FFI-RAPPORT

16/00577

Validation of a Parabolic Equation method against long range blast wave measurements

Knut Waagan

Validation of a Parabolic Equation method against long range blast wave measurements

Knut Waagan

Norwegian Defence Research Establishment (FFI) 6th June 2016

Keywords

Støy
Akustikk
Beregningsmetoder
Skytefelt

FFI-rapport:
FFI-RAPPORT 16/00577

Prosjektnummer
382001

ISBN
P: ISBN 978-82-464-2758-4
E: ISBN 978-82-464-2759--1

Godkjent av / Approved by
Eirik Svinsås, *Research Manager*
Jon E. Skjervold, *Director*

(U) Summary

This report is about the validation of a method, based on a Parabolic Equation model, for predicting acoustic noise. The method is designed for the low-frequency, long-ranging noise induced by heavy weapons and explosions. It is able to take detailed meteorological information into account, which is important for this application. Hundreds of relevant blast wave measurements are available from the Norwegian Trials campaign at Finnskogen. Fairly detailed weather data are also available from the campaign. We have compared our simulations with measurements from Finnskogen, and made the following main conclusions:

1. The PE model worked as well as can be expected given the parametric uncertainties.
2. Taking the weather into account is clearly necessary in noise mapping of heavy weapons.
3. The weather data improved the prediction accuracy of the PE model.
4. Prediction accuracy varied with weather type, season, distance and sound frequency.

A total of 299 unique combinations of detonation events and propagation paths have been considered, some of which were simulated several times with different parameter settings. The selected events were from six summer days and three winter days. Propagation distances varied from 1 to 23 km. Wind and temperature profiles were obtained from measurements that used a tethered balloon. Temperature inversions, which strongly influence sound propagation, occurred during both the summer and winter experiments. In the process of selecting and analysing the shot recordings and weather data, we found that there were errors and issues in the database registration, which are specified in this report. Future users of the database should therefore especially consult our chapters on shot selection and weather data.

(U) Sammendrag

Denne rapporten omhandler validering av en metode, basert på en Parabolic Equation-modell, for prediksjon av akustisk støy. Metoden er designet for lavfrekvent langtrekkende støy generert av tunge våpen og eksplosjoner. Den kan utnytte detaljert meteorologisk informasjon, noe som er sentralt for denne anvendelsen. Hundrevis av relevante lydmålinger er tilgjengelige fra Norwegian Trials-kampanjen på Finnskogen. Relativt detaljerte værdata er også tilgjengelige fra kampanjen. Vi har sammenliknet våre simuleringer med målinger fra Finnskogen, og kommet til følgende hovedkonklusjoner:

1. PE-modellen fungerte så bra som en kan forvente gitt parameterusikkerhetene.
2. Å ta hensyn til været er klart nødvendig for støykartlegging av tunge våpen.
3. Værdataene forbedret nøyaktigheten til PE-modellen.
4. Prediksjonsnøyaktigheten varierte med værtype, årstid, avstand og lydfrekvens.

Totalt 299 unike kombinasjoner av detonasjonshendelser og propagasjonsbaner har blitt undersøkt, og noen av dem ble simulert flere ganger med ulike parameterverdier. De utvalgte hendelsene var hentet fra seks ulike sommerdager og tre vinterdager. Propagasjonsavstandene varierte fra 1 til 23 km. Vind- og temperaturprofiler ble hentet fra målinger med værsonde. Temperaturinversjoner, som kan påvirke lydutbredelse kraftig, fant sted under eksperimentene både sommer og vinter. Under prosessen med å velge ut og analysere skudd- og værdata fant vi at det er noen feil og problemer med databaseregistreringen, som er spesifisert her. Fremtidige brukere av databasen anbefales derfor å rådføre seg med denne rapporten, spesielt kapitlene om skuddseleksjon og værdata.

Contents

1 Introduction

Military training activity produces acoustic noise that can affect neighbours, necessitating the ability to predict the noise dispersal. The software Milnoise serves as prediction tool for the Norwegian Defence. Predominantly, outdoors acoustics is concerned with traffic and industrial noise. Heavy weapons noise differs by being louder, lower in sound frequency and intermittent. In addition, the propagation is nonlinear near the source. With this particular application in mind, we have implemented a sound propagation model as presented in [18]-[19]. The purpose of this report is to validate the model, and our implementation, against measurements.

By far the most suitable data set available is from the Norwegian Trials at Finnskogen in the 1990s. The sound sources used, C4 charges from 1-64 kg, resemble the military sources; the terrain was predominantly Norwegian forest; the propagation distances were from 1-20 km. Weather data were gathered with a tethered sonde up to a few hundred meters above ground level, and there are data on the acoustic properties of the ground. The topography at the site is moderate, by Norwegian standards, ranging 280-450 m above sea level with few steep features.

A schematic overview of our propagation model, a parabolic equation (PE) model, is shown in Figure 1.1. Four categories of input data are indicated: source, weather, topography and ground impedance. The output data are sound levels. The weather data are of particular interest, as our main aim is to enable more detailed representation of refraction in the atmosphere.

The PE model is a rather established tool in outdoor acoustics, but most studies concern higher frequencies and shorter distances. We expect the model to capture the refractive effects accurately given precise weather data. Small scale turbulence effects may very well cause some difficulty, though. The treatment of the ground and the near-source nonlinearities are actually less well understood phenomena, however the resulting uncertainties may in practice be dominated by the strong impact of atmospheric refraction.

Since the main objective is to validate the PE model, use as detailed weather data as possible. In practice, meteorological data will always be a limiting element. Therefore, rather than as a validation of the propagation model, an alternative interpretation of this work is as a study of the predictive usefulness of the tethersonde data.

The report is organised in the following way: First, the Norwegian Trials data are introduced, and we describe how recordings were selected. The weather and ground data are then discussed, and interpreted as input data for the PE model. There is also a short section on source data. The simulations for summer conditions are presented first. Sections 3.1-3.2 discuss the simulations of 81 well documented cases from summer conditions. Those are perhaps the most important sections of this report. The remainder of that chapter presents simulations that further illuminate the findings. The winter simulations are presented in a similarly organised, separate chapter. Detailed plots of simulations and measurements can be found in the Appendix. The remainder of this introduction serves to introduce the propagation model, as well as some technical definitions.

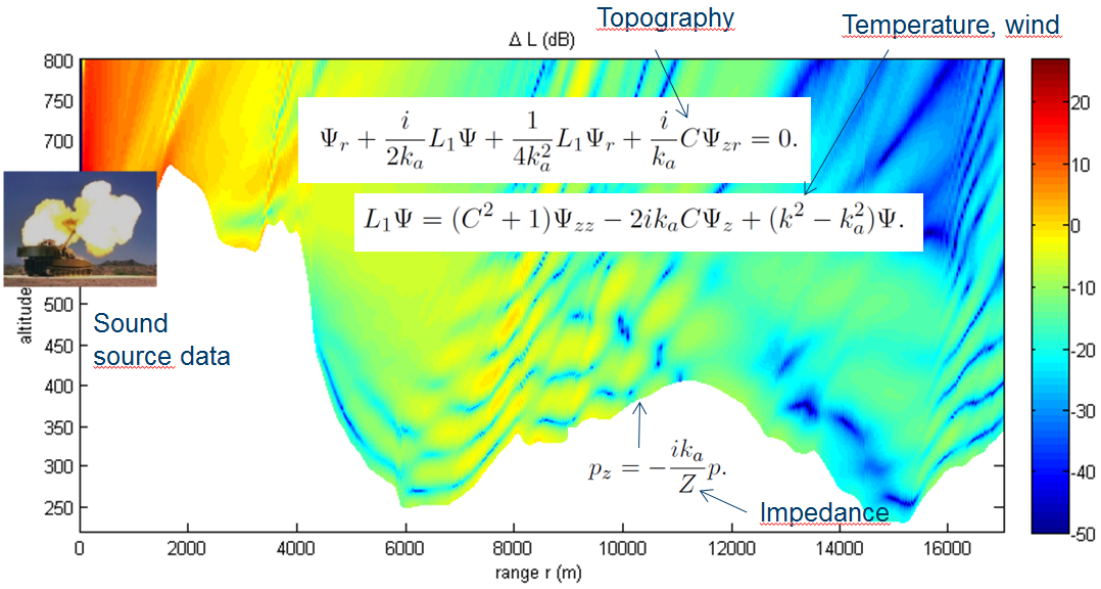

Figure 1.1 *Overview of the model. The sound pressure is given by $p = \Psi e^{-ikr}/\sqrt{r}$. Colours indicate relative sound levels for a 20 Hz harmonic source. The shown boundary condition is a bit simplified.*

1.1 Basic notions and definitions

Cylindrical symmetry around the source location is assumed in the model, hence the sound pressure p is considered a function of time t, the horizontal distance r, referred to as range, and height above ground z.

Fourier transforming in time, we get the complex pressure $p_f(r, z)$ for each frequency f. The sound pressure level is defined as

$$L_p(f) = 10\log_{10}\left|p_f/p_{\text{ref}}\right|^2, \quad p_{\text{ref}} = 2\times 10^{-5}\ \text{Pa}. \tag{1.1}$$

For a point source it can be decomposed as

$$L_p(f) = L_0(f) - 10\log_{10}(R/R_0)^2 + \Delta L_f, \tag{1.2}$$

where L_0 is the sound pressure level in a homogeneous free atmosphere at some reference distance R_0, the second term is the geometric loss, and ΔL_f is called the relative sound level. Hence, ΔL_f contains all information about refraction, terrain and ground effects and is independent of the source. Equation (1.2) is only valid for linear sound propagation out from a point source. Linearity may not hold near the source, but the nonlinear effects are, as an approximation, incorporated in the source data L_0. More details on source data can be found in [6].

The sound exposure level (SEL) is defined by

$$\text{SEL} = 10\log_{10} t_{\text{ref}}^{-1}\int |p/p_{\text{ref}}|^2\, dt = 10\log_{10} t_{\text{ref}}^{-1}\int \left|p_f/p_{\text{ref}}\right|^2 df, \tag{1.3}$$

with the reference time $t_{\text{ref}} = 1$ s and $p_{\text{ref}} = 2 \times 10^{-5}$ Pa. All the calculations are performed in the frequency domain. Frequencies are sampled over 12th octaves, i.e. $f_j = 2^{j/12} f_0$ for integer j. The sound exposure level in third octave bands SEL3(f_c) for a center frequency f_c are reported. We use a standard trapezoidal rule to compute SEL3 from twelfth octave samples.

The third octave bands from 1-100 Hz are considered here. Some of these are inaudible, hence it is common to 'C-weigh' the data, meaning that a standardised high pass filter cutting off at 20 Hz is applied. We denote the C-weighted SEL by SELC.

Sound gets refracted in the atmosphere due to variations in the sound speed c. We compute c from air temperature T according to the relation

$$c = 340 \text{ m/s} \sqrt{\frac{T}{288.15\text{K}}}. \tag{1.4}$$

The horizontal wind speed component u in the direction of propagation defines the effective sound speed $c_{\text{eff}} = c + u$. We use the so-called effective sound speed approximation, which consists of an unmoving atmosphere with c replaced by c_{eff}. By wave number k we therefore refer to the effective wave number $2\pi f / c_{\text{eff}}$, strictly speaking.

The sound waves will interact with the ground, which is modeled as an impedance surface, meaning that the normal derivative of the complex pressure satisfies

$$\frac{\partial p_f}{\partial n} = -\frac{ik}{Z} p_f \tag{1.5}$$

at the ground surface, with the complex specific impedance Z depending strongly on frequency.

1.2 The PE method

The details of the PE method are described in [18]-[19]. We use the wide-angle PE equation of [11] (see [12]), with the exception that piecewise linear topographic profiles, rather than twice differentiable profiles are considered. The main equations are included in Figure 1.1. Some numerical parameter choices for this study must be specified: The top of the domain was 15% of range, but never less than 250 m. We used 'reduction of range-dependence' as in [19] with an accuracy threshold of 5 m. As a 'scattering threshold' we generally used -35 dB, meaning that we did not allow the relative sound level ΔL to drop below -35 dB.

2 Norwegian Trials data from Finnskogen

The campaigns at Finnskogen took place in September 1994 and February 1996. The geometry of the experiment is shown in Figure 2.1. C4 explosive was detonated at 2 m height on the locations marked in red. Towers with microphones were situated at five locations (yellow), and there were five weather towers with up to 30 m height (green). The tethersonde was operated at position 403. There are additional tethersonde data from positions 0 and 112, but we have not used them since they had more limited coverage. The weather measurements are summarised in [4]. We have accessed the Finnskogen data from the NORTRIAL database, described in [1] and [2], using the well-documented Matlab interface that comes along with it.

2.1 Shot selection

The recordings that we selected are listed in appendix A.4, and in this section the selection procedure is described. Each shot recording in the database has been assigned a quality label in the Nortrial database. Quality A recordings have a good signal-to-noise ratio and no other obvious issues. Quality B1 recordings are considered reliable except that the signal-to-noise ratio may be an issue. Other categories have not been considered here. In addition to quality labels, we have restricted ourselves to the times when the tethersonde was operated. Histograms of propagation distances are shown in Figure 2.2. We expect the farthest to be very challenging.

From summer 1994, we found 81 quality A cases that could be used. They are mostly from microphone towers 306 and 112. By a 'case' we mean a combination of a detonation event and a receiver position. For many cases there is more than one recording from a tower. If so, we picked the most elevated microphone. We have enumerated the cases according to the order they appear in the database listing, which seems to be chronological for summer data, and by tower, then chronological, for winter data.

The data from tower 0 appear not to be correctly registered, hence they were excluded. It appears as if the sampling rate cited is off by about a factor of two, although there could be other issues. This may have affected previous investigations of these data, and our advice is to ignore results using tower 0. We have performed the simulations however, in case the correct data were to be retrieved. This would add 46 quality A cases to the other 81.

From the winter trials, we have picked quality A data from February 21-23rd. We mostly consider data from tower 306, of which there are 83 cases. There are 73 quality A cases from 212 and 412, however it is clear that the charge sizes have been incorrectly registered there. By comparing to recordings of the same detonation events at 306, we have corrected the charges. This is also an issue for the summer data, but there was only one mismatch (case 122) and two that could not be verified (cases 40, 88), and it appears that we have gotten the charge sizes right.

A total of 61 quality B1 data from summer 1994 have briefly been considered. Since we had limited time to verify the quality, only those with SELC>70 dB were picked, of which six cases were excluded after inspection. Charge sizes were incorrect for many of these cases, and we excluded those were data entries disagreed.

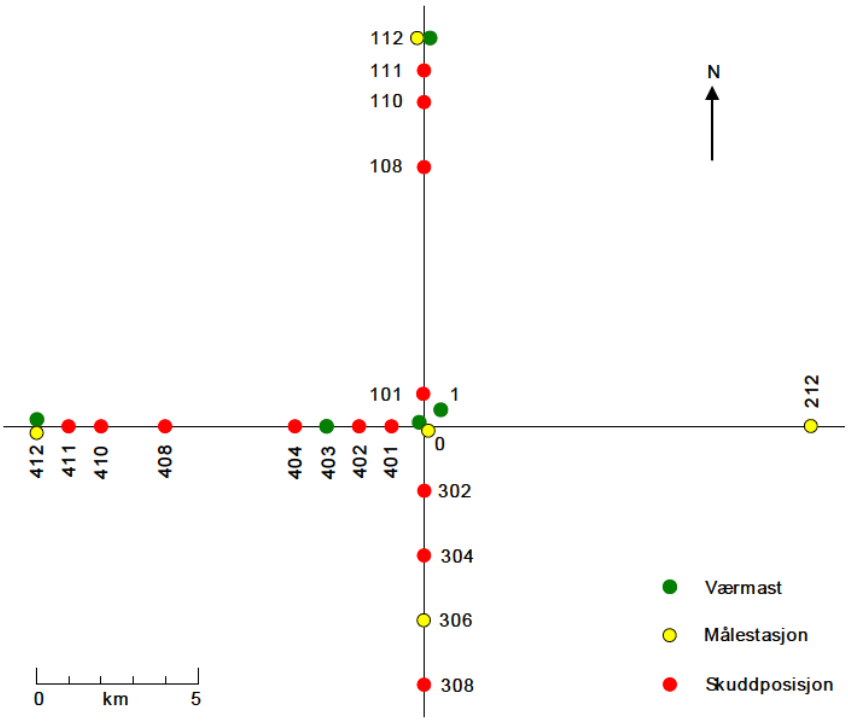

Figure 2.1 *Positioning of shots and measuring stations. Green dots are weather masts, yellow dots are sound recorder locations, red are shot positions. Tethersonde data are from 403. From [1].*

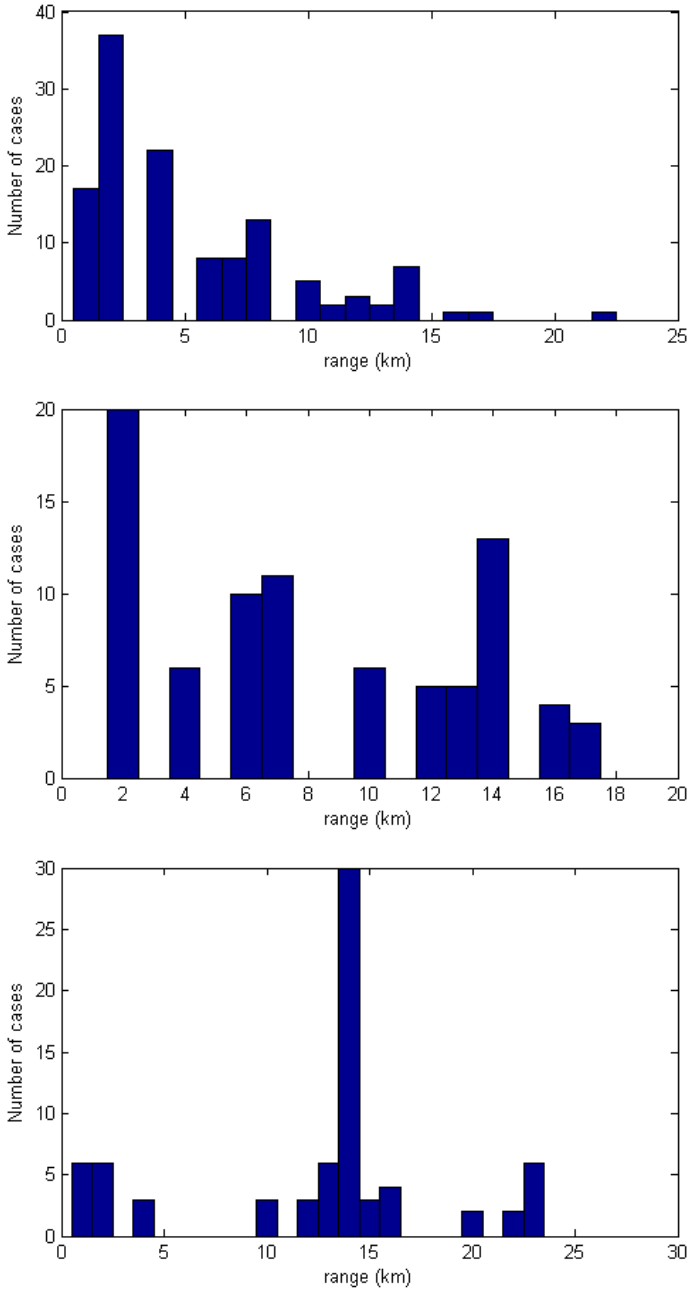

Figure 2.2 *Histograms of propagation distances. Top: Summer quality A, 81 cases, Middle: Winter quality A from tower 306, 83 cases. Winter quality A, other towers, 73 cases.*

2.1.1 Signal duration

The duration of the recordings varied, and could last up to 15 seconds. The actual blast wave signals may have lasted up to a few seconds at long range, but often they were much shorter. Integrating over the whole recording could lead to overestimation of the SEL3 values because of noise. We therefore devised a very simple truncation algorithm: The timing t_p of peak pressure was identified, and then the surrounding time interval $t_p - a < t < t_p + b$ was selected. For the summer quality A data, we set $a = 0.5$ s and $b = 2$ s. The resulting SEL3 spectra were practically identical to those using the whole recording. For the winter recordings, this was not the case, and we also changed the parameters to $a = 1$ s and $b = 1.5$ s, in order to accommodate some oddly shaped blast waves. These parameters were also used as control for the summer B1 data, and that gave small deviations from the untruncated recordings. Ideally, the B1 data should have been treated individually.

2.2 Weather data

The selected summer measurements are from six days in 1994. From September 13-14th, which seems to have featured cloudy weather and little temperature variation; and September 19-22nd, when the weather was clear with temperature inversions in the morning and large temperature variation throughout the day. An example of this weather type is shown in Figure 2.3. Winds were weak to moderate near ground, but 'low level jets' were observed at a few hundred meters height. These probably had significant impact on propagation, including during temperature inversions. The winter measurements were selected from February 21-23rd. The weather was then calm and clear with deep inversions, and large temperature variation throughout the day.

2.2.1 Tethersonde data interpretation

The tethersonde measured temperature, wind and wind direction at times t_k and heights z_k above ground. We used the Matlab interpolation routine 'griddata' to turn this into a map of the atmosphere across a continuum over t and z. The result for one single day is shown in Figure 2.3. This interpolation routine responds strongly to how the parameters are scaled. We found through trial and error that dividing z with 5000 m/day gave reasonable looking results. Above the reach of the sonde we set wind and temperature constant.

For use in a propagation model, this two-dimensional map has to be reinterpreted into a four-dimensional map over time and space. The simplest strategy would be to follow the terrain, i.e. assume the meteorology is only a function of time and height above ground. A second strategy is to assume the meteorology is a function of time and altitude, i.e. height above sea level, only. This is likely a decent approximation except near the ground, and was our primary strategy. Exceptions were made for the following reason: The 403 station, where the sonde was operated, was at 320 m elevation, whereas station 306 was in a valley bottom at 280 m. As a solution, we let the weather follow the terrain whenever the ground elevation was below 320 m.

The tethersonde captured many details that were either intermittent fluctuations or just spurious artifacts. Neither are likely to be very useful for us, hence we applied some smoothing in the vertical

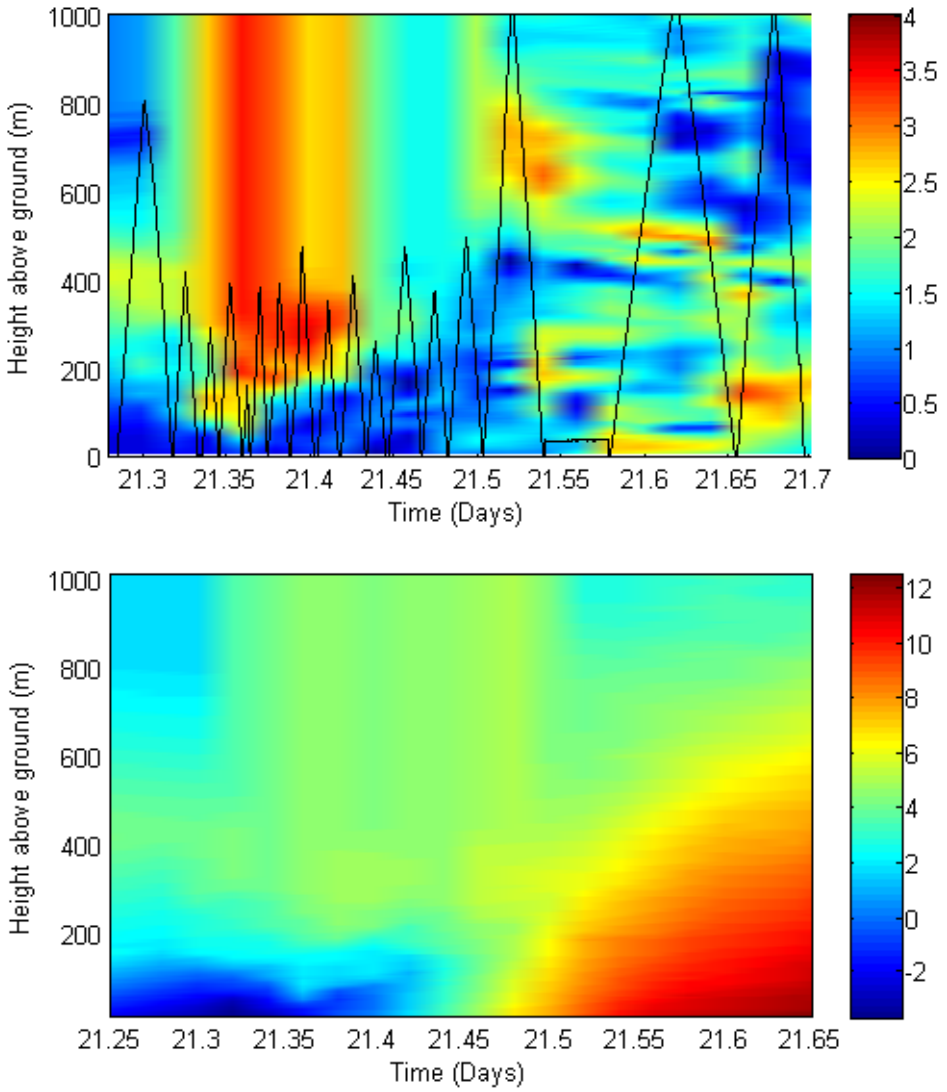

Figure 2.3 *Top: Wind speed (m/s) as a function of time and height above ground on September 21st 1994. The tethersonde height is indicated by the black curve. Bottom: Temperature (°C) on September 21st.*

direction to the data. The smoothing simply consisted of a running average. Unless otherwise noted, the temperature data were averaged over a 50 m window, and the wind data over 300 m. Another typical way to deal with this problem is to fit some function, such as a lin-log profile, to the data, but due to the large variety of observed profiles, smoothing seemed a better, less intrusive, option.

The summer tethersonde data were available in a postprocessed form in NORTRIAL, and we chose those. On September 21st there was a problem with the postprocessing, therefore the raw temperature data had to be used for that day. From the winter trials only unprocessed data were available. They were of course a bit noisier. The Matlab code we wrote to treat and interpolate the sonde data is included in appendix A.3, for completeness. There were many specific 'glitches' in the data that we corrected individually, and they are best listed in this way.

The lowest 10 m above ground, i.e. 320-330 m elevation, were not covered by the sonde data. We let the temperature be constant here, and let the wind taper off linearly to zero in the lowest 10 m above ground level. We also tested some surface layer models for the lowest few tens of meters above ground, and they are described later.

2.3 Ground data

It is crucial to have reasonably accurate values for the ground impedance Z. We calculated ground impedances from rigid porous medium models, based on parameters found in the database.

2.3.1 Summer

It is rather well-established that the Delany-Bazley model, although widely used in outdoor acoustics, is unsuitable for low frequencies, see e.g. [16] and [17]. We used a Taraldsen model ([17], [5]) instead. It requires one input parameter, the resistivity σ. The database provides a classification of the ground at Finnskogen, along with suggested values of σ, based on [14] and [15], see Figure 2.4. We used a halfspace model, as we had little information about vertical structure. Mostly the backing layer consisted of hard moraine. We suspect that deeper and more reflective layers played some role for infrasound at least at tower 112, based on looking at the spectra. At tower 306, sand sediments made up the backing layer. It has been demonstrated that this could lead to seismic effects ([10], [8]), which we have not attempted to include, partly because it may be difficult or impossible to model with an impedance boundary condition.

2.3.2 Winter

Snow 30-40 cm deep was reported from the winter trials, with significant terrain variability. Snow is expected to have a strong impact on sound levels in a way that is challenging to model. We tried to model the snow-covered ground as a rigid, homogeneous layer with a hard backing, as described in [5] and [12]. The Zwikker-Kosten model ([21], [12]) was chosen for the porous medium. This leaves three parameters to be chosen: resistivity σ, porosity Ω and snow depth d. Some clues to appropriate values were found in [13], however there seemed to have been a lack of data below

Ny klasse 0 (FFI klasser 0,2,5) : Barskog i forskjellige årsklasser, tettvokst stor barskog, ungskog på tidligere hogstfelt. Typisk overflate strømningsmotstand i denne typen skogsbunn er 30 000 Pa·s/m2 .

Ny klasse 1 (FFI klasser 3,4) : Flere år gammel glissen skog på tidligere hogstfelt, hogstfelt med eventuelt innslag av frøtrær. Litt usikkert angående typiske impedansverdier, men for tett, tørr torv eller tynt moselag over sandaktig jord, kan verdien for strømningsmotstand være ca. 100 000 Pa·s/m2.

Ny klasse 2 (FFI klasser 8,9) : myr eller myrlignende vegetasjon. Dette er fuktig myr med tykt, moselignende vegetasjon. Typisk overflate strømningsmotstand er 15 000 Pa·s/m2.

Ny klasse 3 (FFI klasser 6,7,10,11) : Grasbakke, myr, åpent lende, dyrket innmark, kultivert grassland, eng, dyrket innmark. Typisk overflate strømningsmotstand er 350 000 Pa·s/m2.

Ny klasse 4 (FFI klasse 1) : Vann. Overflate strømningsmotstand er svært høy, fungerer som "hard flate" akustisk sett. Strømningsmotstand ca 20 000 000 Pa·s/m^2.

Figure 2.4 *Ground classification. Values of specific resistivity σ are given. Classes 0-1 are forest types, 2 marsh, 3 open country and 4 water.*

40 Hz. We ended up with $\sigma = 8$ kPa s/m^2, $\Omega = 0.7$ and $d = 70$ cm. Obviously, the latter choice deviated from observed depths. On the other hand, the resulting impedance values captured the low frequency effects quite well, which was most important, since the main goal was to study the PE model and the weather data.

2.4 Source spectra

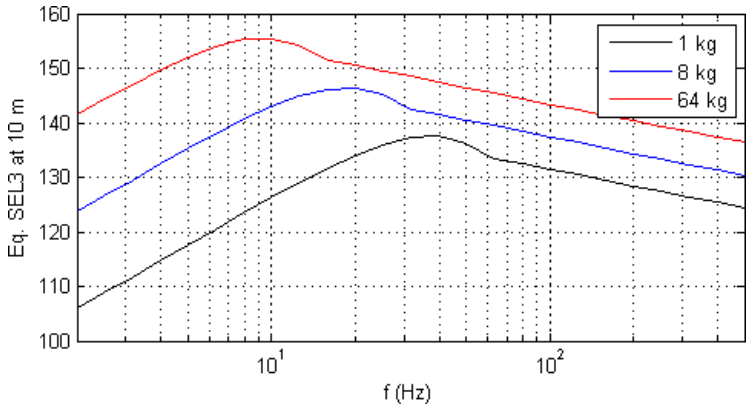

Figure 2.5 *The source spectra used.*

The source model is the so-called FOFT model described in [7]. The FOFT model is described for TNT, so we applied a conversion factor of 1.34 to the charge sizes. The model consists of a

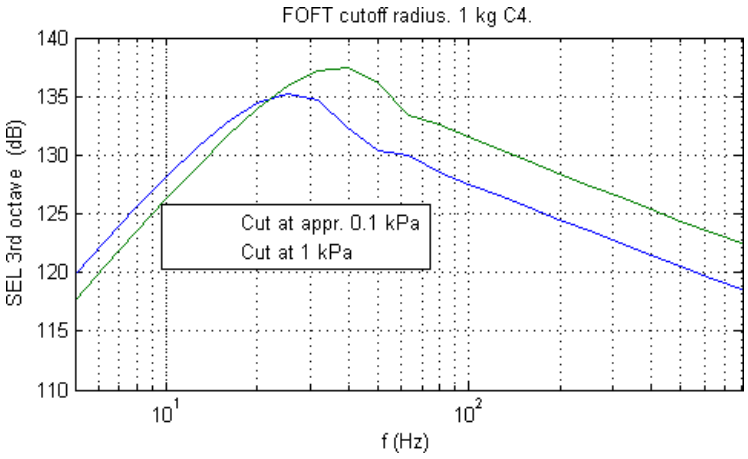

Figure 2.6 *Source spectra for 1 kg C4 for different 'nonlinearity criteria'. The picture looks similar for other charges sizes.*

blast wave from a free explosion evaluated at a range where the propagation is linear. The wave is then propagated backwards linearly to a reference length r_0. The range at which nonlinearities can be ignored is open for interpretation. We have chosen a peak pressure of 1 kPa as a criterion. The formulas indicate that it should rather be around 0.1 kPa, but at that range ground interaction and refraction are certainly more important. These two strategies differ by a few dB in the source spectra, as illustrated in Figure 2.6. Interesting experiments on ground interaction in the nonlinear range are reported in [3], where ground effects over grassland are observed already at 5 kPa.

3 Summer conditions study

We have gathered spectra for all 81 quality A summer cases in appendix A.2. The third octave SEL spectra from the PE simulations and the measurements can be compared for each case. For reference, we have included two simpler models: (1) PE simulations without refraction and topography, which resemble the Low Frequency Module currently implemented in Milnoise, and (2) a FOFT source model with a double charge. The double charge is a simple way to take the ground into account, because at close range most energy is reflected from the ground. Including this model in the plots demonstrates the effect of the propagation conditions. Next to each spectrum plot, the sound speed that was used in the simulation is shown as a function of altitude, with both the effective and the thermal sound speeds included.

3.1 All A data

Figure 3.1 shows the SELC values for all 81 cases. Predicted SELC is plotted against measured SELC. Hence, the prediction error can be read off as the vertical (or horizontal) distance to the black diagonal line. The PE predictions (blue circles) were scattered fairly symmetrically around the line, and the errors increased with decreasing SELC. The simple FOFT source model (light blue dots) overestimated SELC with minor exceptions, as should be expected over soft ground. The simple PE model (red dots) tended to underestimate. Both reference models deviated more for weak received signals.

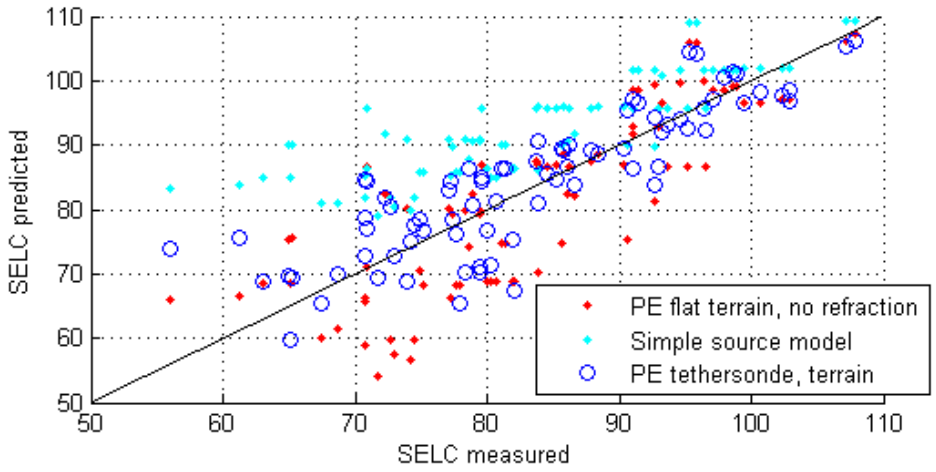

Figure 3.1 *SELC values, predicted vs. measured. All summer A data.*

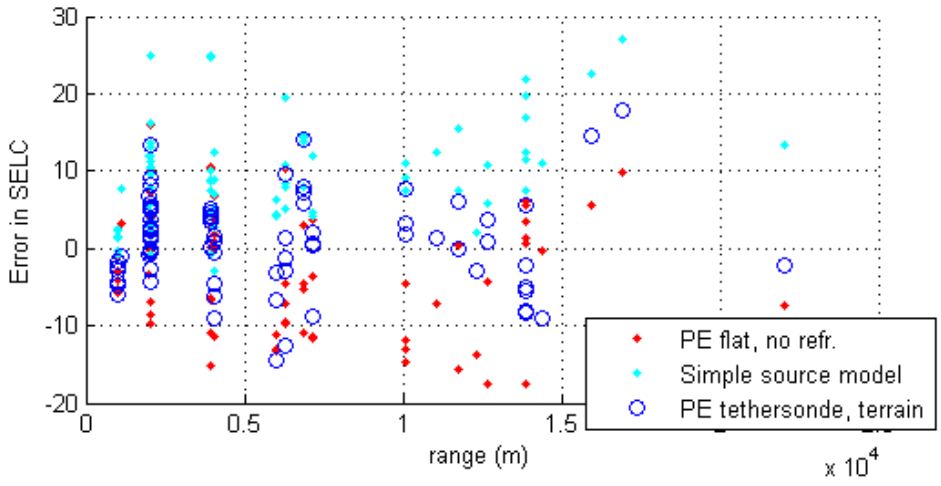

Figure 3.2 *Signed prediction error in SELC vs. range. All summer A data.*

Figure 3.2 shows the signed prediction errors in SELC plotted against range r. The sign convention, which is used throughout this report, is such that positive values mean overprediction of sound levels. The errors were smallest at 1 km, and seem to increase until 6 km, beyond which there is no obvious pattern. It seems that the influence of the propagation conditions increased with range, as the three models increasingly deviated.

Figure 3.3 contains the error in SEL3 for all A data. The most striking feature is below 10 Hz, where the measurements at tower 306 consistently showed a strong sound reduction of up to tens of dB. As far as we know, there is no theoretical nor observed precedence for this phenomenon, hence it is best disregarded for now. The effect was evident also in [16], and, along with the above mentioned issues with tower 0, it can explain the difficulties reported there below 10 Hz. At tower 306, seismic effects have been predicted in the infrasound range, but the predicted magnitude was much smaller than the phenomenon observed here.

These experiments can not be regarded as statistically independent, and a statistical analysis is beyond the scope of this work. Certain features are clear, however, from the average quantities shown in Figures 3.4-3.5. Including weather improved both RMS (root mean square) error as well as median error, and increasingly so with frequency. The bias towards underestimation caused by ignoring weather is evident in the mean signed error. The variance of the error increased with frequency when weather was included. The lack of a strong bias in the predictions agrees with meteorological variability being the main source of uncertainty.

It is evident that weather and topography became more important as frequency and range increased. Hence, up to a certain range, a simpler algorithm such as the Milnoise LF module should suffice. Quantifying when and where is nontrivial, but the data may give us a clue. The band 1-25 Hz is regarded as particularly challenging, hence we consider the 25 Hz 3rd octave band. Figure 3.6 plots, against range, the differences in SEL3 between the full and the simple PE simulations. There are clear deviations at 2 km, and at 4 km, meteorology very obviously must be taken into account. At shorter ranges, ground interaction, or perhaps some other issue such as source modelling, are at least as critical as meteorology.

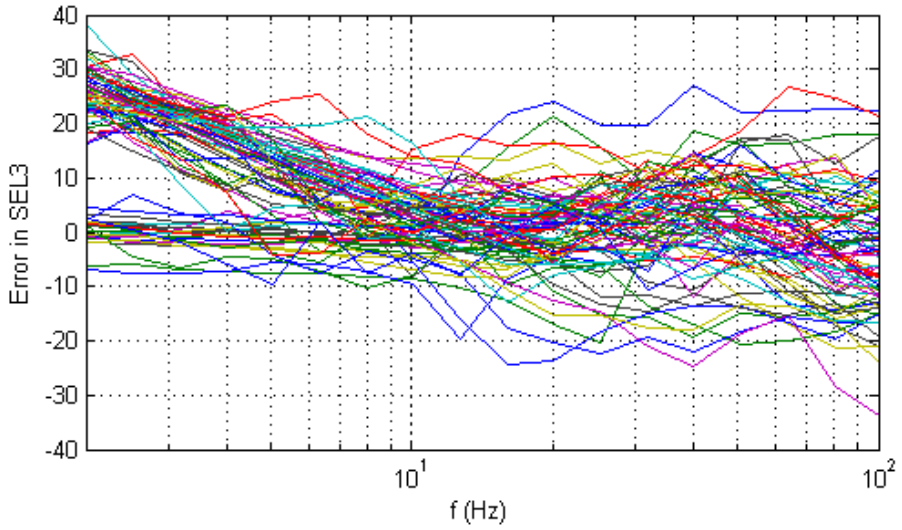

Figure 3.3 *Signed error in SEL3. All summer A data.*

3.2 Weather types

The accuracy of sound propagation models should be expected to depend on the weather type. The accuracy of the weather forecast may vary with type, and the influence of atmospheric turbulence can be large when upward refraction or ground effect dominates.

As weather type indicators we chose the temperature gradient $\tau = \Delta T/\Delta z$, evaluated as the change from 600 to 330 m altitude, and the wind component U in the direction of propagation at 600 m altitude. We also considered the effective sound speed gradient $\Delta c_{\text{eff}}/\Delta z$, evaluated at the same heights as temperature. A scatter plot of the weather indicators for each case is provided in Figure 3.7. Cases with temperature inversion, i.e. with positive τ, were clearly separated, so we let them form one class. Downwind there will typically be some downward refraction, hence we divided the remaining cases at $U = 2$ m/s. The SEL3 errors are all plotted in Figure 3.8 with one colour for each weather type. The inversion cases were best captured, and the upwind/neutral cases the worst with a lot of underestimation. The latter was not unexpected.

Figure 3.9 shows the RMS errors for each weather class. It is evident that weather is crucial during inversion as well as downwind, while otherwise the weather data does not improve the RMS error much. Figure 3.11 shows SELC for each weather type. The SEL3 values at 32 Hz can be seen in Figure 3.10. The significance of weather is very clear at this frequency. The simple PE model underestimated during the downward refracting weather types. The full PE model clearly handled those weather types better, except for some long-range downwind cases, which were overestimated. The upwind/neutral situation is less clear: At longer range, the weather data enhanced underestimation, while at shorter range, they seem to have been quite useful. Generally, precision was much better for received SEL3 values above 80 dB than below.

SEL3 values for each of the three weather classes is provided as scatter plots in A.1-A.3, with one plot for each third octave band. The observations we have stated for 32 Hz hold generally. We

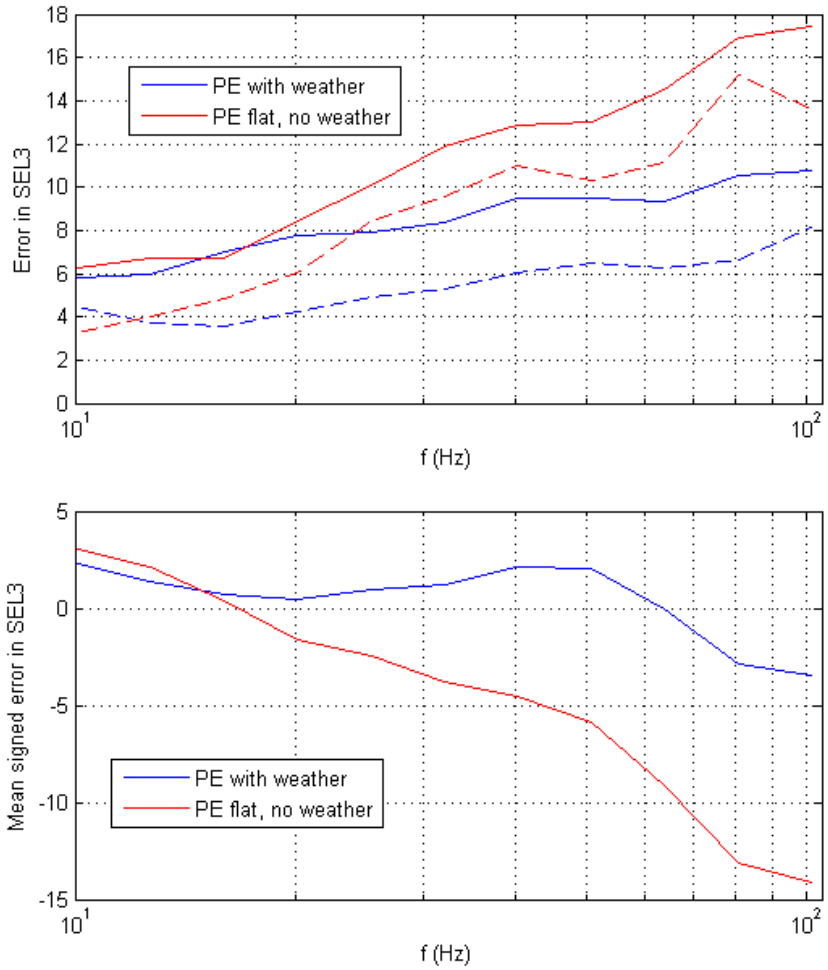

Figure 3.4 *Top: Error in SEL3. Solid: RMS, dashed: median. Bottom: Mean signed error in SEL3. All summer A data.*

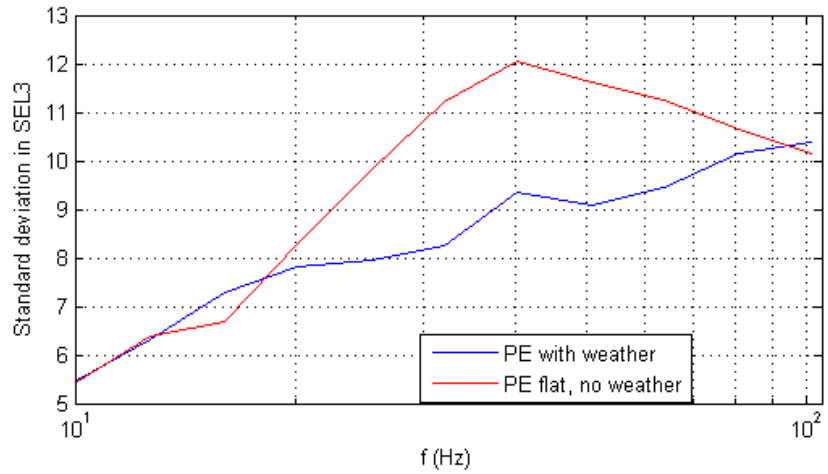

Figure 3.5 *Standard deviation from mean in SEL3 error. All summer A data.*

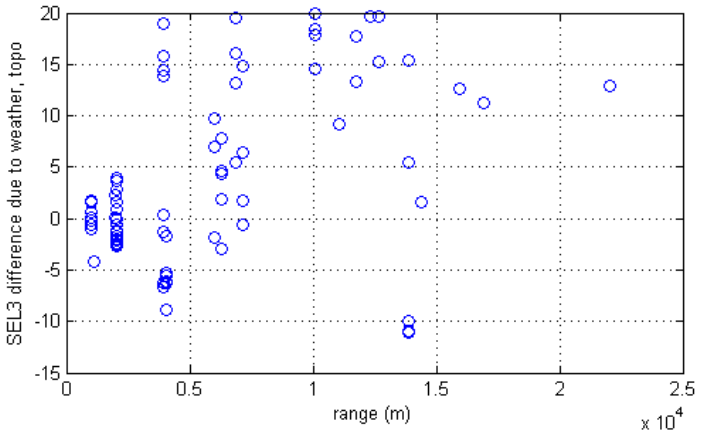

Figure 3.6 *Difference at 25 Hz in SEL3 between full and simple PE model. All summer A data.*

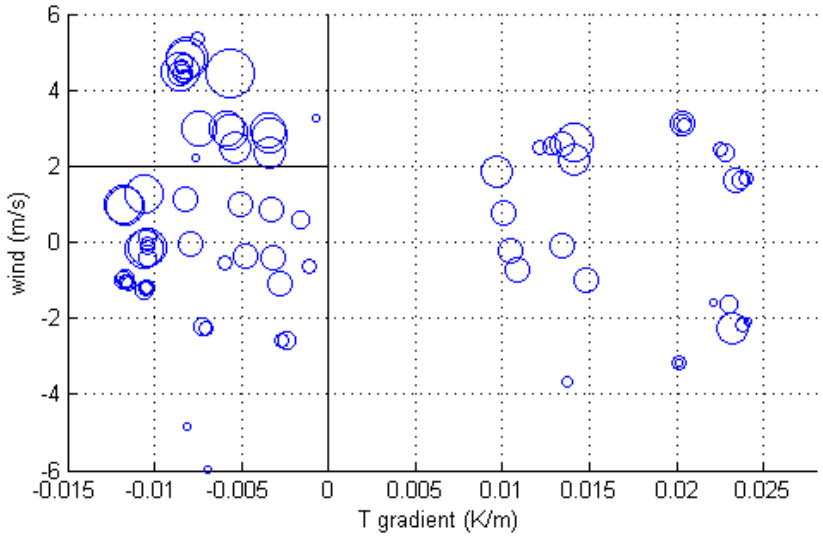

Figure 3.7 *Scatter plot of meteorological conditions. All summer A data. Circle sizes indicate range. Weather classifications marked with black lines.*

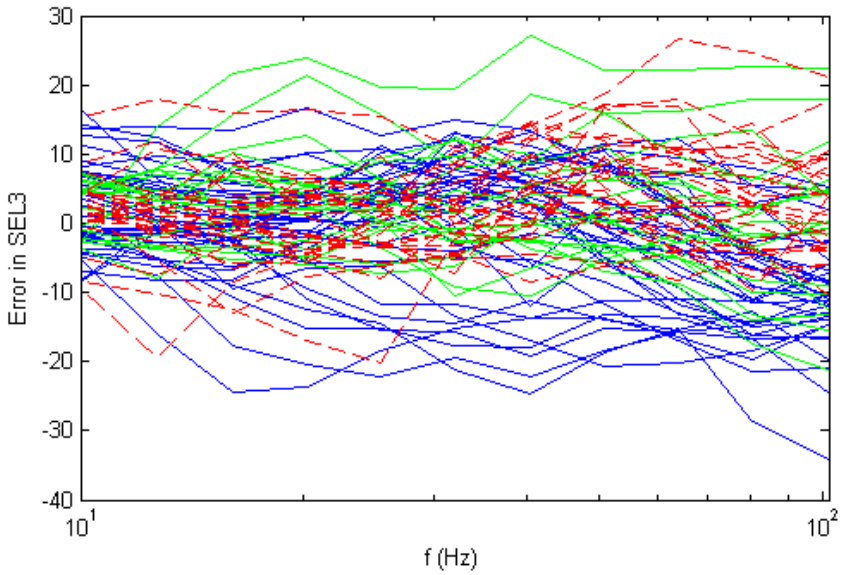

Figure 3.8 *RMS prediction error vs. f. Solid lines: Full PE, dashed: simple PE. Red: Inversion, green: downwind, blue: neither. Circle sizes are proportional to range. Summer A data.*

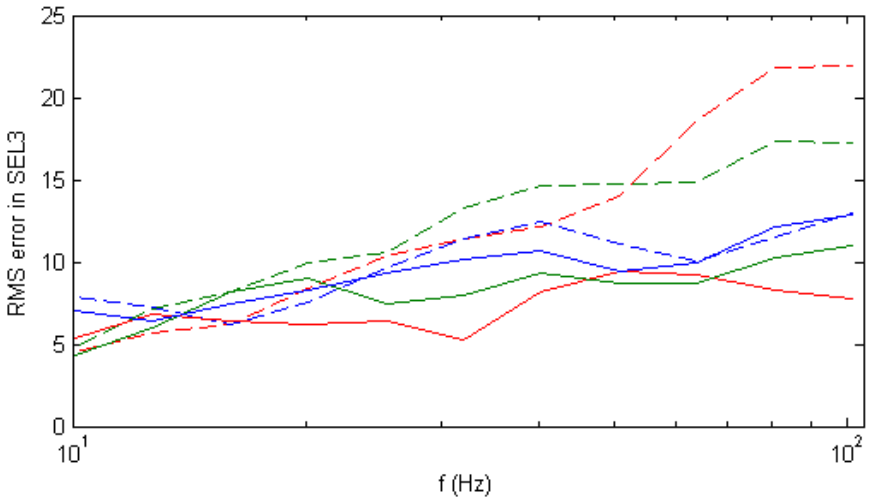

Figure 3.9 *RMS error for different weather types. Red: inversion, green: downwind, blue uwind/neutral. Solid lines are from the full PE simulations and dashed lines are from simple PE simulations. Summer A data.*

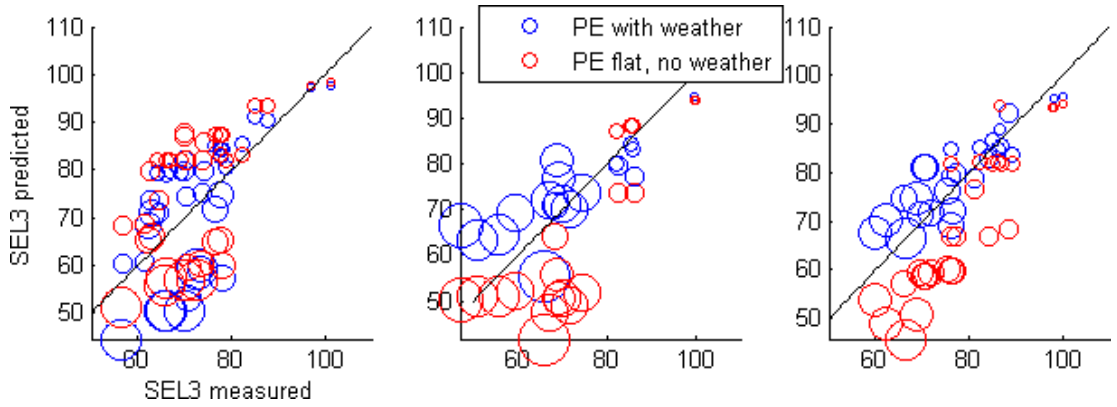

Figure 3.10 *SEL3 at 32 Hz for each weather type. Left: Upwind/neutral, middle: Downwind, right: inversion. Summer A data.*

also note a tendency towards over-prediction in the mid frequencies, perhaps to do with ground interaction or source modelling. At the lowest frequencies ground interaction and possibly other effects appear to have dominated over refraction in many cases.

3.3 Parameter variation

For this section, the numerical simulations of the summer quality A cases were repeated with various changes in the input data. This serves for one thing to illustrate some of the parametric uncertainty. A more ambitious aim is to determine which parameter choices are better.

3.3.1 Topography

As mentioned, the terrain profiles were gentle by Norwegian standards. Topography had a direct effect, but it was relatively subtle. To illustrate this, we have performed the simulations without any refraction: Once with and once without topography. Figure 3.12 shows the difference in SEL3 due to including topography or not. Range and frequency played a role here as expected.

3.3.2 Vertical regularisation

The vertical smoothing of temperature and wind is a balance act between capturing the essential features and excluding intermittent and/or spurious effects. As a less smoothed alternative we averaged temperature over 15 m and wind over 50 m. The scatter plots for each third octave are shown in A.4-A.6. SEL3 values for 32 Hz are shown in 3.13. We find that the increased detail tended to decrease accuracy, in some cases strongly so. In upwind conditions, detailed profiles may improve the underprediction problem, but at the price of occasional overestimates. Our findings are consistent with [20], in the sense that they recommend some averaging rather than instantaneous profiles. We have also tried to average temperature over 50 m as above and wind over 100 m, but it seems the rather large smoothing length of 300 m for the wind was favourable.

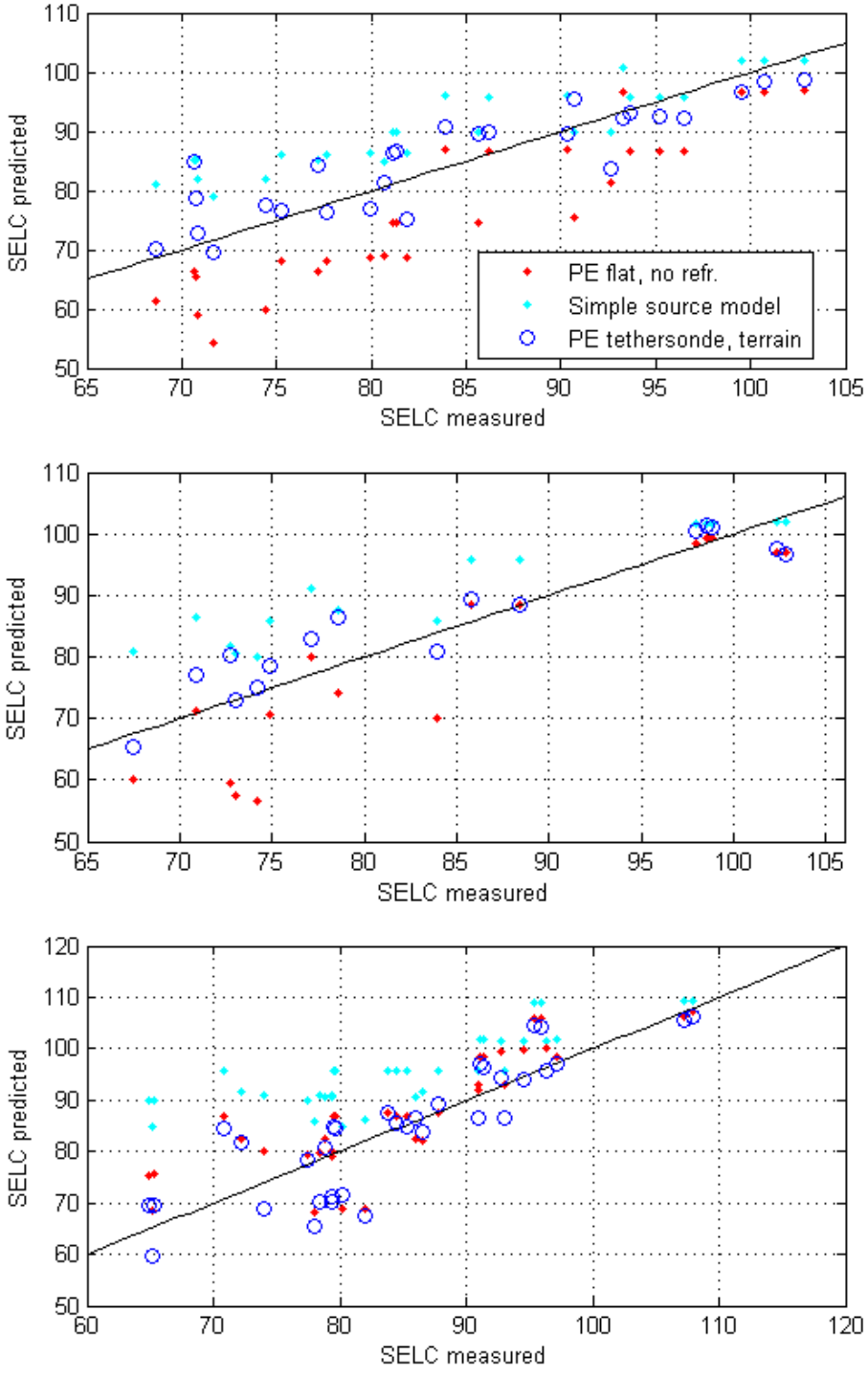

Figure 3.11 *Predicted vs. measured SELC. Bottom: Neutral/upwind, middle: downwind, top: inversion. Summer A data.*

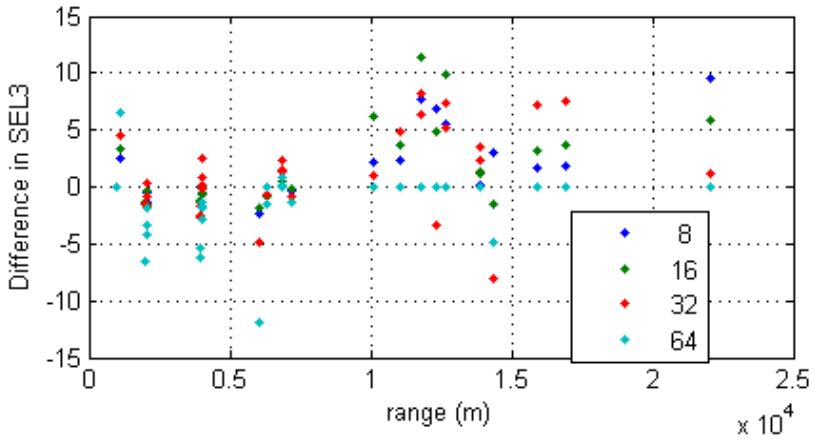

Figure 3.12 *Difference due to topography for 4 frequencies (denoted in Hz). No refraction. All summer A data.*

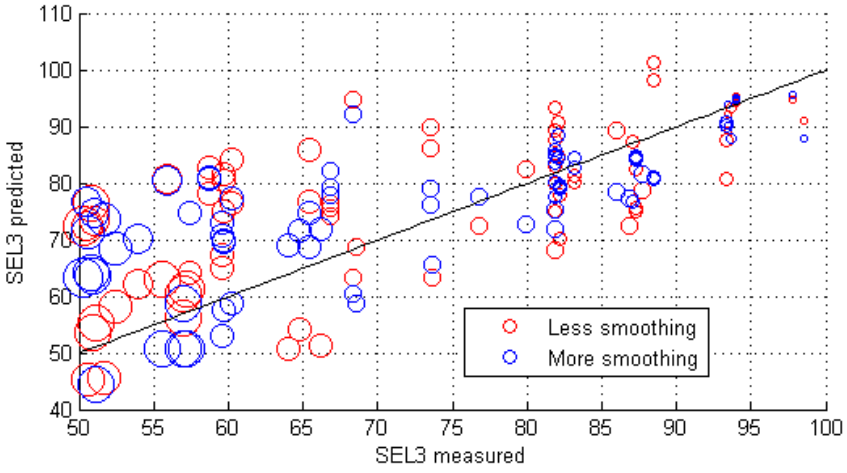

Figure 3.13 *Vertical smoothing of meteorology data at 32 Hz.*

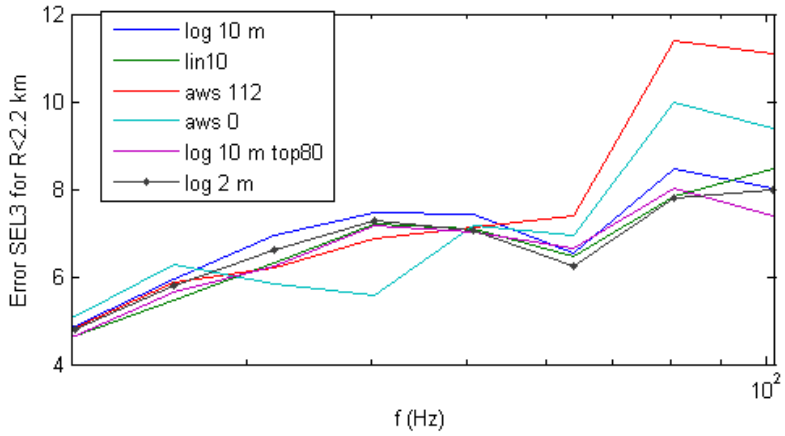

Figure 3.14 *RMS error in SEL3 for various surface layer models. Ranges less than 2.1 km. The SL models were used up to 30 m, except 'log 10 m top80' which went up to 80 m.*

3.3.3 Surface layer

The surface layer (SL) is likely to be very complicated at a forest location like Finnskogen. We have still attempted some ways of taking it into account. Each attempt consisted of replacing the tethersonde data in the lowest few tens of meters above ground. We have tested the following ideas:

1. 'lin10'. No treatment (except for the usual linear tapering of the tethersonde wind data, hence the name).
2. 'log z_0'. Wind is replaced a with logarithmic profile

$$u(z) = u(z_t)\log(z/z_0 + 1)/\log(z_t/z_0 + 1) \tag{3.1}$$

   with roughness length z_0 up to height z_t.
3. 'aws N'. A lin-log fit to the data from a weather tower at position N. Wind below 30 m above ground was then tapered to zero with the lin-log profile, keeping wind direction fixed. The temperature below 30 m was changed so that the gradient equaled that of the lin-log profile.

The simulation output was quite sensitive to the surface layer model, particularly for the higher frequencies. The scatter plots in Figure A.13-A.9 demonstrate this. None of the attempts seemed to improve on the simple 'lin10' model. The weather tower-based surface layer profiles notably increased the errors, which again shows that instantaneous, local profiles must be used with care. Figure 3.14 compares the RMS error at short range for each SL model. Only the short range cases were included as they presumably are the most affected by the lowest parts of the atmosphere.

Looking at the weather tower data makes it clear that the SL profiles will vary a lot across the terrain. Figure 3.15 compares the temperature gradient between 10 and 30 meters at three locations over time. Most likely the profile depends a lot on local vegetation, and may behave somewhat stochastically. The wind profiles appeared more predictable, as they fit logarithmic profiles. At tower 0, a suitable roughness length seemed to be 10 m, while at 112, 2 m fit better. The ground class data explain the difference as 112 was in a field, and 0 was in open forest. The weather tower at 403 was inside dense and tall forest, and measured rather interesting profiles, as noted in [4].

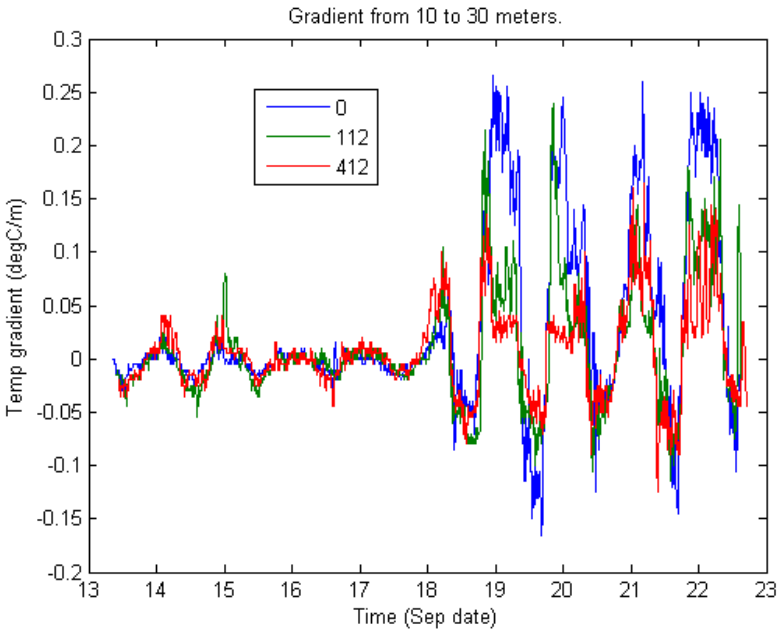

Figure 3.15 *Temperature gradient between 10 and 30 m.*

3.3.4 Sound speed following topography

An alternative extrapolation of the sonde data is to assume that the meteorology only depends on height above ground. We show scatter plots from such a simulation in Figure A.7. At 306 we had to follow the terrain in any case, as already explained, therefore we only include data from tower 112 here. Results are not bad, but this alternative approach seems not to be very useful.

3.3.5 Scattering threshold

As mentioned, our scattering threshold was at -35 dB. Clearly, the sound levels still fall below the measured values in some cases. Figure 3.16 shows the RMS error in SEL3 resulting from different threshold values. For this statistic, the best choice was about -25 dB. Most likely, this should depend on the propagation conditions.

3.4 B1 data

The selection of quality B1 data was also simulated. The resulting SELC values look much as expected, see Figure 3.17. We divided weather types into downward and upward refracting according to the sign of the effective sound speed gradient. Ranges were either quite close at 2-4 km or above 10 km. The close range values were mostly well predicted, and the tethersonde data seem useful except for the underestimation at long range during upward refraction.

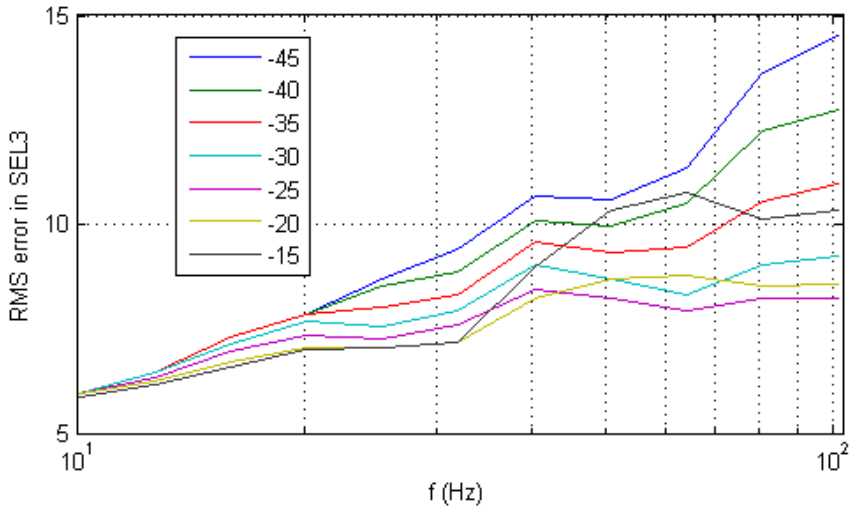

Figure 3.16 *RMS for different scattering thresholds. The thresholds in dB are given.*

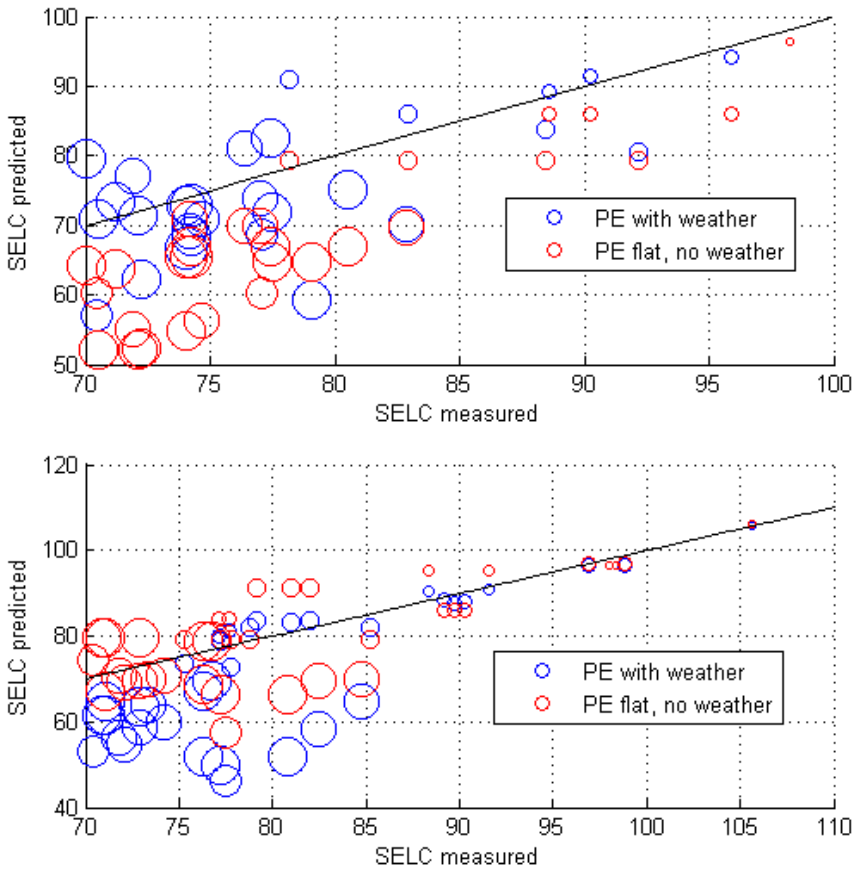

Figure 3.17 *Selected B1 data. Top: downward refraction. Bottom: upward refraction.*

4 Winter conditions study

The spectra for the winter cases are included in appendix A.2. We first discuss the recordings from tower 306. Spectra for the cases with range 2 km are shown in Figure 4.1. These cases were used as templates to find suitable impedance values. It is clear that the ground effect was remarkably strong with a cut-off between 10 and 20 Hz. The cut-off was reasonably well captured by the simulations. Above 20 Hz sound levels varied a lot with weather, which makes it harder to assess the accuracy of the ground model.

All predicted SELC values are shown in Figure 4.2. There are large deviations compared to the summer cases. Without weather there was, as during summer, a bias towards underestimation. The SEL3 errors for all cases are plotted in 4.3. Accuracy decreased with frequency. We note that the unexplained damping of sound levels below 10 Hz is not present in the winter data.

The statistics in 4.4 look quite similar to the summer data, but RMS errors and biases are both larger. It is still clear though, that the tethersonde data improved predictions.

Temperature inversions were deeper in winter, hence weather type indicators are evaluated higher up: The temperature gradient $\tau = \Delta T/\Delta z$ is the change from 820 to 350 m altitude. The same applies for c_{eff} gradient. The wind indicator U is evaluated at 710 m altitude. Weather type indicators are plotted in Figures 4.5-4.6. For classification of weather types we simply divide into upward and downward refraction according to the sign of the c_{eff} gradient. SELC errors are plotted against the c_{eff} gradient in Figure 4.7. The RMS errors did not vary much between these two weather classes, except that they were large for the simple PE model during downward refraction.

It is clear that the winter data are very challenging to model. This is, at least partly, due to the snow cover. It may be that the strong ground damping made scattering effects more prominent. Other possible explanations are that the postprocessing had been applied to the summer tethersonde data and not the winter data, and that therefore there are more spurious features in the winter sound speed profiles. Also, it may be that the weather conditions happened to be more challenging during the winter trials. There was a larger proportion of long ranges in the winter data, which explains some, but not all of the increased difficulty.

4.1 Parameter studies

A few variations of the simulation setup was attempted for the winter trials.

4.1.1 Ground impedance

Two ground impedance strategies are compared in Figure A.12. Different snow depths are supplied to the hard-backed Zwikker-Kosten model. Other parameters remain constant. The 35 cm choice yields too large sound levels for the lower frequencies, but otherwise the results are practically identical.

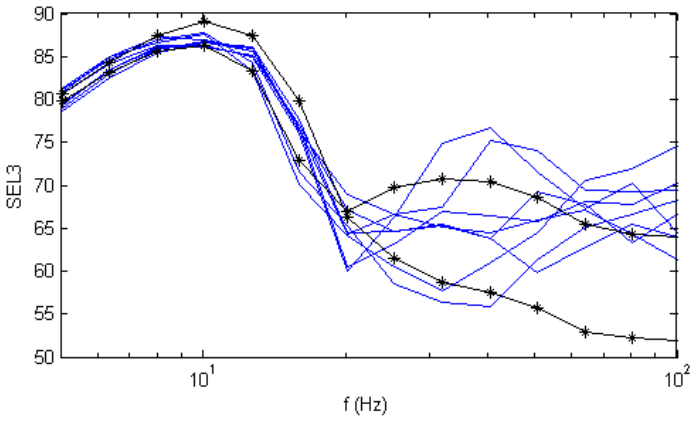

Figure 4.1 *Range 2 km at tower 306. 1 kg charges. Microphone heights vary. Blue lines are measurements and black lines are simple PE simulations.*

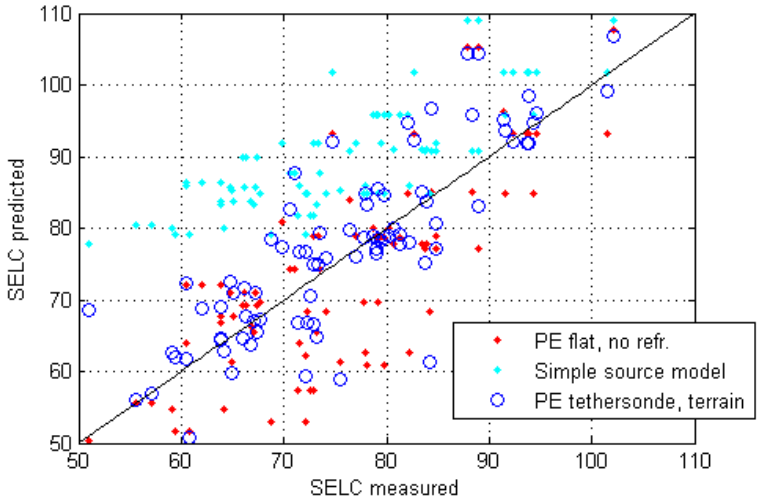

Figure 4.2 *All cases.*

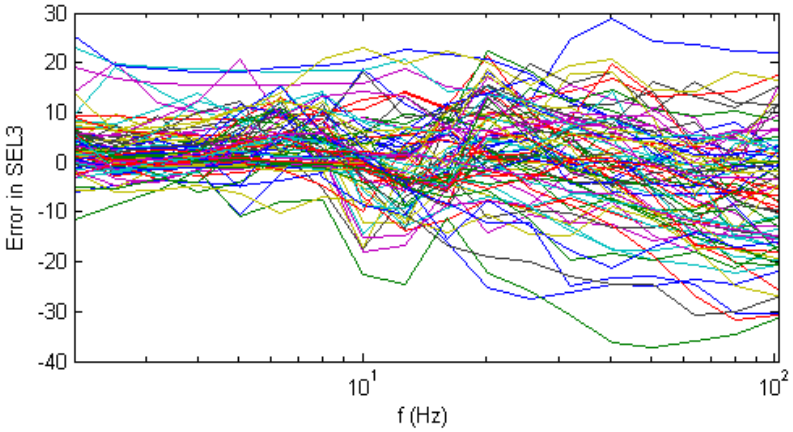

Figure 4.3 *Errors in SEL3 for all winter cases at tower 306.*

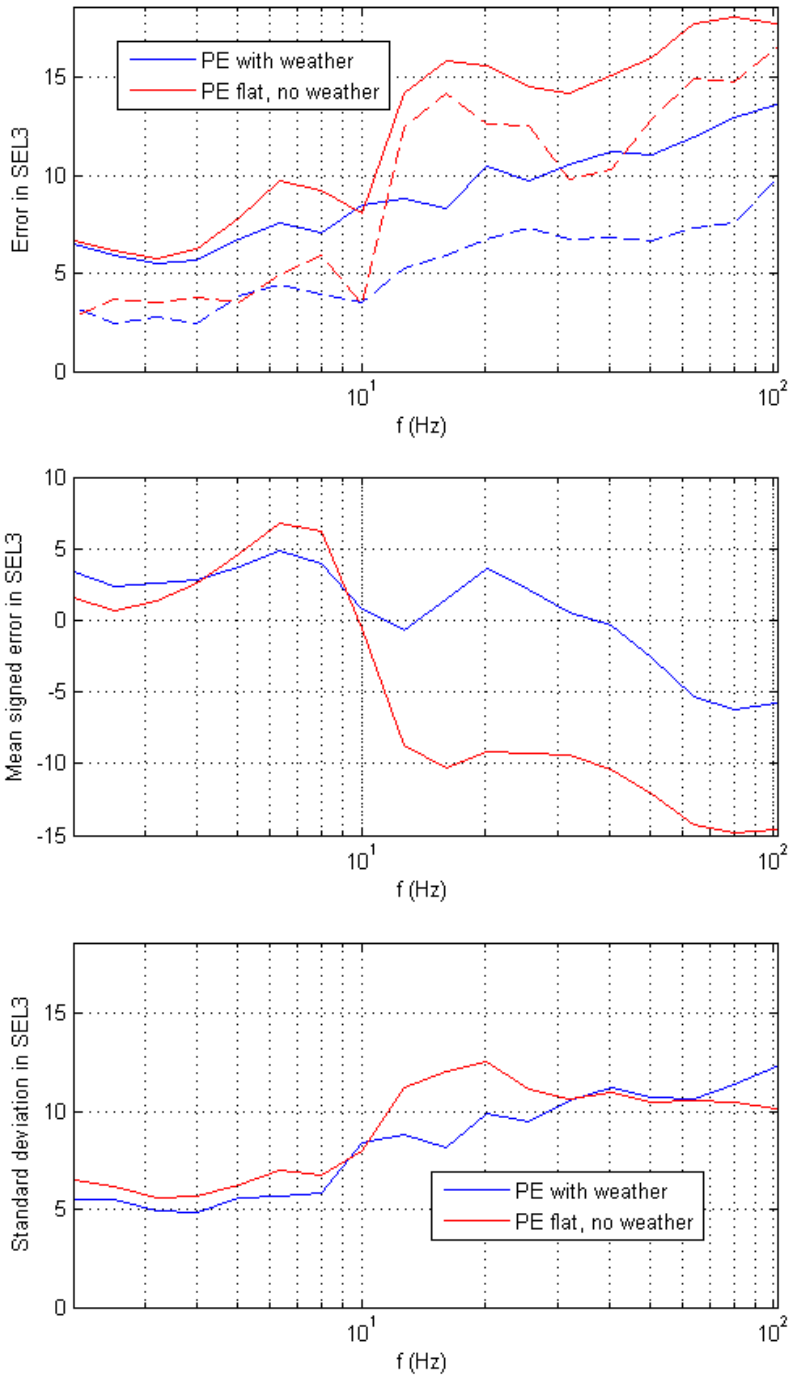

Figure 4.4 *Mean quantities for the winter A cases from tower 306. Dashed lines are median errors, solid lines are RMS errors.*

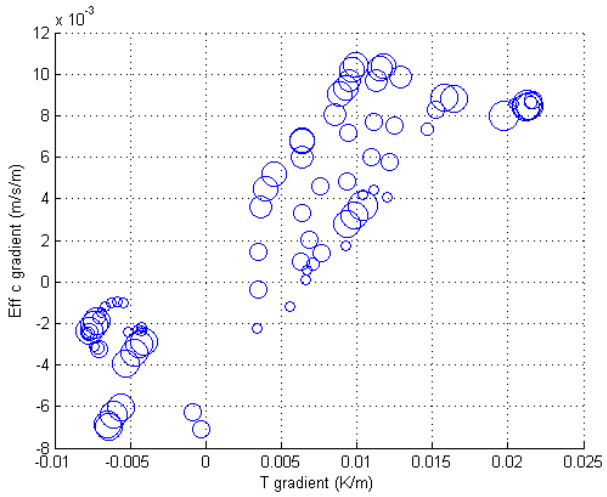

Figure 4.5 *Sound speed gradient vs. temperature gradient. Winter. Circle size is proportional to range.*

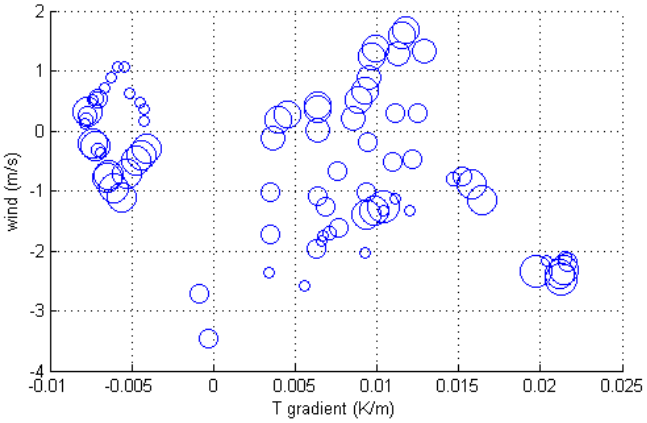

Figure 4.6 *Wind vs. temperature gradient. Winter. Circle size is proportional to range.*

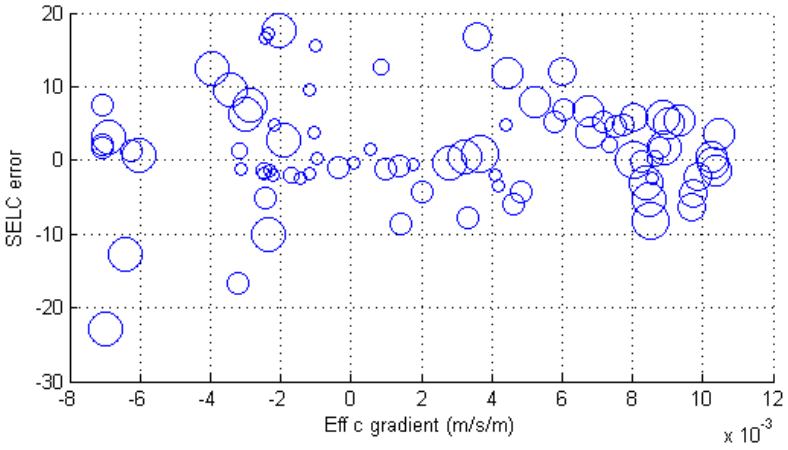

Figure 4.7 *SELC error vs. effective sound speed gradient. Winter. Circle size is proportional to range.*

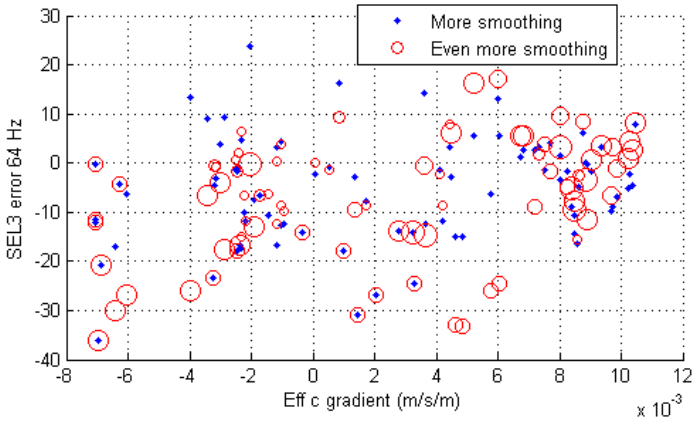

Figure 4.8 *SEL3 at 64 Hz*

4.1.2 Surface layer

The simple 'lin10' model seems to outperform the logarithmic SL wind profile, see Figure A.13 in the Appendix.

4.1.3 Vertical regularisation

We tried out doubling the vertical smoothing lengths. Resulting SEL3 values at 64 Hz are shown in Figure 4.8. The data are plotted against effective sound speed gradient. It seems that more smoothing might be beneficial near neutral conditions, i.e. when the sound speed gradient is small. For downward refraction, too much smoothing reduces precision. We remark that the logarithmic surface layer tapering of wind was used for all simulations shown in 4.8. The plots of the sound speed in appendix A.2 suggest that the unprocessed temperature data could be less reliable than unprocessed summer data. Hence we tried an experiment with a 300 m smoothing window in both temperature and wind speed. Results were markedly different, but none consistently better than the other.

4.2 Data from towers 212 and 412

The remaining cases of quality A were from towers 212 and 412. As mentioned, the charge sizes had to be retrieved from tower 306 data entries, hence we regard these data with enough suspicion to treat them separately. SELC values are shown in Figure 4.9. There were 59 long distance cases with range exceeding 10 km, and the remaining 15 were at 4 km or less. The third octave scatter plots can be seen in Figures A.14-A.15.

We note that four of the downward refraction cases are badly underestimated. These were at ranges 22-23 km from around the same time. At this range one should expect that the tethersonde data are insufficient, because there may be important downward refracting conditions higher up in

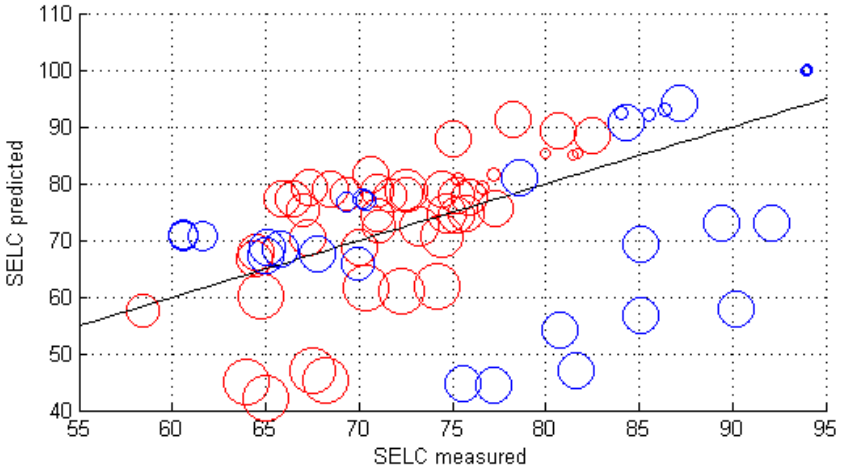

Figure 4.9 *SELC values at 212 and 412. Red: downward refraction, blue: upward.*

the atmosphere, and also because the horizontal homogeneity assumption is less likely to be valid. There are nine upward refracting cases that are badly underestimated. These are all from the same 14 km path (108->412) and around the same time, indicating that there is a weather feature that is not captured properly. We note also a tendency towards overestimation of the stronger signals. We believe this is due to ground interaction, because of deeper, or a different type of, snow around these receiver locations. Indeed, we observe that the cut-off frequency is lower at tower 412 than at 306, when examining the spectra for the close range cases.

5 Summary

We make the following conclusions from this validation study:

1. The PE model worked as well as can be expected given the parametric uncertainties.
2. Taking the weather into account is clearly necessary in noise mapping of heavy weapons and explosions.
3. The tethersonde weather data improved predictions.
4. Model performance in summer was good during downward refracting conditions, and less so during upward refraction. Difficulty with upward refraction is commonly observed in outdoor acoustics, and believed to be due to scattering from turbulence.
5. The PE model with tethersonde data gave on average very good predictions, in the sense that there was little modelling bias. There was one exception: At long range during upward refraction, we observed strong underestimation. During downward refraction, there was on average a few dB overestimation.
6. Ground interaction in winter was very strong and difficult to model.
7. Winter data were not as accurately predicted as summer data, at least partly due to the ground interaction. Tethersonde data were still helpful.
8. The importance of weather increased with frequency and range.
9. Louder sounds were more accurately predicted than softer sounds. This has to do with both range and refractive conditions.
10. The ground impedance data for summer conditions seemed to be fairly accurate.
11. Infrasound prediction required weather data from 2-4 km range. At closer range other effects were equally or more important.
12. The level of detail to take into account from localised weather profiles needs to strike a balance between capturing essential features and avoiding small scale fluctuations.
13. Surface layer modelling influenced the simulation results. Simple SL models were better than using instantaneous profiles from weather towers.

Generalisation of these conclusions may be limited to the weather types tested; in particular, strong winds did not occur during the experiments. Also, it should be noted that actual training activity often takes place in somewhat more rugged terrain than at Finnskogen.

The main goal, to validate the PE model, has been addressed, and we have obtained additional valuable insights. Even so, this study leaves many questions unanswered that could be addressed by further investigation:

1. Could more simple weather profiles be useful? It would be interesting, from a practical viewpoint, to look at sound speed profiles based on reduced data, perhaps even purely based on ground measurements.
2. How important is turbulent scattering? It is likely to be important due to the underestimated long range upwind cases, although this could also occur due to the large scale sound speed profiles being incorrect. A correlation study of closely timed detonations would clarify this.
3. What is the best way of modelling these scattering effects? This is an on-going research field in outdoor acoustics. Current methods are computationally expensive, and have limited

applicability to complicated long-range scenarios. Hence, this is a rather challenging question. Perhaps some empirically based statistical strategy should be sought, such as in [9].

4. How can the surface layer best be handled? This question is closely connected to the previous one.
5. Can the ground impedance values be improved? For summer, this might be possible from looking at short range cases.
6. How should ground impedance be computed over snow? This is certainly worth more attention, although it seems to be a very challenging topic.
7. Why are the winter data less accurately predicted than the summer data? Extreme, possibly inaccurate, impedance values in combination with scattering effects seem very likely reasons. It could also be related to the weather data, but that is difficult to judge without understanding the ground interaction.
8. The treatment of the nonlinear propagation near the source leaves a few dB of uncertainty. In practice, this may be hard to tease out from the uncertainty in ground impedance, and may be site specific. The shorter range NORTRIAL measurements from Haslemoen are more suited for this.
9. Vegetation and topographic roughness were not taken into account here, except perhaps indirectly via the impedance boundary. This is a tricky issue in itself, and especially when there are so many other unknown factors.
10. How good is the assumption of horizontal homogeneity of atmospheric conditions? At times at least, it is remarkably good, as shown in [4]. A more systematic study would be useful.
11. Comparison with other propagation models, such as ray-tracing, Fast Field Program and engineering standards may be interesting. These methods lack generality, but, when applicable, are more efficient than PE methods.

A Appendix

A.1 Scatter plots

Third octave sound exposure levels, SEL3, are presented here as scatter plots with measurements along the x-axis and predictions along the y-axis. The diagonal is drawn as a solid line, and the center frequency is indicated above each plot.

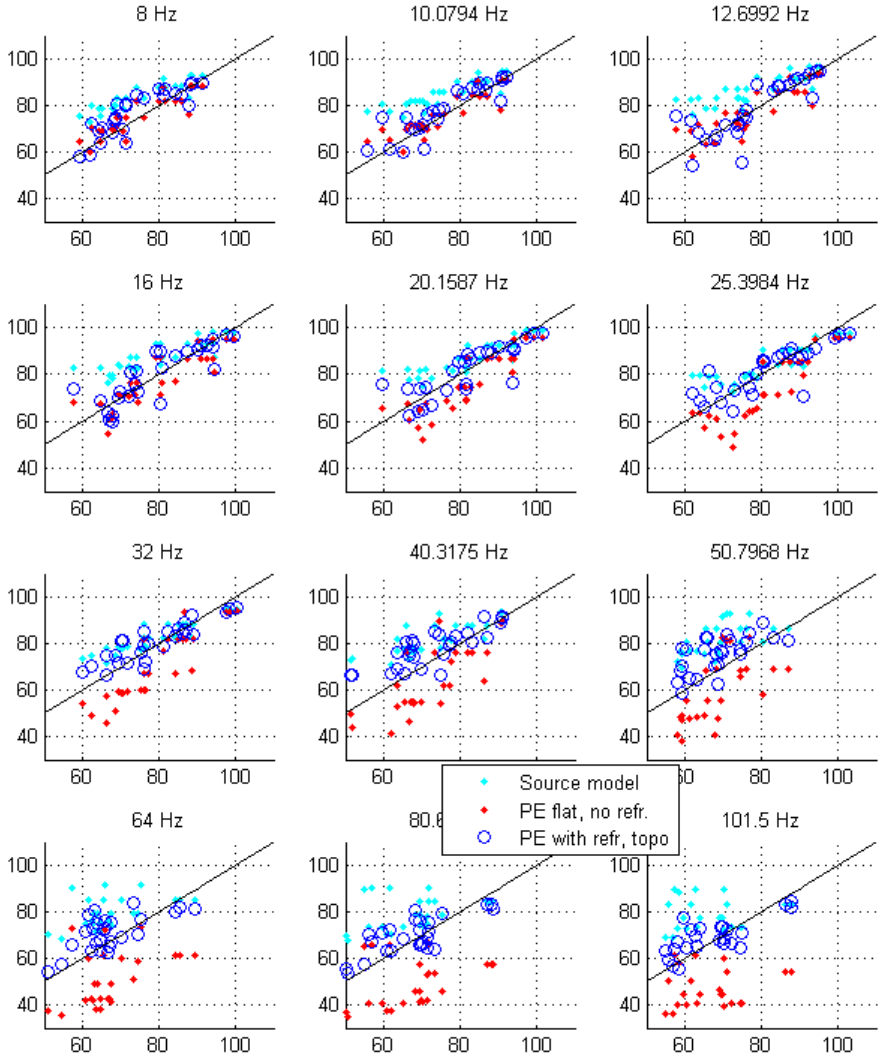

Figure A.1 *Predicted vs. measured 3rd octave SEL during temperature inversion, summer A data, 27 cases.*

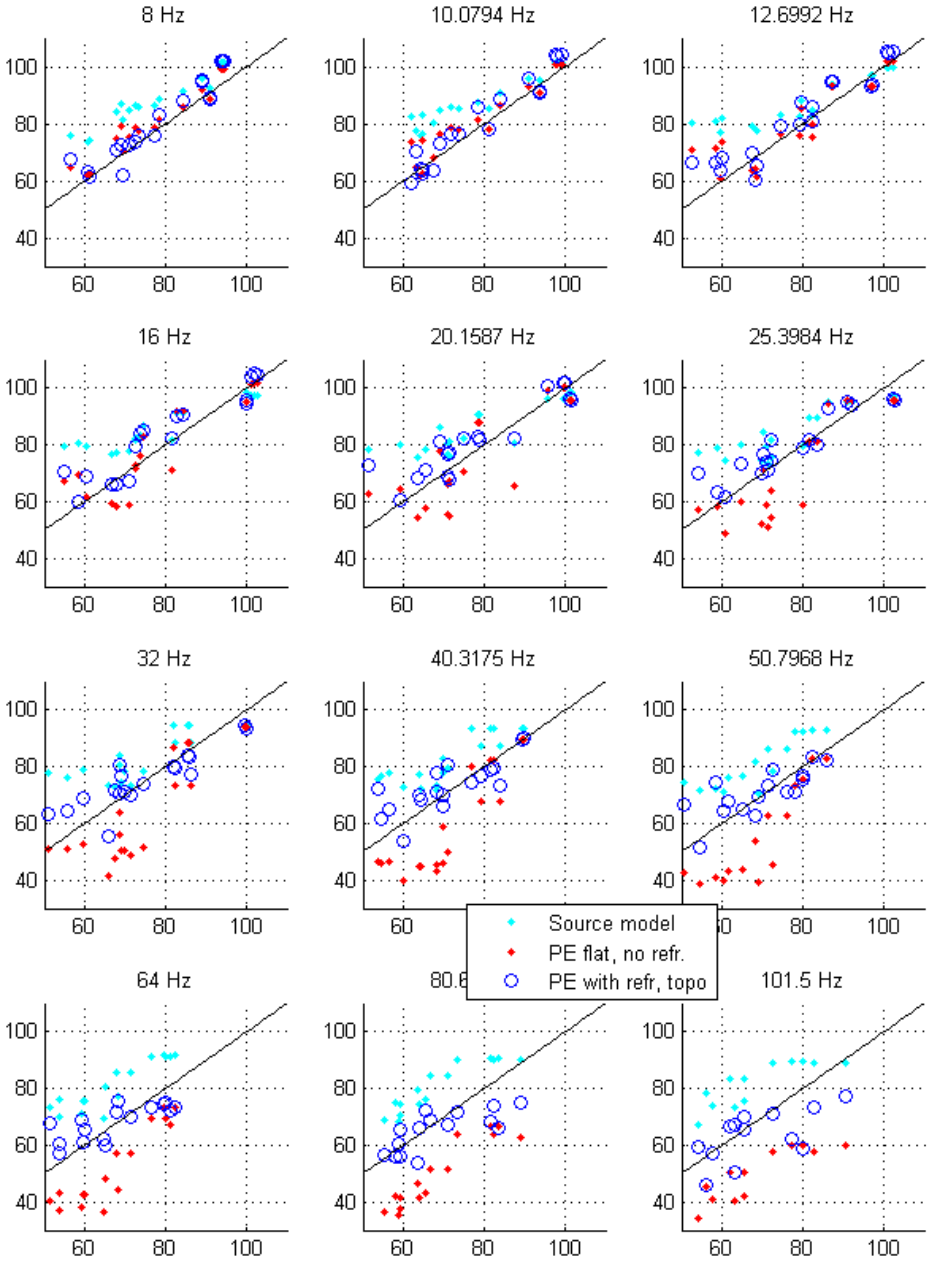

Figure A.2 *Predicted vs. measured 3rd octave SEL downwind, summer A, 19 cases.*

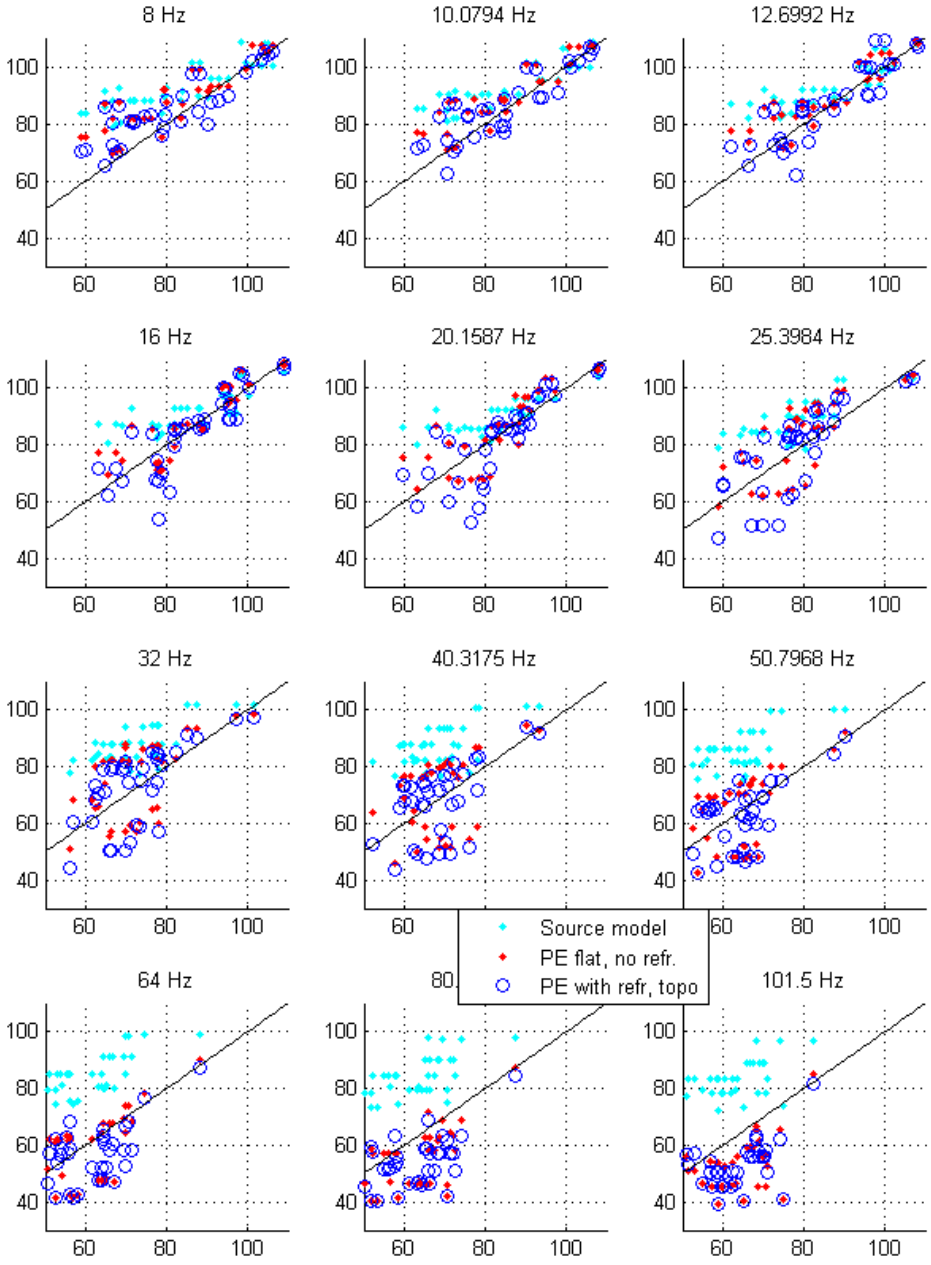

Figure A.3 *Predicted vs. measured 3rd octave SEL upwind or neutral, summer A, 34 cases.*

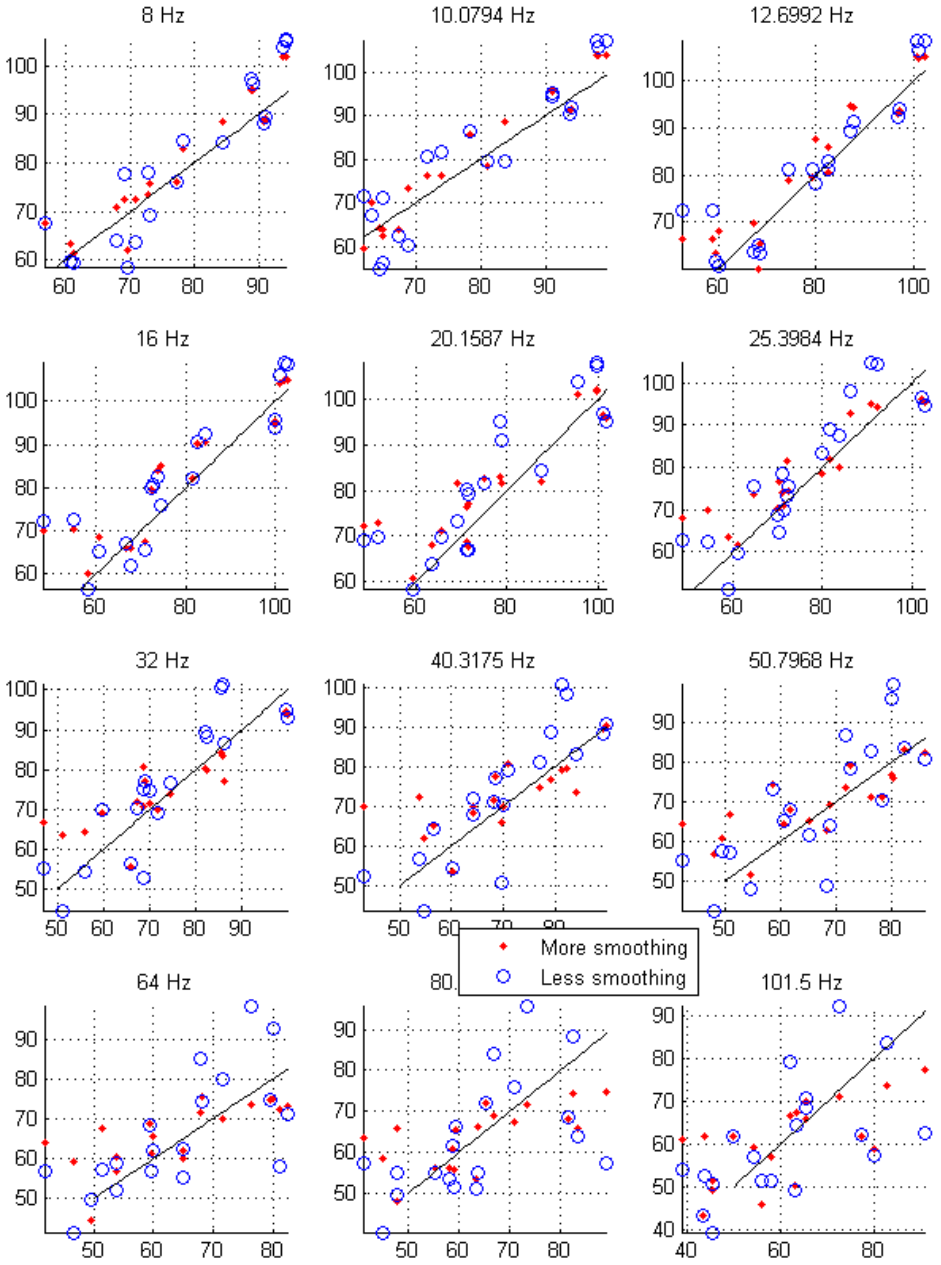

Figure A.4 *Smoothing study, summer A, temperature inversion.*

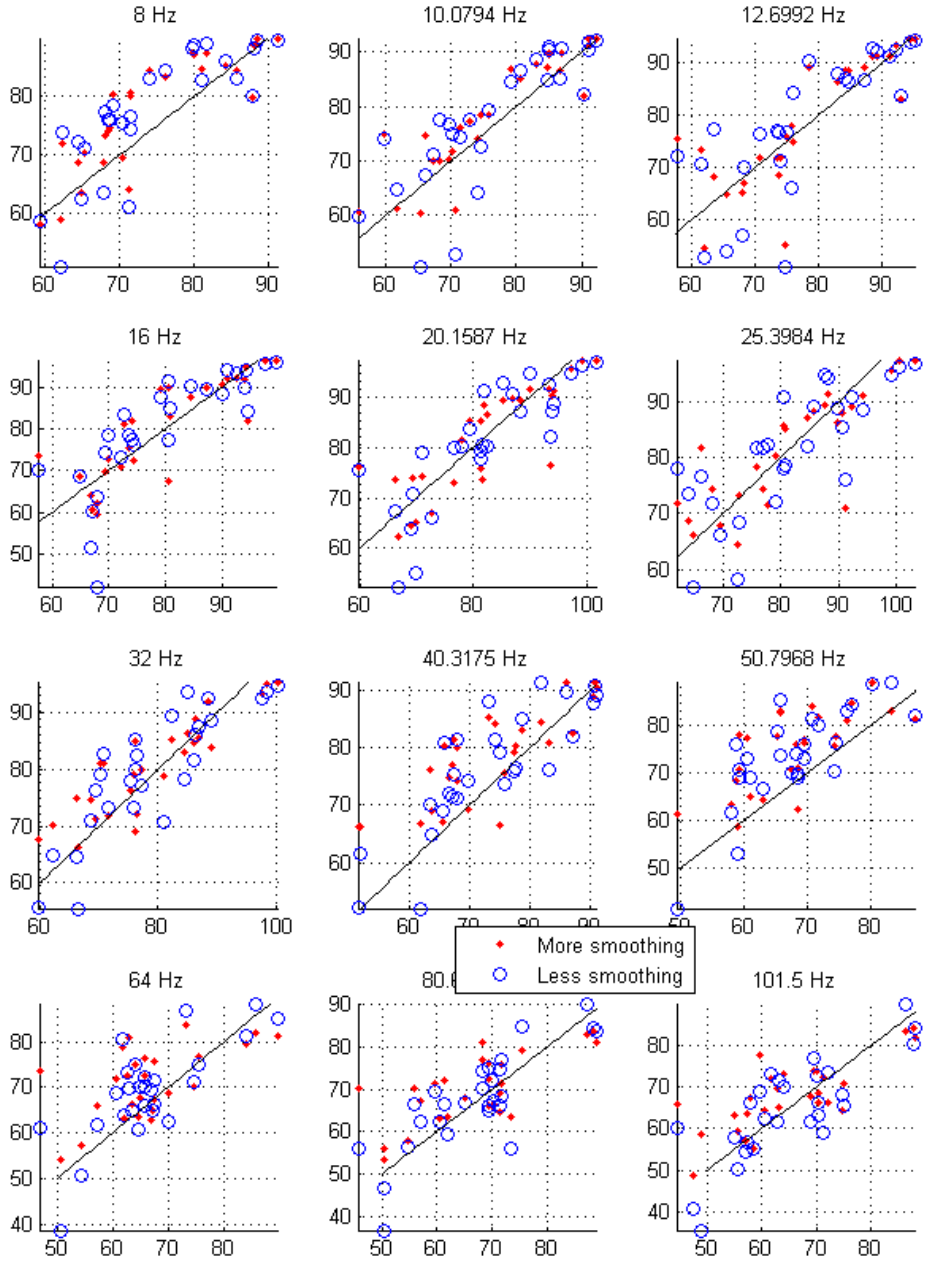

Figure A.5 *Smoothing study, summer A, downwind.*

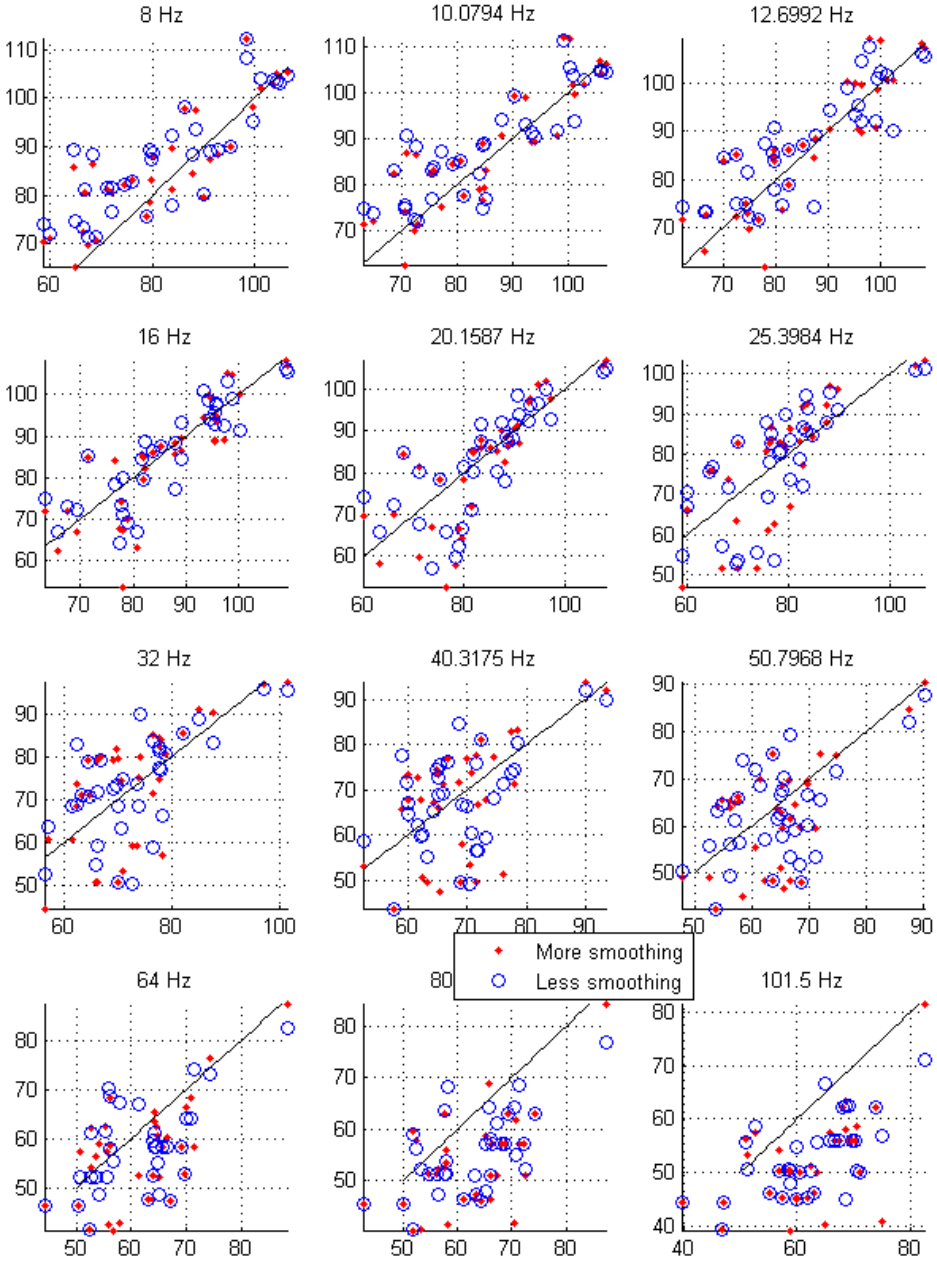

Figure A.6 *Smoothing study, summer A, upwind/neutral.*

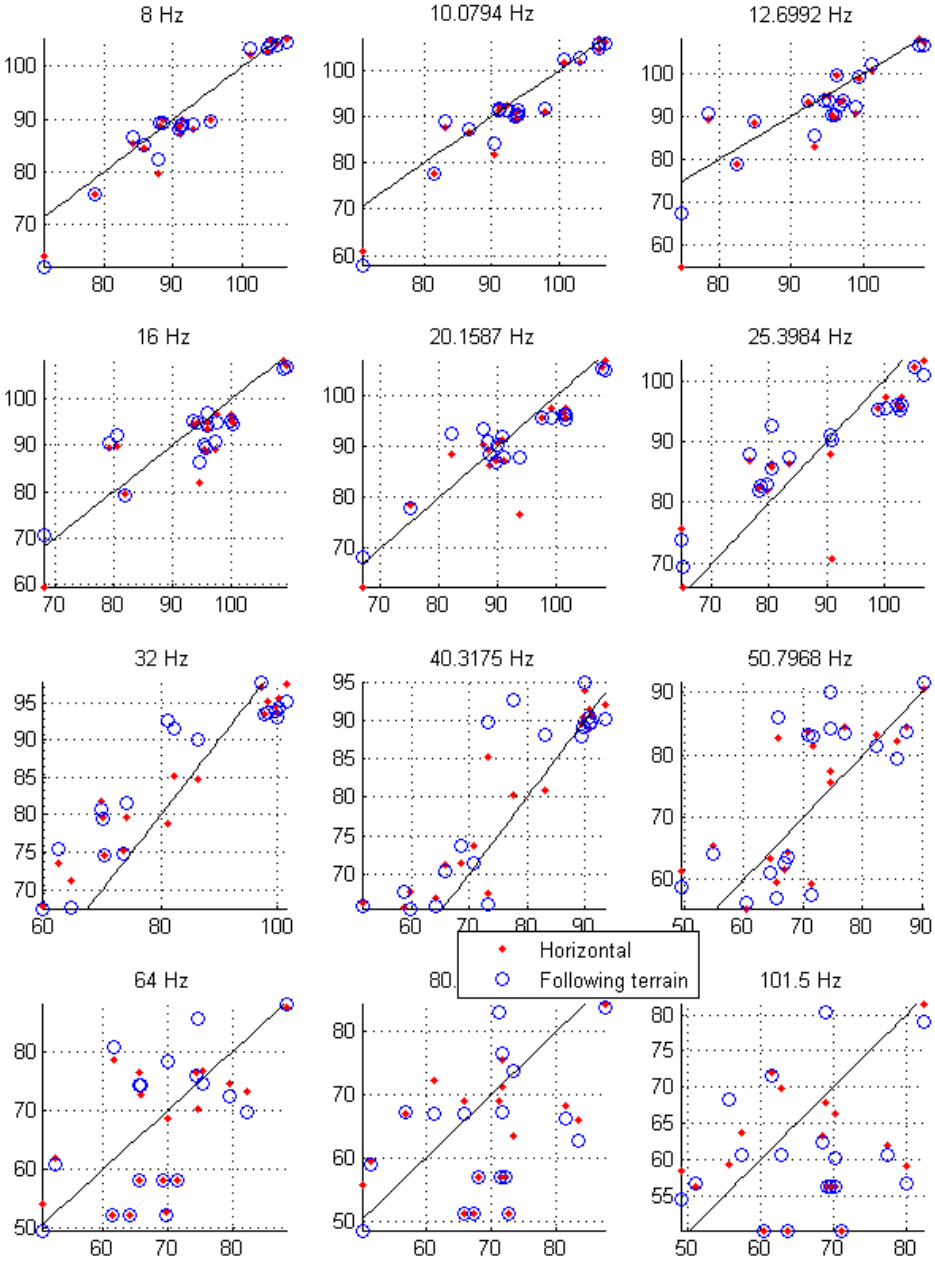

Figure A.7 *Terrain-following sonde data. Summer A, tower 112, 18 cases.*

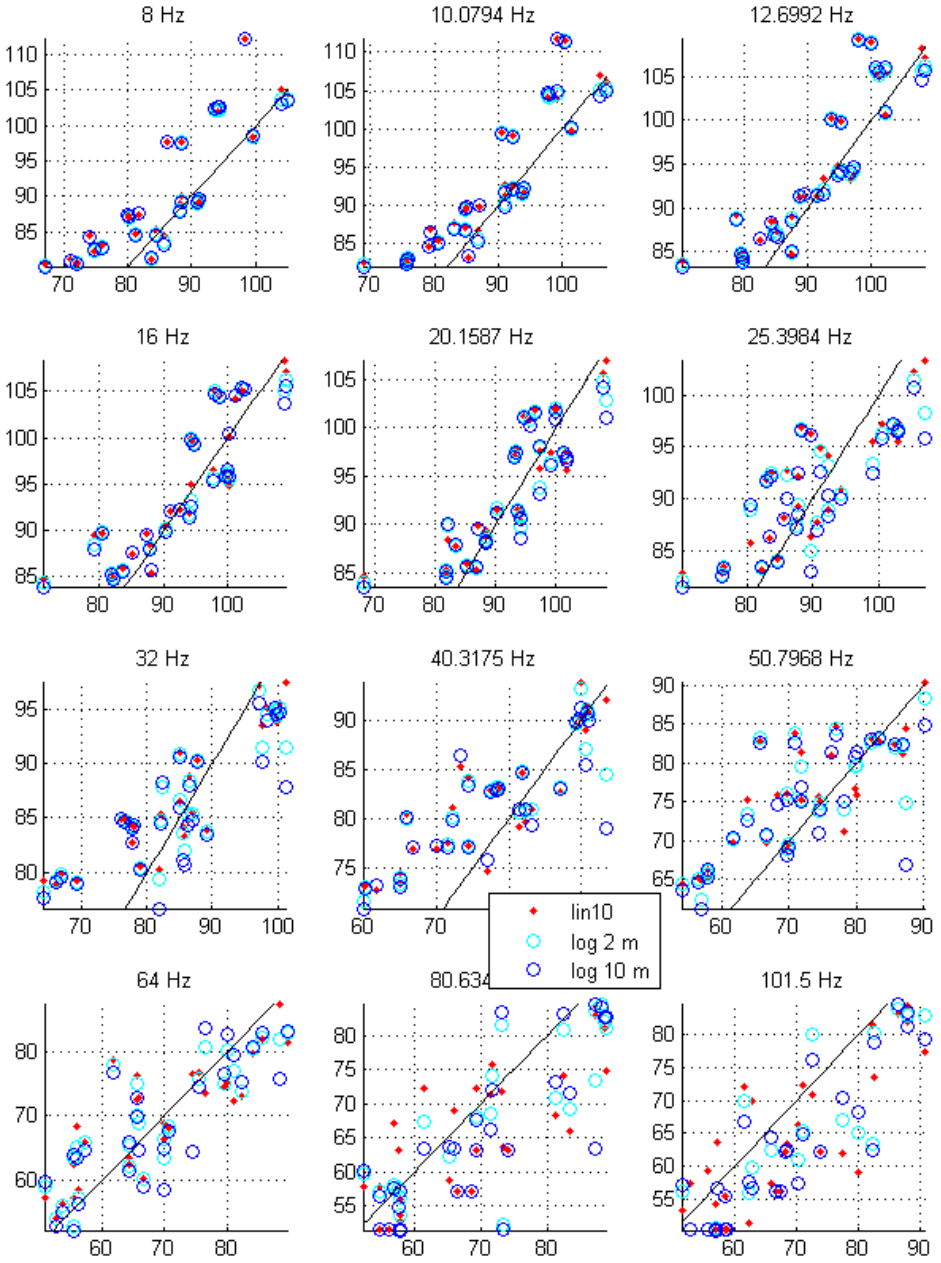

Figure A.8 *Logarithmic surface layer profiles. Summer A. Range less than 2.1 km, 29 cases.*

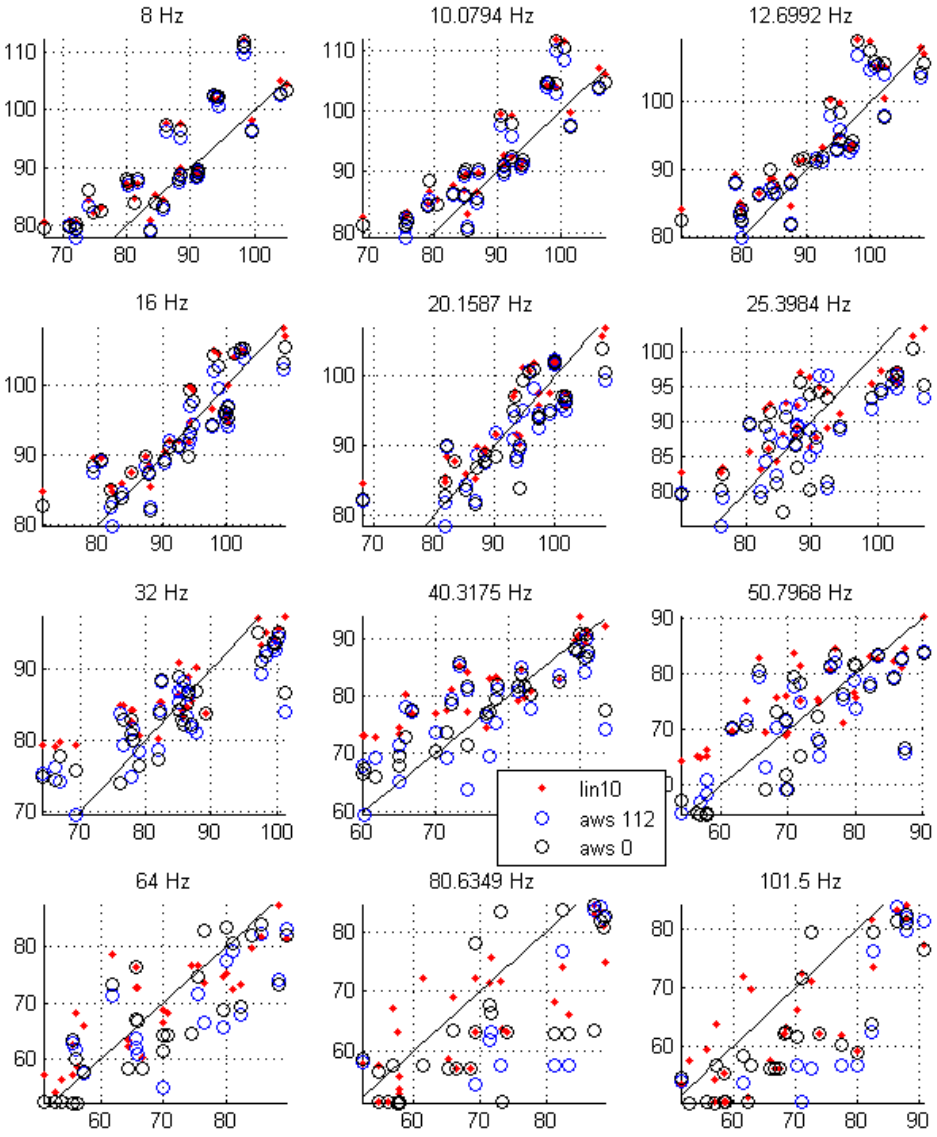

Figure A.9 *Weather tower data as SL models. Range less than 2.1 km, 29 cases.*

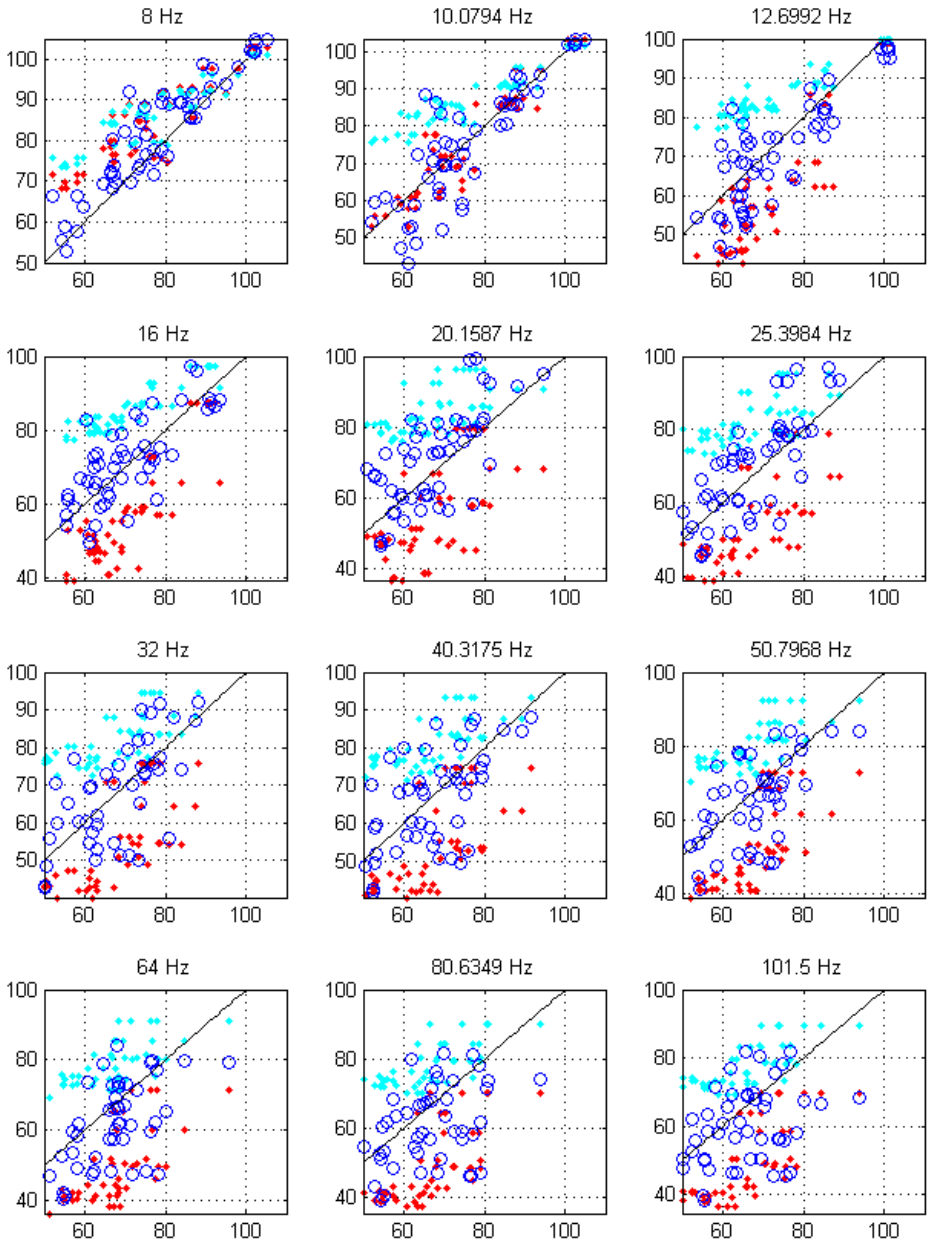

Figure A.10 *Downward refraction, winter A, tower 306, 49 cases*

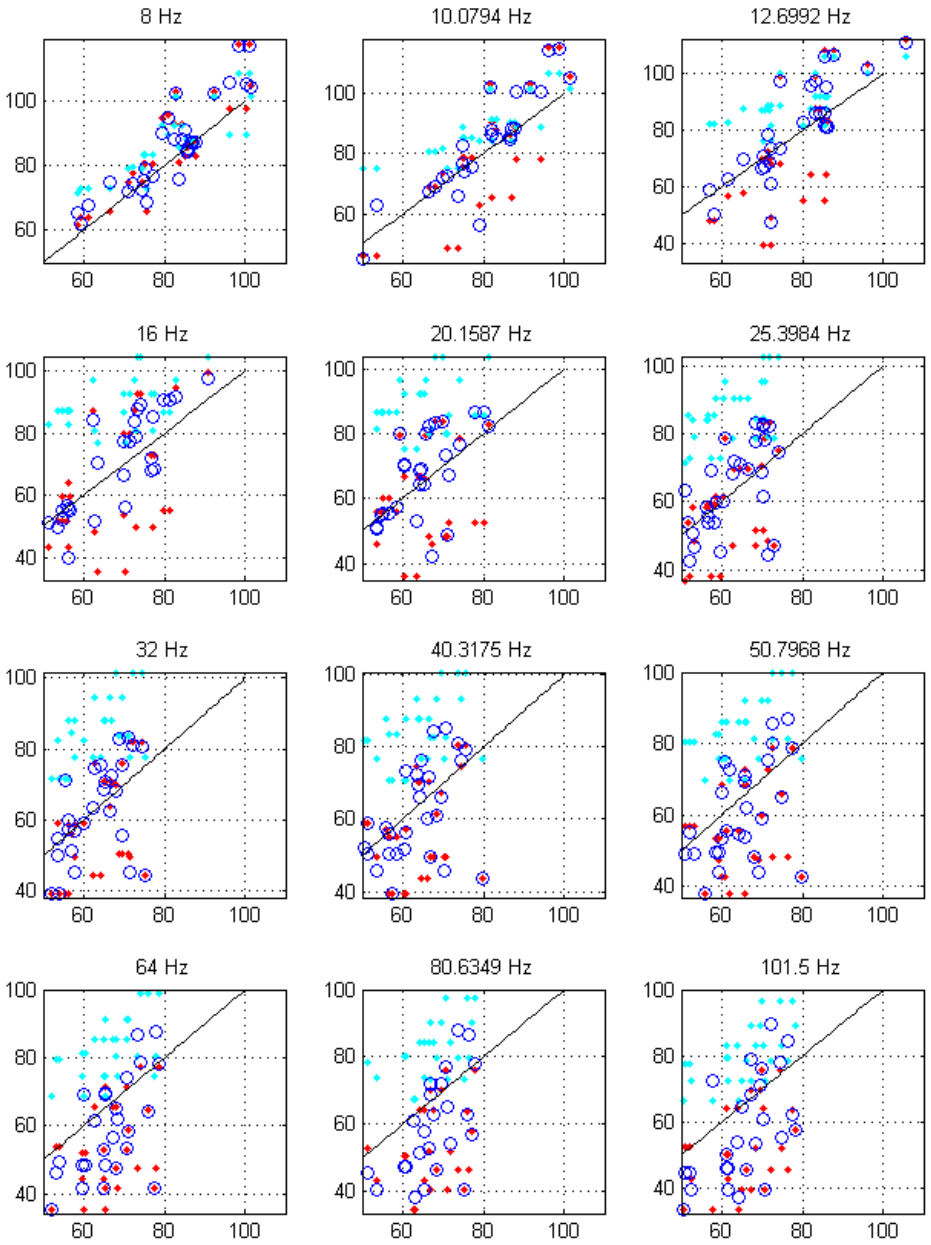

Figure A.11 *Upward refraction, winter A, tower 306, 34 cases*

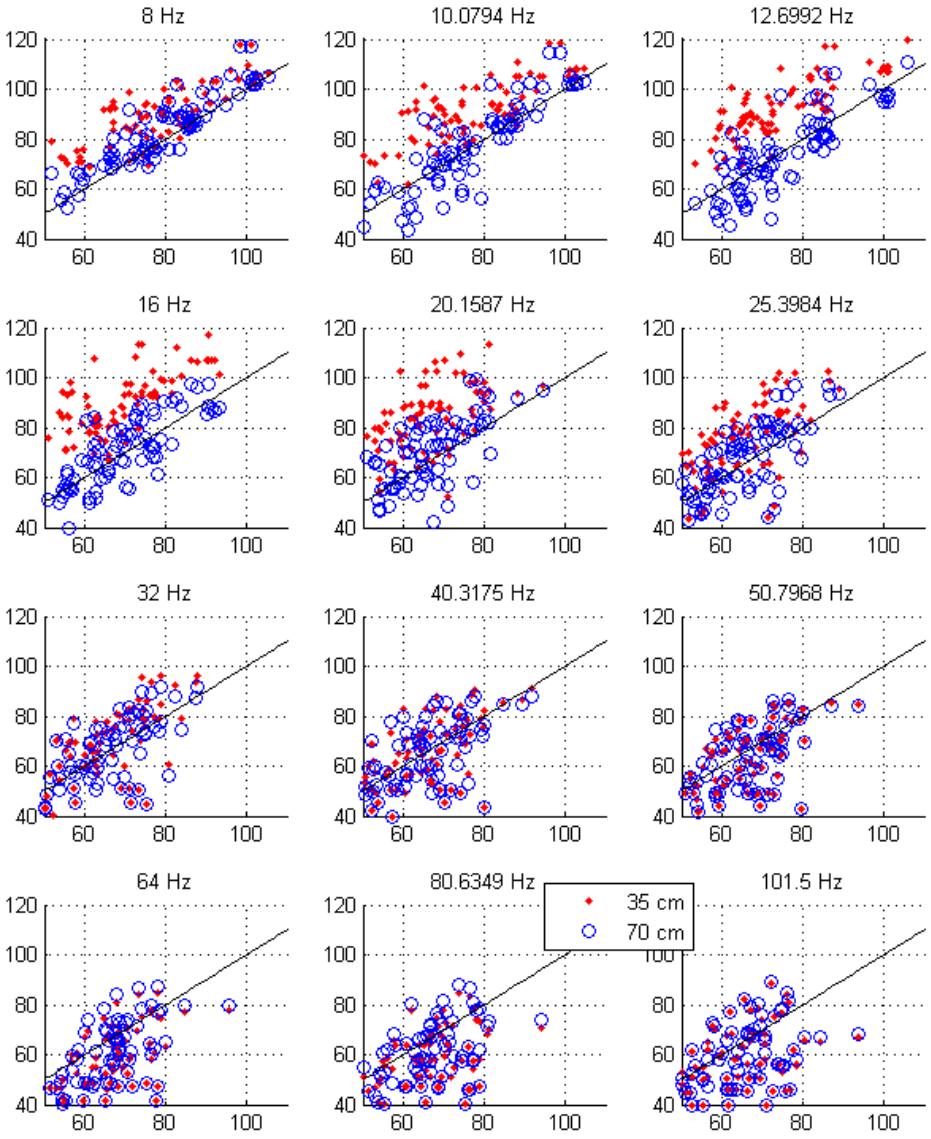

Figure A.12 *Winter A, tower 306, 83 cases. Snow depth in impedance model varied.*

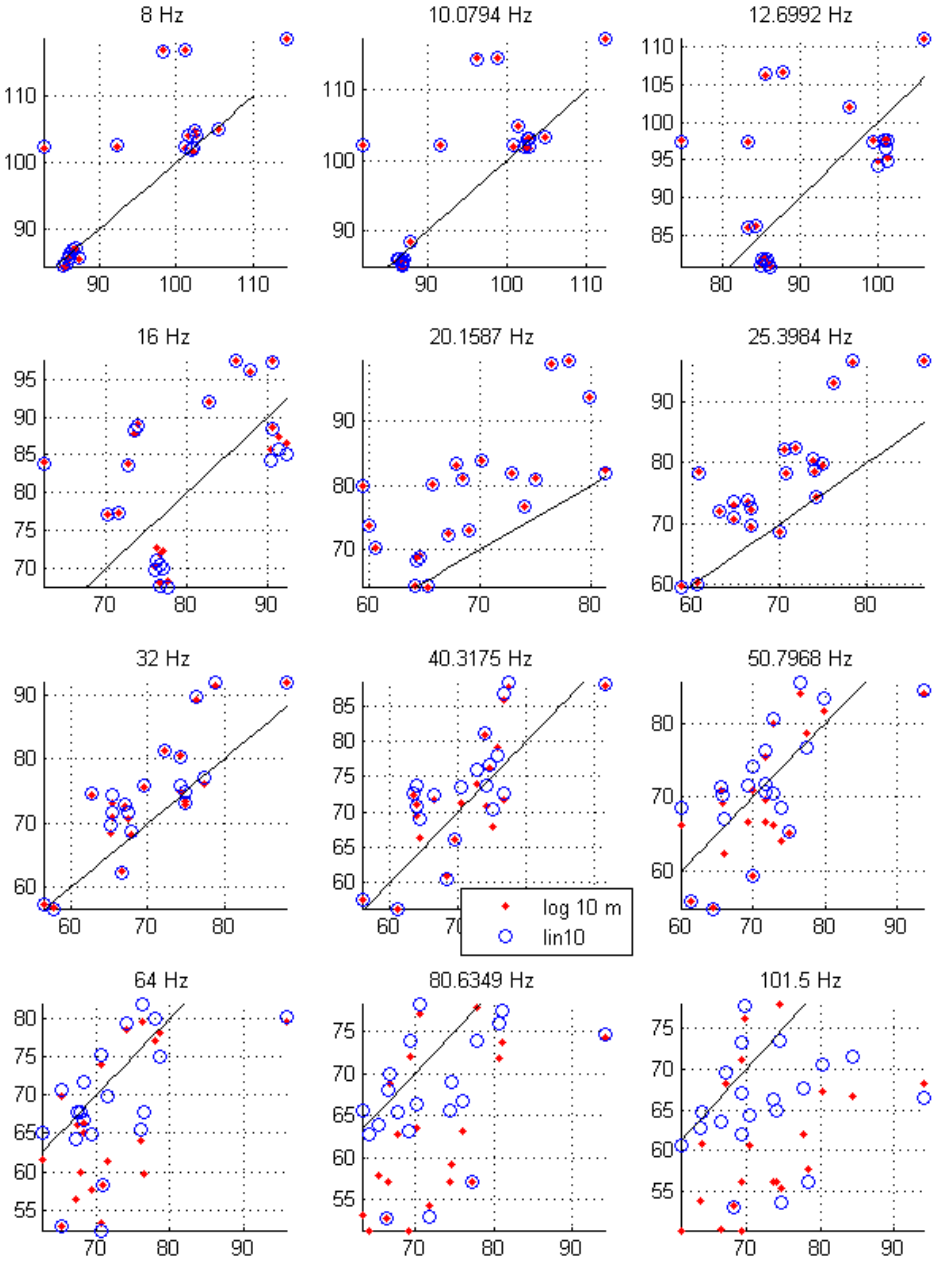

Figure A.13 *Winter A, tower 306, 2 km range, 20 cases. Surface layer models.*

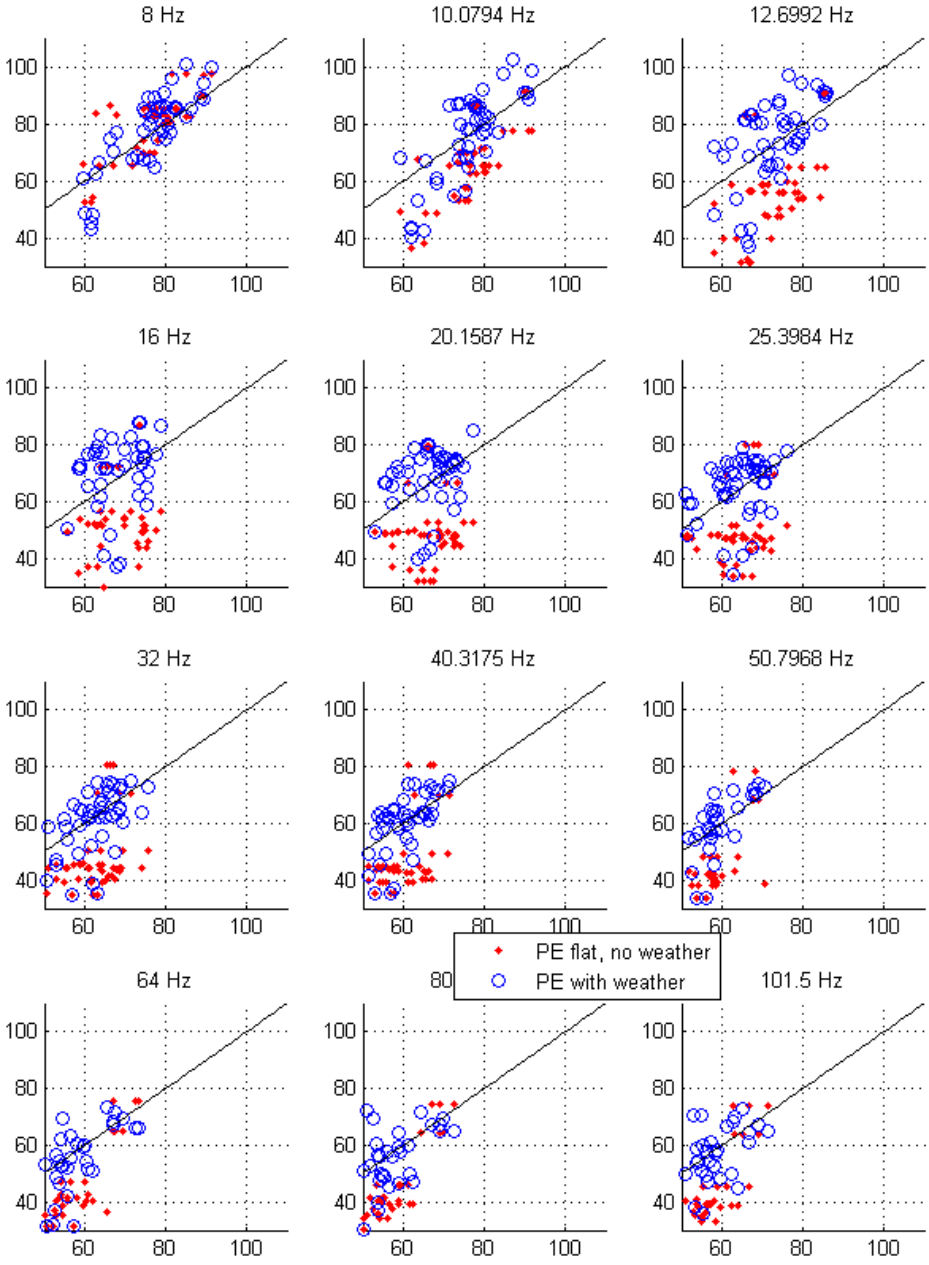

Figure A.14 *Winter A, towers 212 and 412. Downward refraction, 45 cases.*

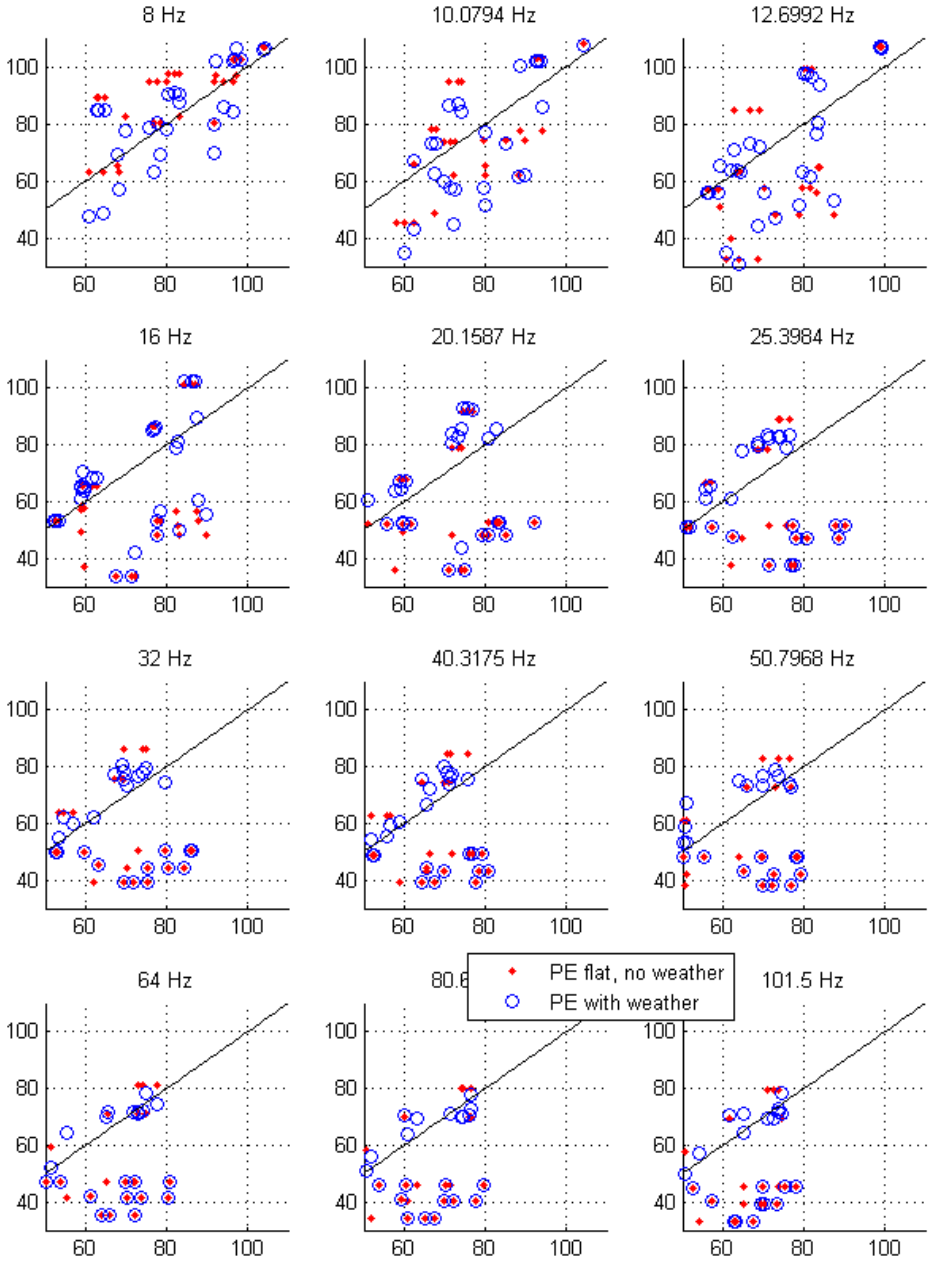

Figure A.15 *Winter A, towers 212 and 412. Upward refraction, 29 cases.*

A.2

For each plot the following information is listed: A case number assigned by us, the event number of the detonation, the source and receiver, locations, the charge size, the receiver heights, the date and time. Spectra across 4-100 Hz are plotted with a logarithmic *f*-axis. The red solid lines are measured spectra. Blue simulated, dashed black the simple PE results, and blue circles the source model. Horizontal black lines in the sound speed plots indicate the minimum of source and receiver elevation. The sound speed profiles used in m/s are plotted against altitude: effective sound speed in blue and thermal sound speed in red.

A.2.1 Summer A data

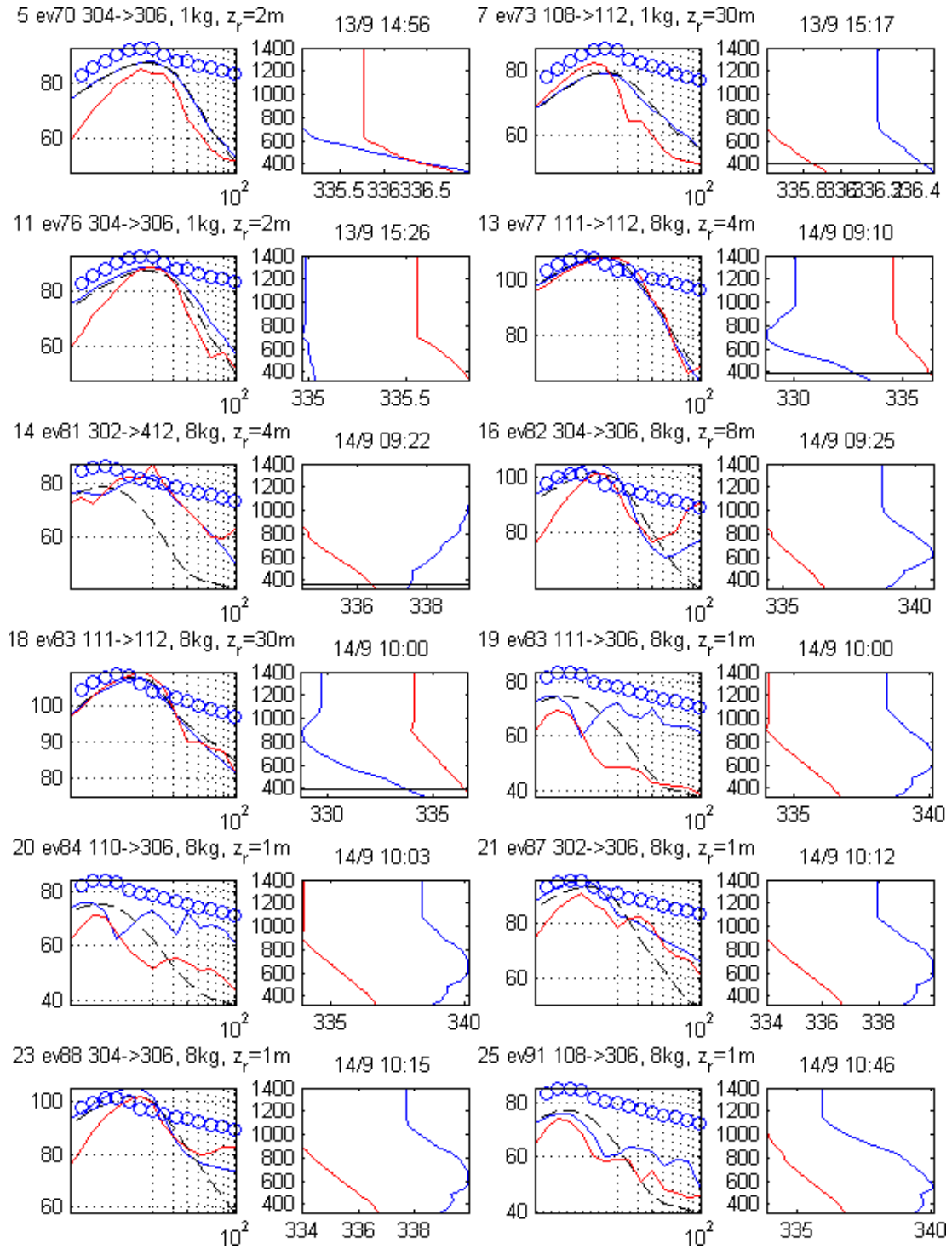

Figure A.16

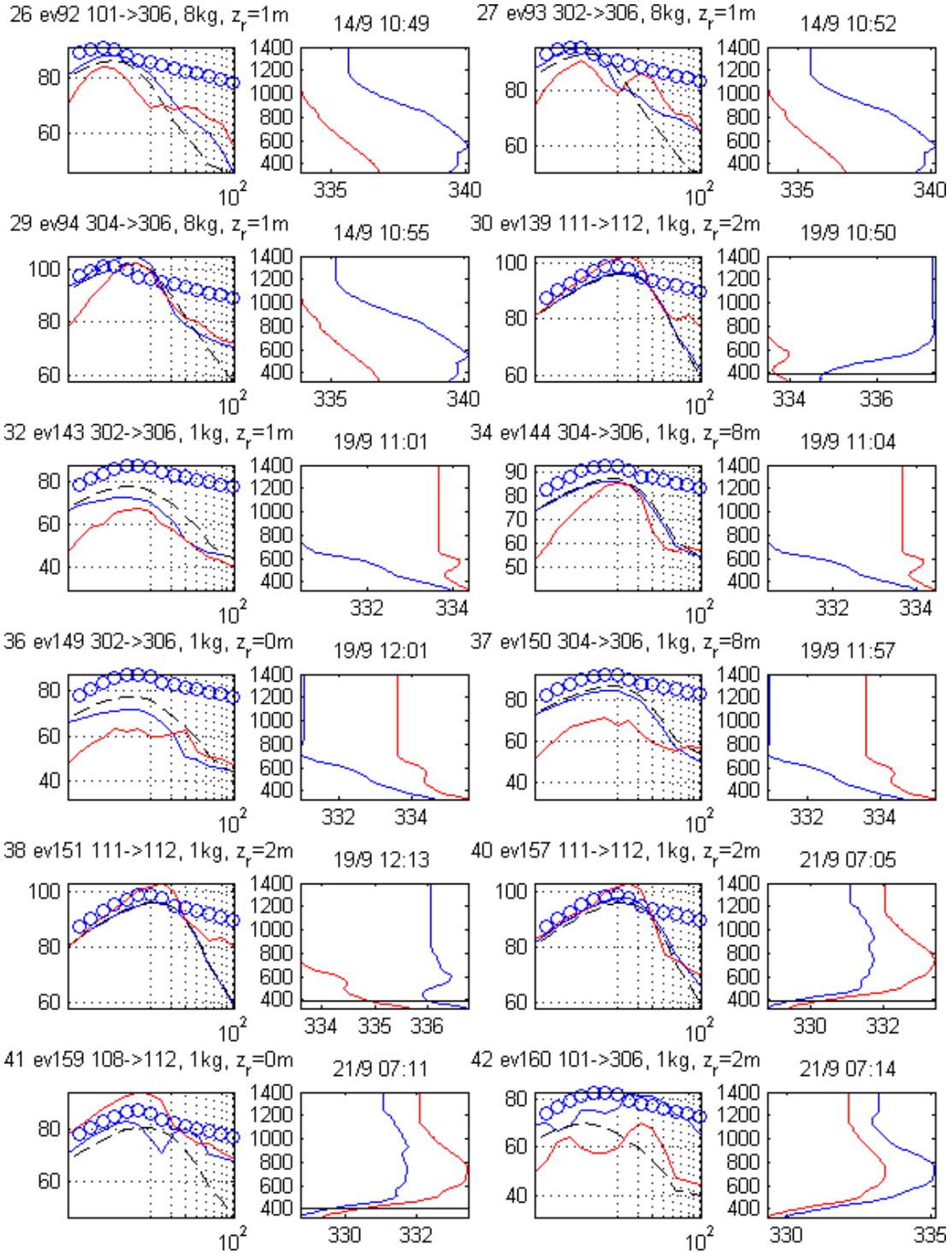
26 ev92 101->306, 8kg, z_r=1m
14/9 10:49
27 ev93 302->306, 8kg, z_r=1m
14/9 10:52
29 ev94 304->306, 8kg, z_r=1m
14/9 10:55
30 ev139 111->112, 1kg, z_r=2m
19/9 10:50
32 ev143 302->306, 1kg, z_r=1m
19/9 11:01
34 ev144 304->306, 1kg, z_r=8m
19/9 11:04
36 ev149 302->306, 1kg, z_r=0m
19/9 12:01
37 ev150 304->306, 1kg, z_r=8m
19/9 11:57
38 ev151 111->112, 1kg, z_r=2m
19/9 12:13
40 ev157 111->112, 1kg, z_r=2m
21/9 07:05
41 ev159 108->112, 1kg, z_r=0m
21/9 07:11
42 ev160 101->306, 1kg, z_r=2m
21/9 07:14
10^2

Figure A.17

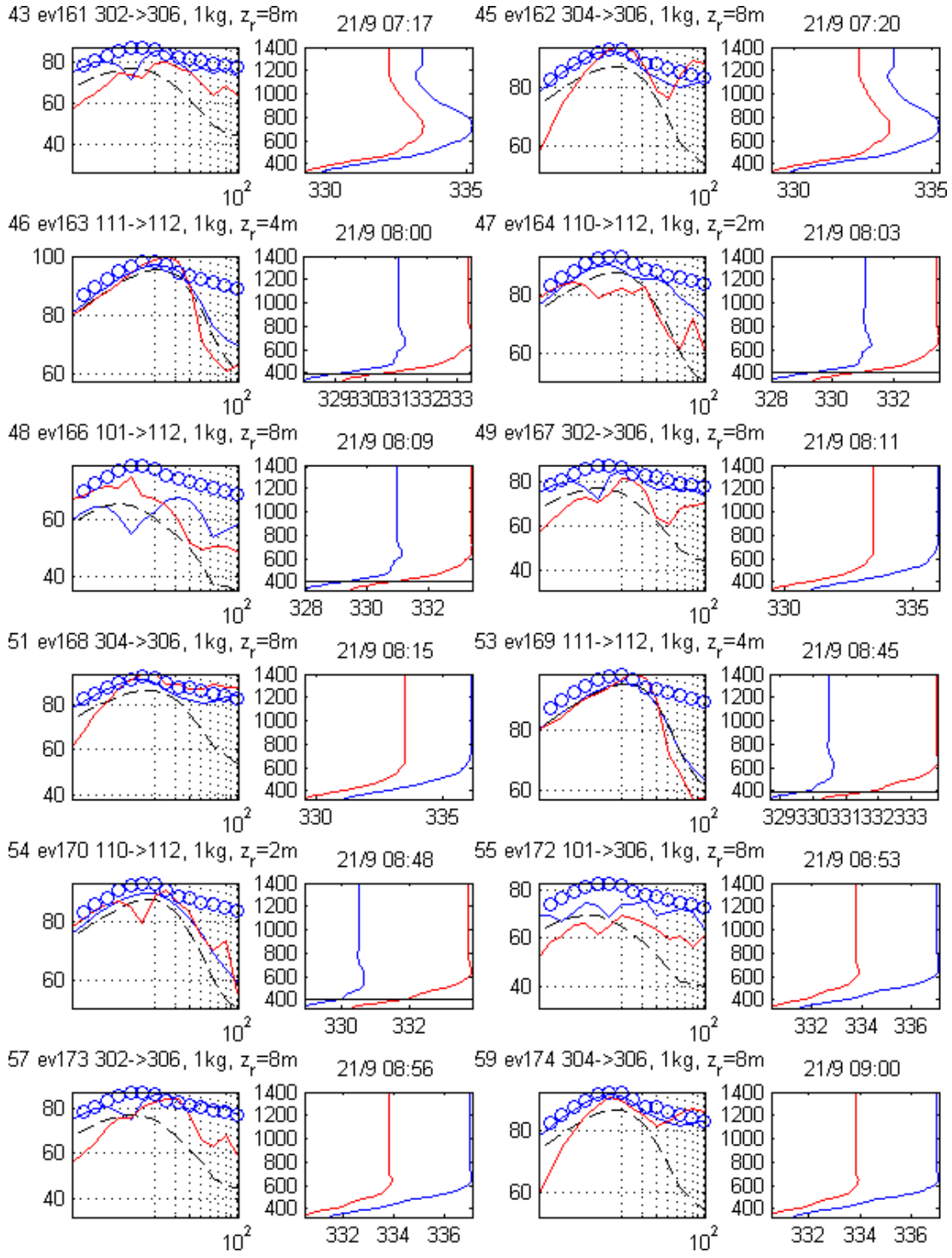
43 ev161 302->306, 1kg, z_r=8m
21/9 07:17
45 ev162 304->306, 1kg, z_r=8m
21/9 07:20
46 ev163 111->112, 1kg, z_r=4m
21/9 08:00
47 ev164 110->112, 1kg, z_r=2m
21/9 08:03
48 ev166 101->112, 1kg, z_r=8m
21/9 08:09
49 ev167 302->306, 1kg, z_r=8m
21/9 08:11
51 ev168 304->306, 1kg, z_r=8m
21/9 08:15
53 ev169 111->112, 1kg, z_r=4m
21/9 08:45
54 ev170 110->112, 1kg, z_r=2m
21/9 08:48
55 ev172 101->306, 1kg, z_r=8m
21/9 08:53
57 ev173 302->306, 1kg, z_r=8m
21/9 08:56
59 ev174 304->306, 1kg, z_r=8m
21/9 09:00

Figure A.18

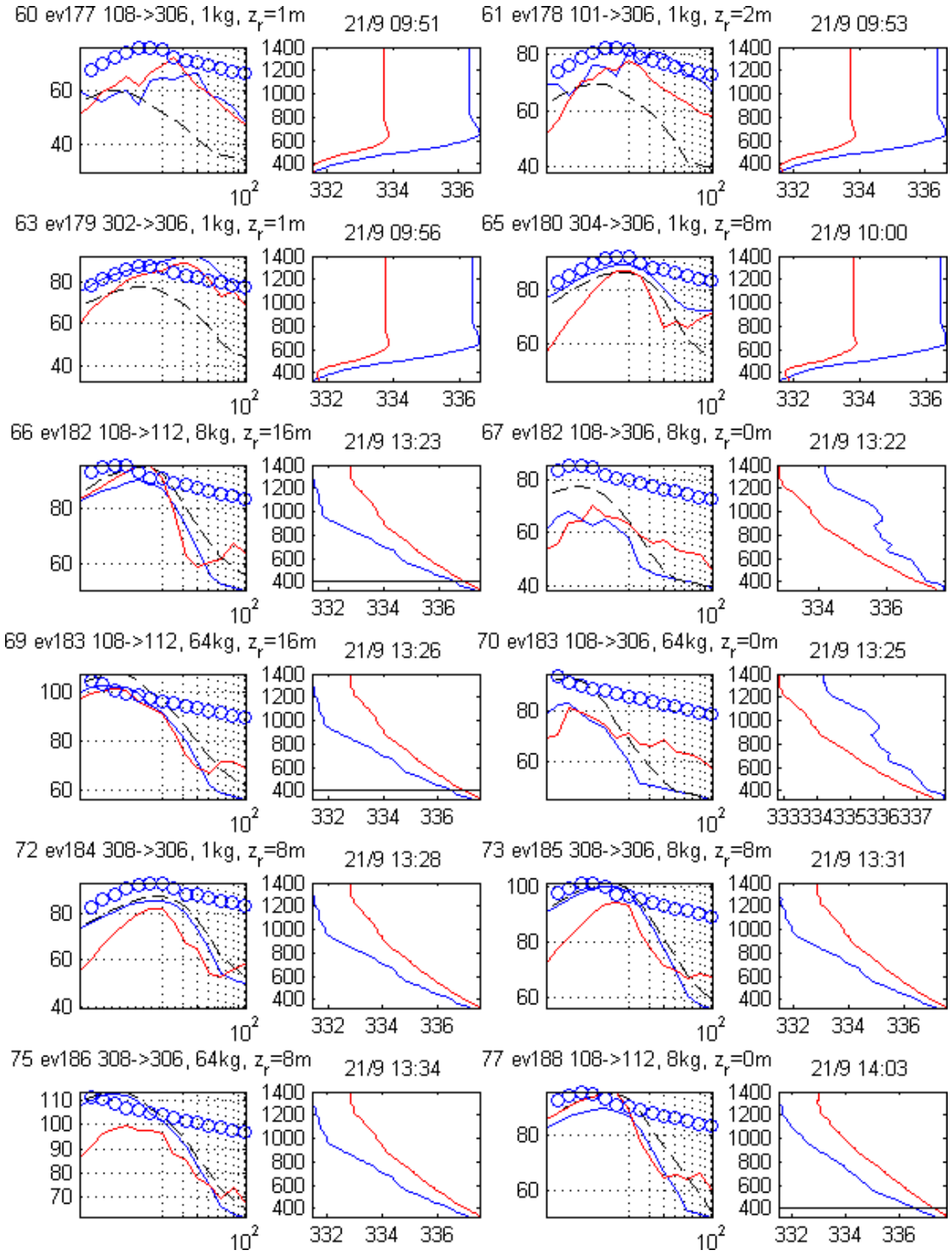
60 ev177 108->306, 1kg, z_r=1m
21/9 09:51
61 ev178 101->306, 1kg, z_r=2m
21/9 09:53
63 ev179 302->306, 1kg, z_r=1m
21/9 09:56
65 ev180 304->306, 1kg, z_r=8m
21/9 10:00
66 ev182 108->112, 8kg, z_r=16m
21/9 13:23
67 ev182 108->306, 8kg, z_r=0m
21/9 13:22
69 ev183 108->112, 64kg, z_r=16m
21/9 13:26
70 ev183 108->306, 64kg, z_r=0m
21/9 13:25
72 ev184 308->306, 1kg, z_r=8m
21/9 13:28
73 ev185 308->306, 8kg, z_r=8m
21/9 13:31
75 ev186 308->306, 64kg, z_r=8m
21/9 13:34
77 ev188 108->112, 8kg, z_r=0m
21/9 14:03

Figure A.19

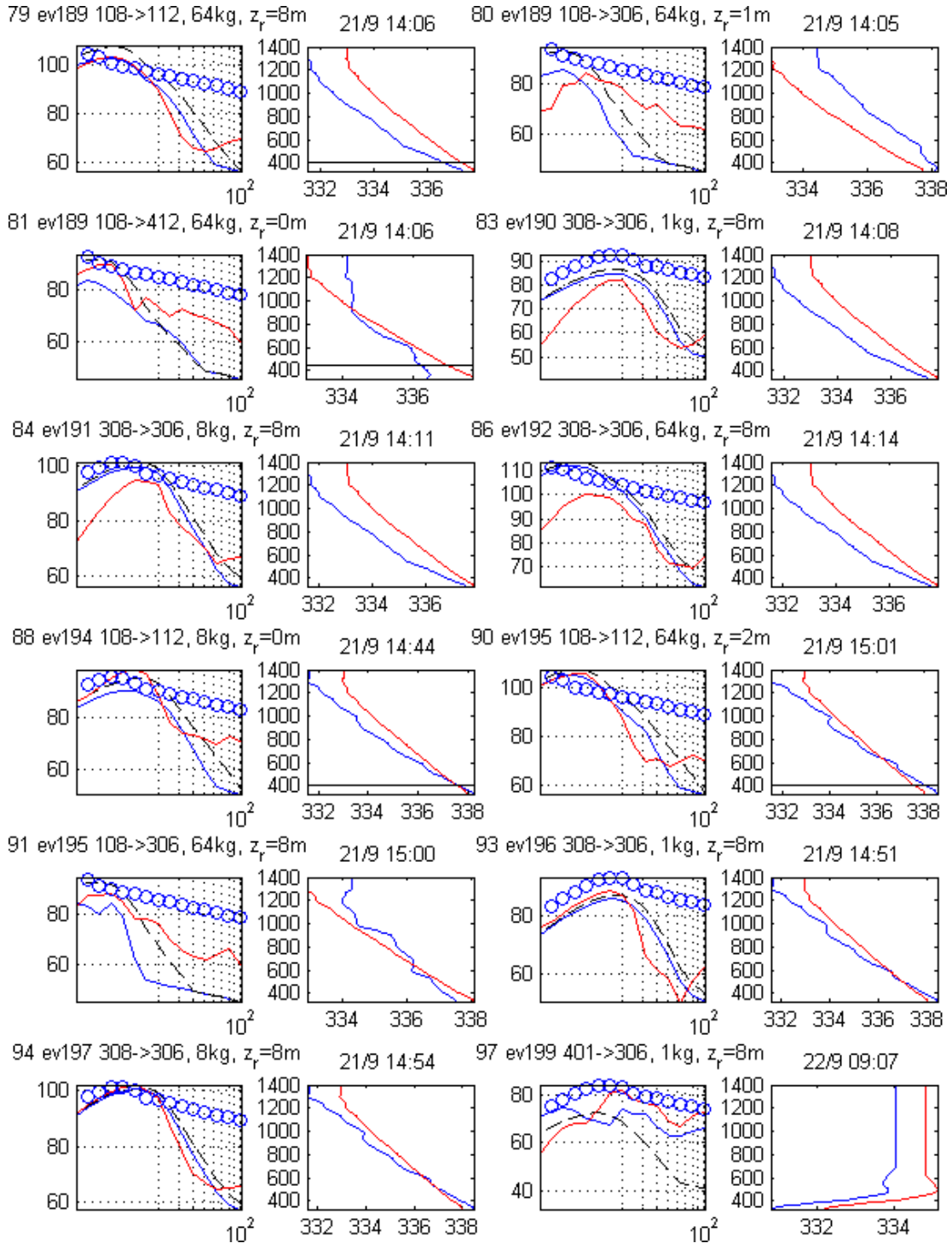
79 ev189 108->112, 64kg, z_r=8m
21/9 14:06
80 ev189 108->306, 64kg, z_r=1m
21/9 14:05
81 ev189 108->412, 64kg, z_r=0m
21/9 14:06
83 ev190 308->306, 1kg, z_r=8m
21/9 14:08
84 ev191 308->306, 8kg, z_r=8m
21/9 14:11
86 ev192 308->306, 64kg, z_r=8m
21/9 14:14
88 ev194 108->112, 8kg, z_r=0m
21/9 14:44
90 ev195 108->112, 64kg, z_r=2m
21/9 15:01
91 ev195 108->306, 64kg, z_r=8m
21/9 15:00
93 ev196 308->306, 1kg, z_r=8m
21/9 14:51
94 ev197 308->306, 8kg, z_r=8m
21/9 14:54
97 ev199 401->306, 1kg, z_r=8m
22/9 09:07

Figure A.20

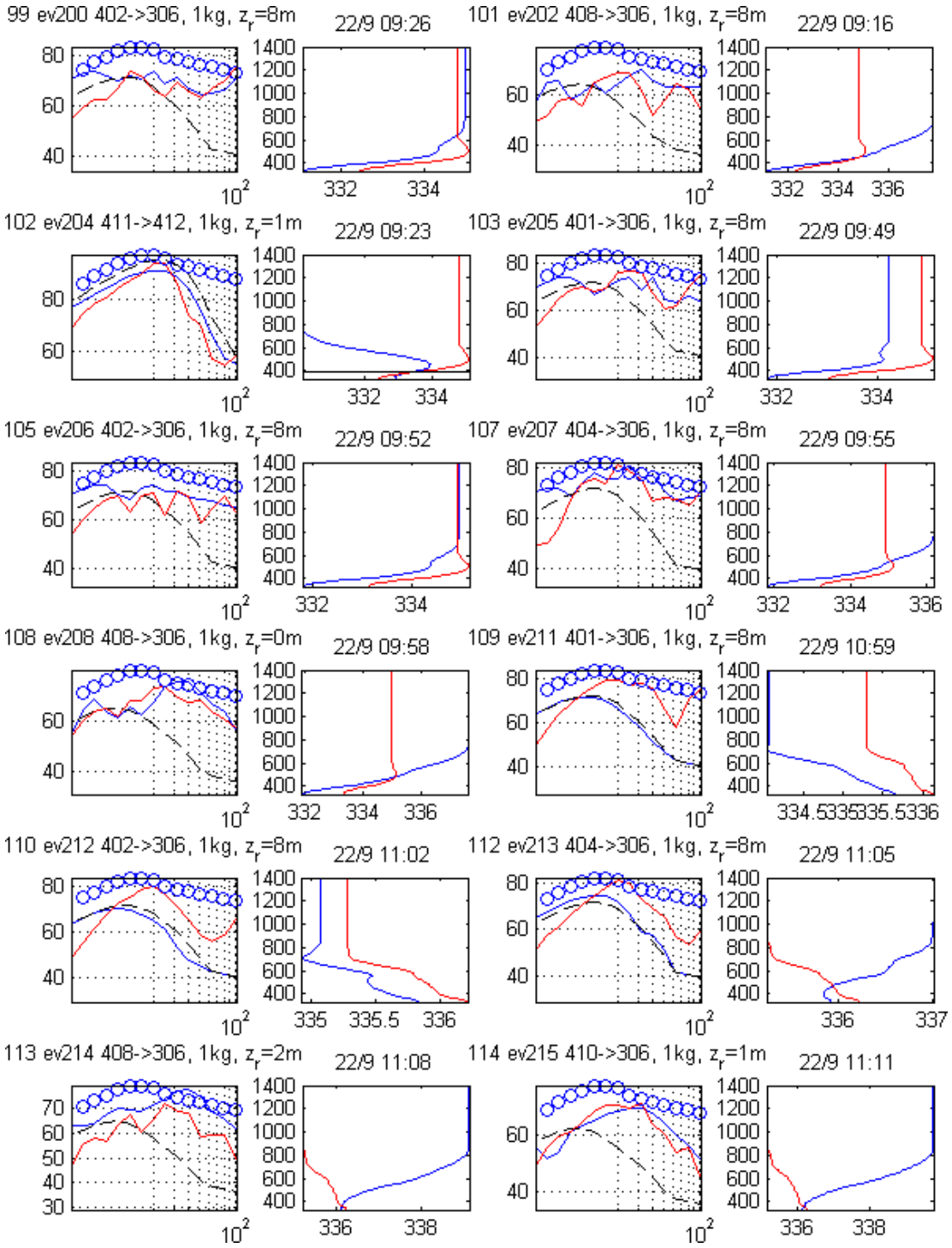
99 ev200 402->306, 1kg, z_r=8m
22/9 09:26
101 ev202 408->306, 1kg, z_r=8m
22/9 09:16
102 ev204 411->412, 1kg, z_r=1m
22/9 09:23
103 ev205 401->306, 1kg, z_r=8m
22/9 09:49
105 ev206 402->306, 1kg, z_r=8m
22/9 09:52
107 ev207 404->306, 1kg, z_r=8m
22/9 09:55
108 ev208 408->306, 1kg, z_r=0m
22/9 09:58
109 ev211 401->306, 1kg, z_r=8m
22/9 10:59
110 ev212 402->306, 1kg, z_r=8m
22/9 11:02
112 ev213 404->306, 1kg, z_r=8m
22/9 11:05
113 ev214 408->306, 1kg, z_r=2m
22/9 11:08
114 ev215 410->306, 1kg, z_r=1m
22/9 11:11

Figure A.21

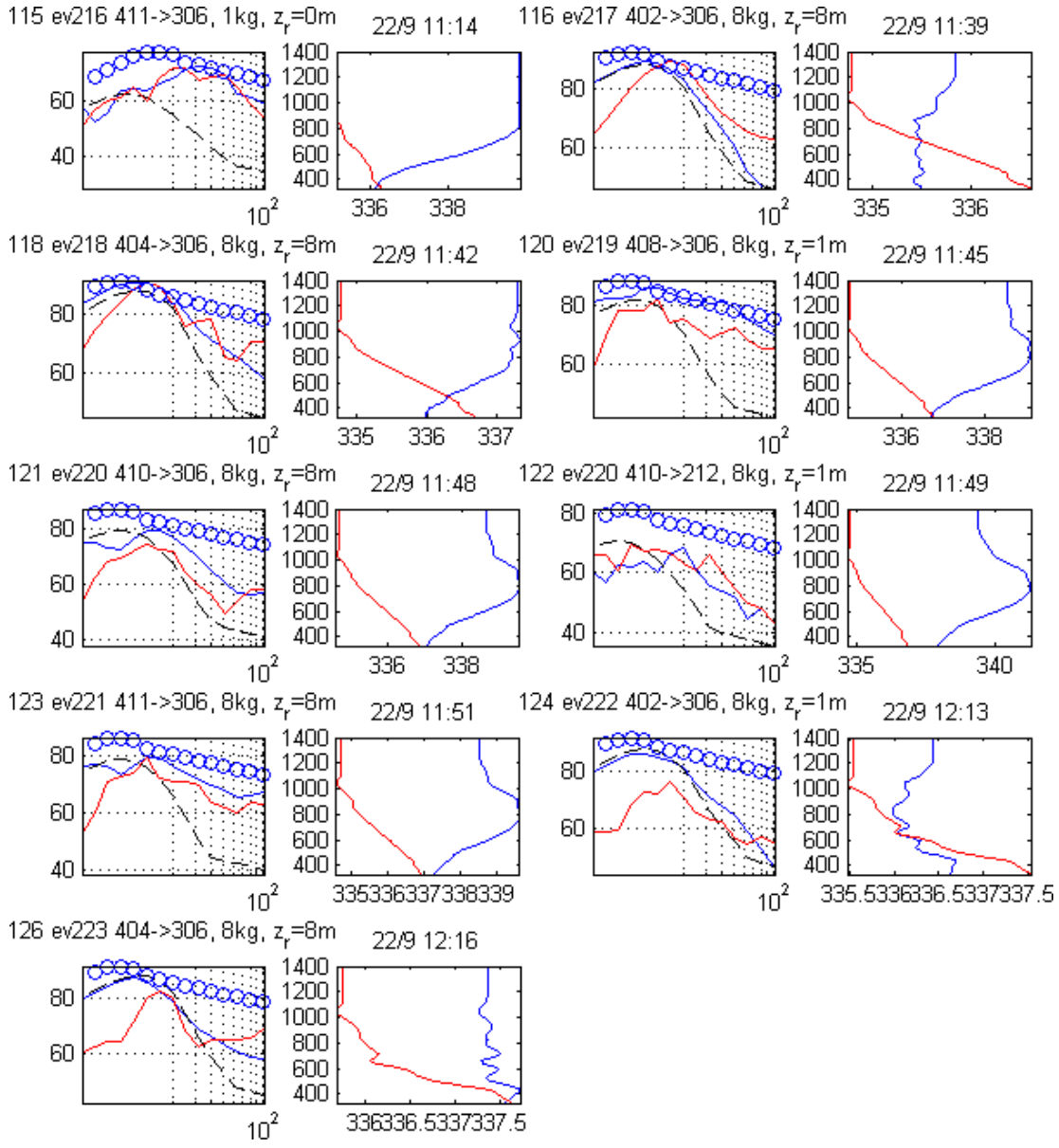

Figure A.22

A.2.2 Winter A data

The first 83 are the ones from tower 306.

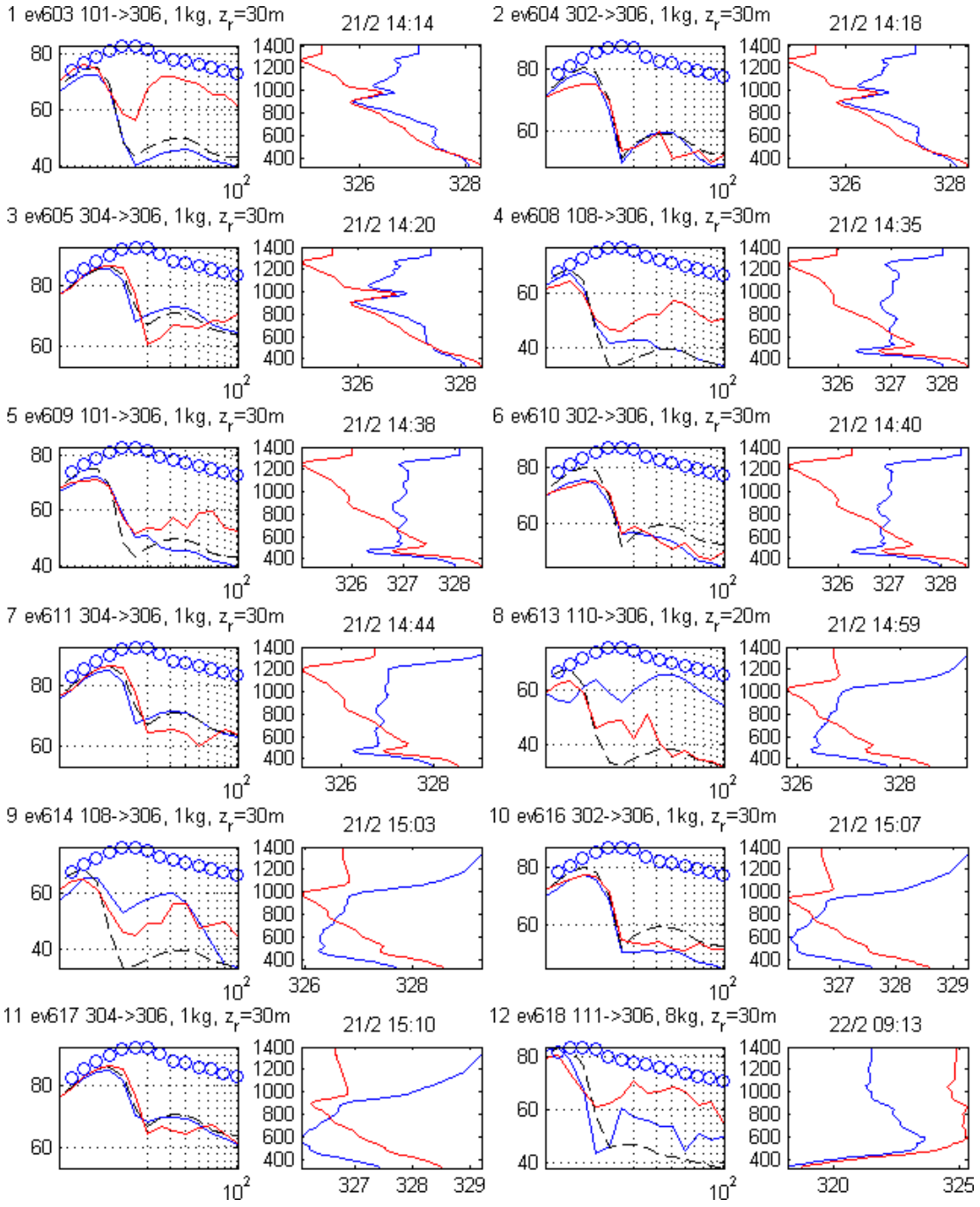
1 ev603 101->306, 1kg, z_r=30m
21/2 14:14
2 ev604 302->306, 1kg, z_r=30m
21/2 14:18
3 ev605 304->306, 1kg, z_r=30m
21/2 14:20
4 ev608 108->306, 1kg, z_r=30m
21/2 14:35
5 ev609 101->306, 1kg, z_r=30m
21/2 14:38
6 ev610 302->306, 1kg, z_r=30m
21/2 14:40
7 ev611 304->306, 1kg, z_r=30m
21/2 14:44
8 ev613 110->306, 1kg, z_r=20m
21/2 14:59
9 ev614 108->306, 1kg, z_r=30m
21/2 15:03
10 ev616 302->306, 1kg, z_r=30m
21/2 15:07
11 ev617 304->306, 1kg, z_r=30m
21/2 15:10
12 ev618 111->306, 8kg, z_r=30m
22/2 09:13
10^2

Figure A.23

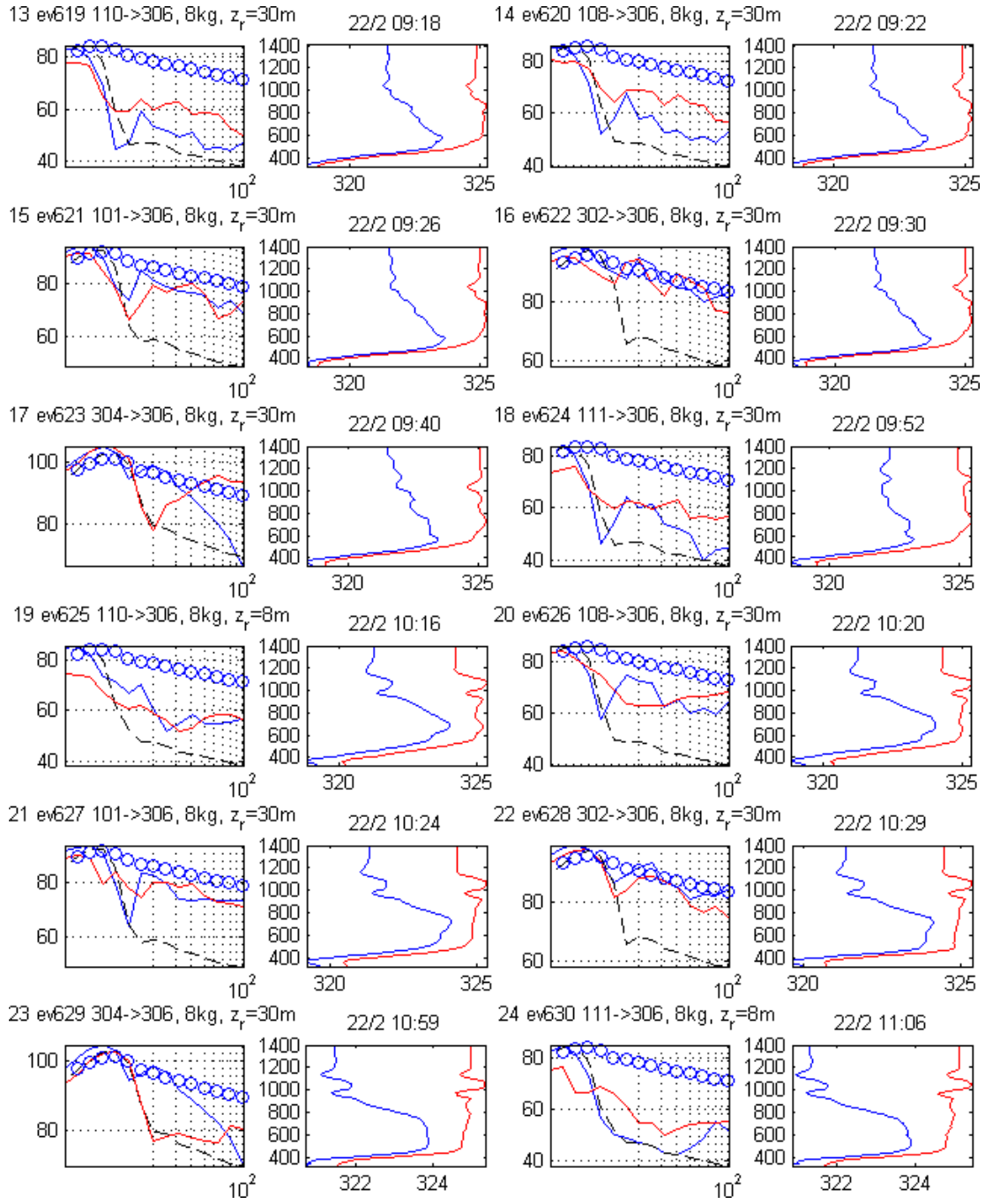
13 ev619 110->306, 8kg, z_r=30m
22/2 09:18
14 ev620 108->306, 8kg, z_r=30m
22/2 09:22
15 ev621 101->306, 8kg, z_r=30m
22/2 09:26
16 ev622 302->306, 8kg, z_r=30m
22/2 09:30
17 ev623 304->306, 8kg, z_r=30m
22/2 09:40
18 ev624 111->306, 8kg, z_r=30m
22/2 09:52
19 ev625 110->306, 8kg, z_r=8m
22/2 10:16
20 ev626 108->306, 8kg, z_r=30m
22/2 10:20
21 ev627 101->306, 8kg, z_r=30m
22/2 10:24
22 ev628 302->306, 8kg, z_r=30m
22/2 10:29
23 ev629 304->306, 8kg, z_r=30m
22/2 10:59
24 ev630 111->306, 8kg, z_r=8m
22/2 11:06
10^2

Figure A.24

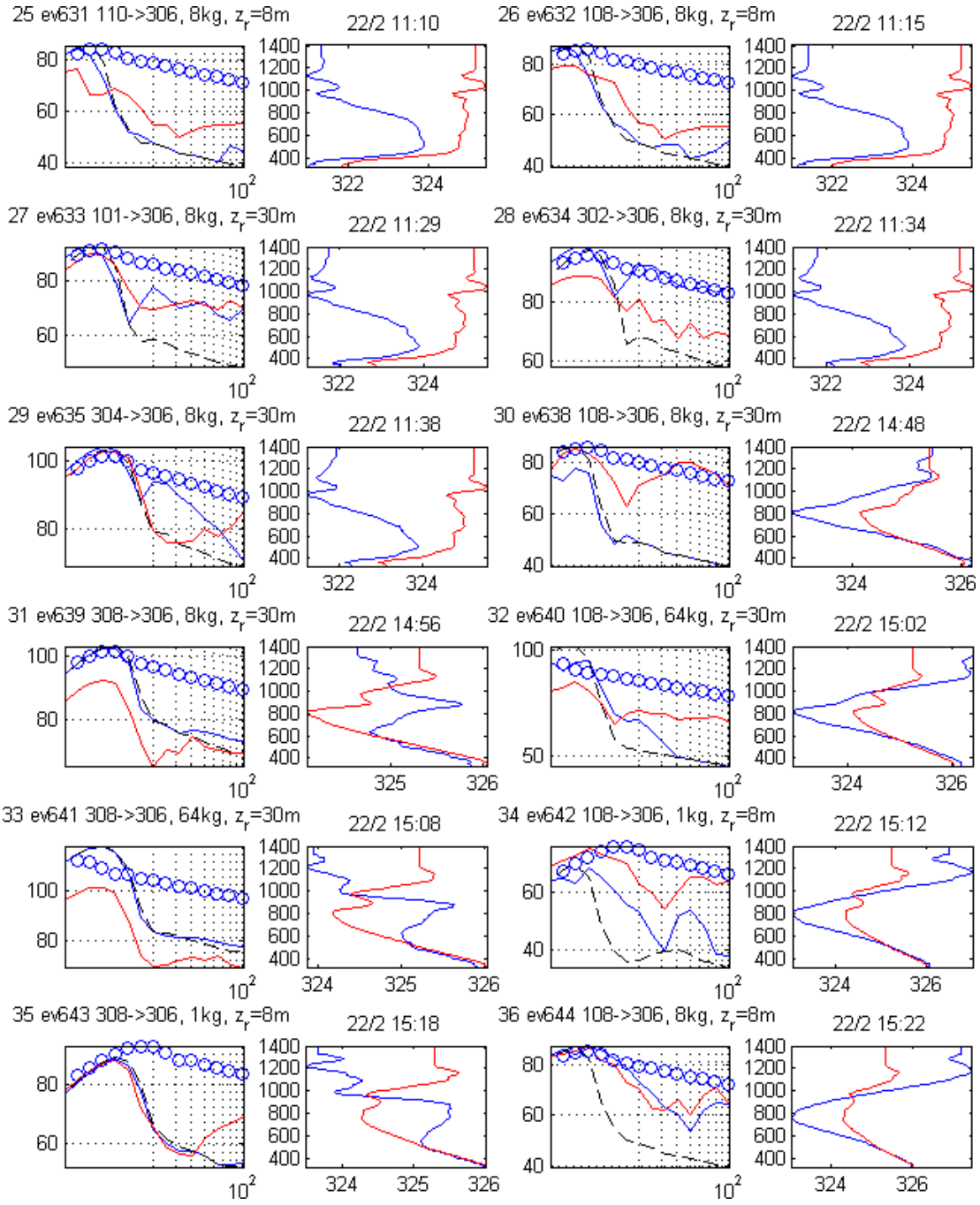
25 ev631 110->306, 8kg, z_r=8m
22/2 11:10
26 ev632 108->306, 8kg, z_r=8m
22/2 11:15
27 ev633 101->306, 8kg, z_r=30m
22/2 11:29
28 ev634 302->306, 8kg, z_r=30m
22/2 11:34
29 ev635 304->306, 8kg, z_r=30m
22/2 11:38
30 ev638 108->306, 8kg, z_r=30m
22/2 14:48
31 ev639 308->306, 8kg, z_r=30m
22/2 14:56
32 ev640 108->306, 64kg, z_r=30m
22/2 15:02
33 ev641 308->306, 64kg, z_r=30m
22/2 15:08
34 ev642 108->306, 1kg, z_r=8m
22/2 15:12
35 ev643 308->306, 1kg, z_r=8m
22/2 15:18
36 ev644 108->306, 8kg, z_r=8m
22/2 15:22
10^2

Figure A.25

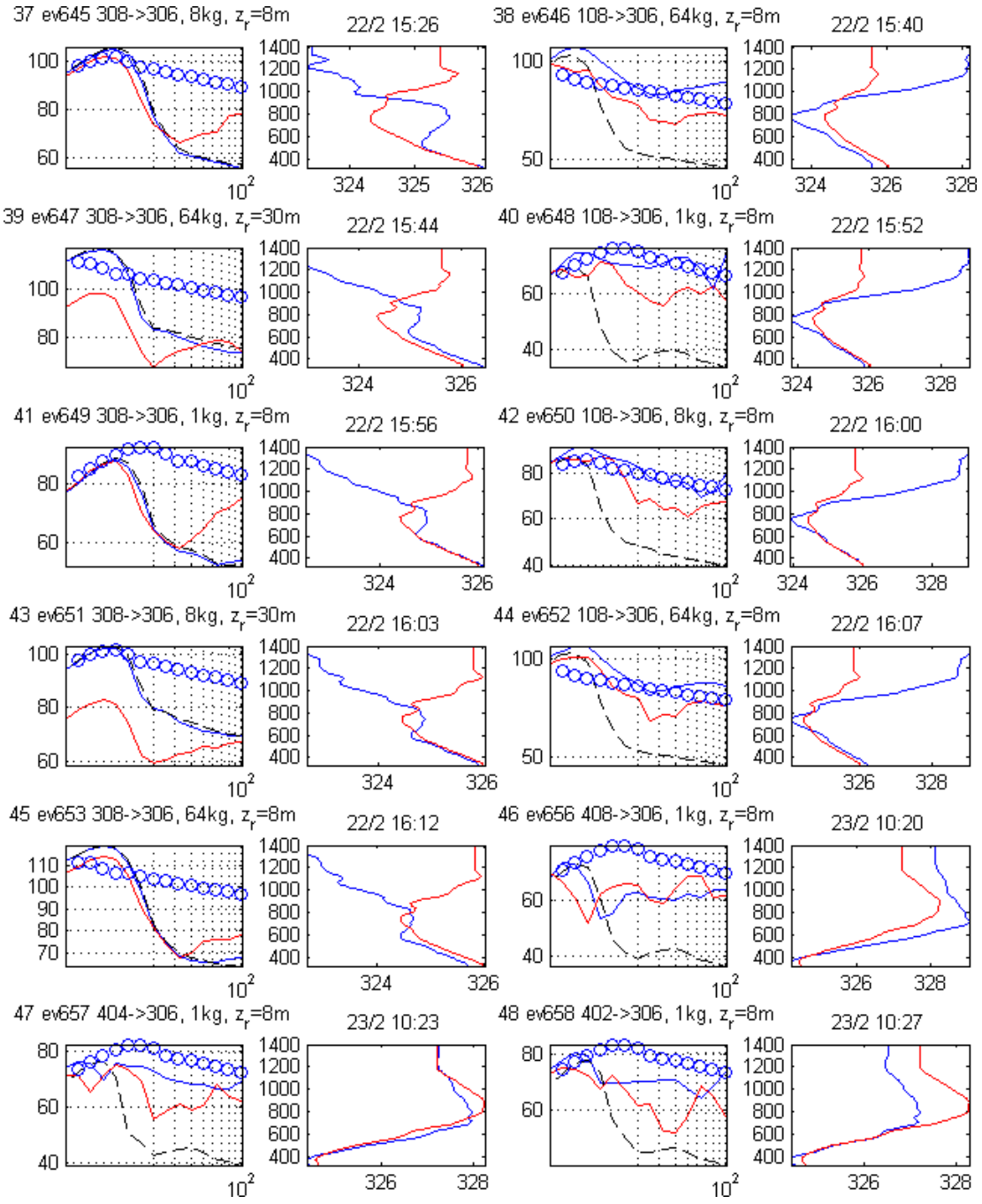
37 ev645 308->306, 8kg, z_r=8m
22/2 15:26
38 ev646 108->306, 64kg, z_r=8m
22/2 15:40
39 ev647 308->306, 64kg, z_r=30m
22/2 15:44
40 ev648 108->306, 1kg, z_r=8m
22/2 15:52
41 ev649 308->306, 1kg, z_r=8m
22/2 15:56
42 ev650 108->306, 8kg, z_r=8m
22/2 16:00
43 ev651 308->306, 8kg, z_r=30m
22/2 16:03
44 ev652 108->306, 64kg, z_r=8m
22/2 16:07
45 ev653 308->306, 64kg, z_r=8m
22/2 16:12
46 ev656 408->306, 1kg, z_r=8m
23/2 10:20
47 ev657 404->306, 1kg, z_r=8m
23/2 10:23
48 ev658 402->306, 1kg, z_r=8m
23/2 10:27

Figure A.26

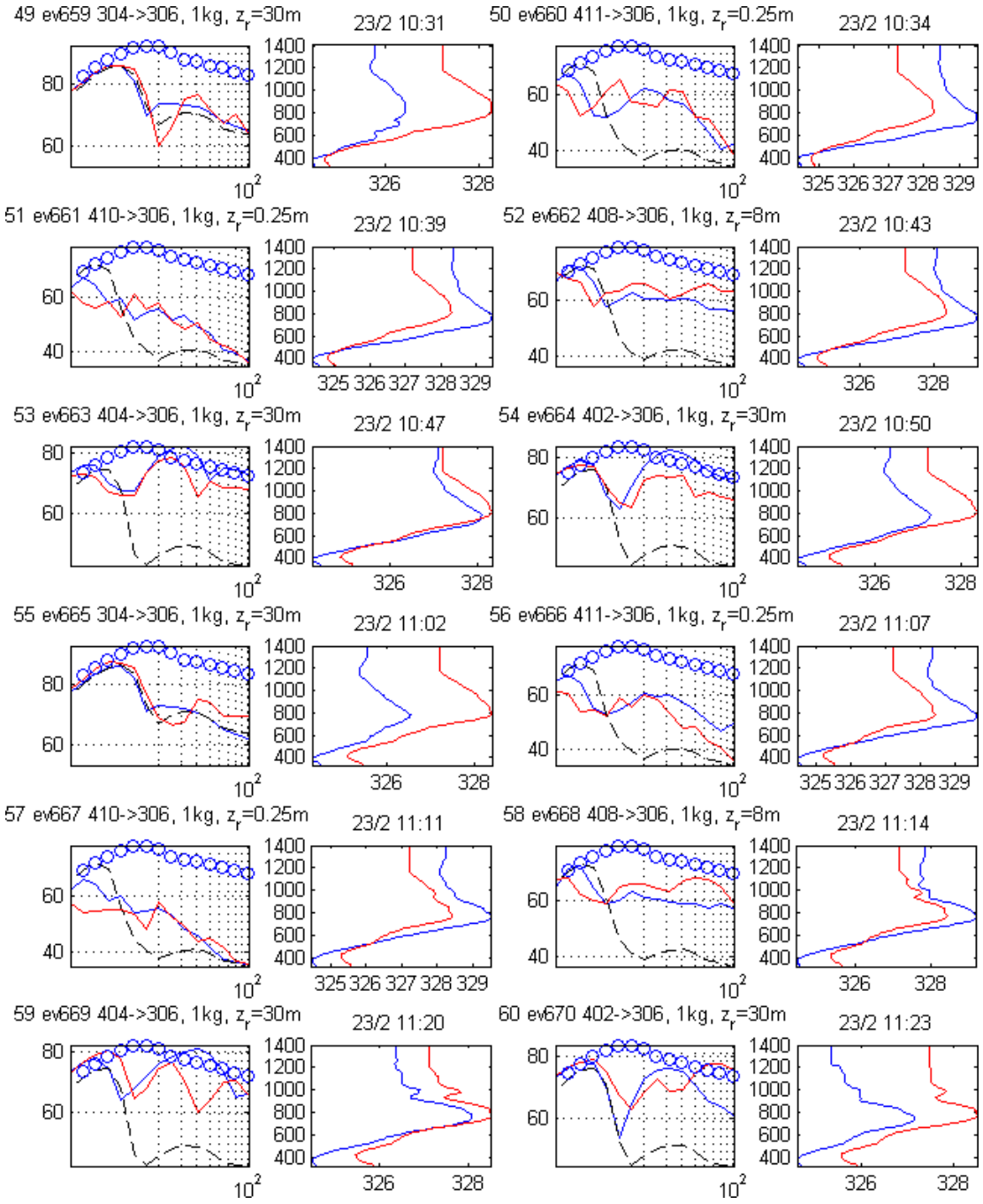
49 ev659 304->306, 1kg, z_r=30m
23/2 10:31
50 ev660 411->306, 1kg, z_r=0.25m
23/2 10:34
51 ev661 410->306, 1kg, z_r=0.25m
23/2 10:39
52 ev662 408->306, 1kg, z_r=8m
23/2 10:43
53 ev663 404->306, 1kg, z_r=30m
23/2 10:47
54 ev664 402->306, 1kg, z_r=30m
23/2 10:50
55 ev665 304->306, 1kg, z_r=30m
23/2 11:02
56 ev666 411->306, 1kg, z_r=0.25m
23/2 11:07
57 ev667 410->306, 1kg, z_r=0.25m
23/2 11:11
58 ev668 408->306, 1kg, z_r=8m
23/2 11:14
59 ev669 404->306, 1kg, z_r=30m
23/2 11:20
60 ev670 402->306, 1kg, z_r=30m
23/2 11:23
10^2

Figure A.27

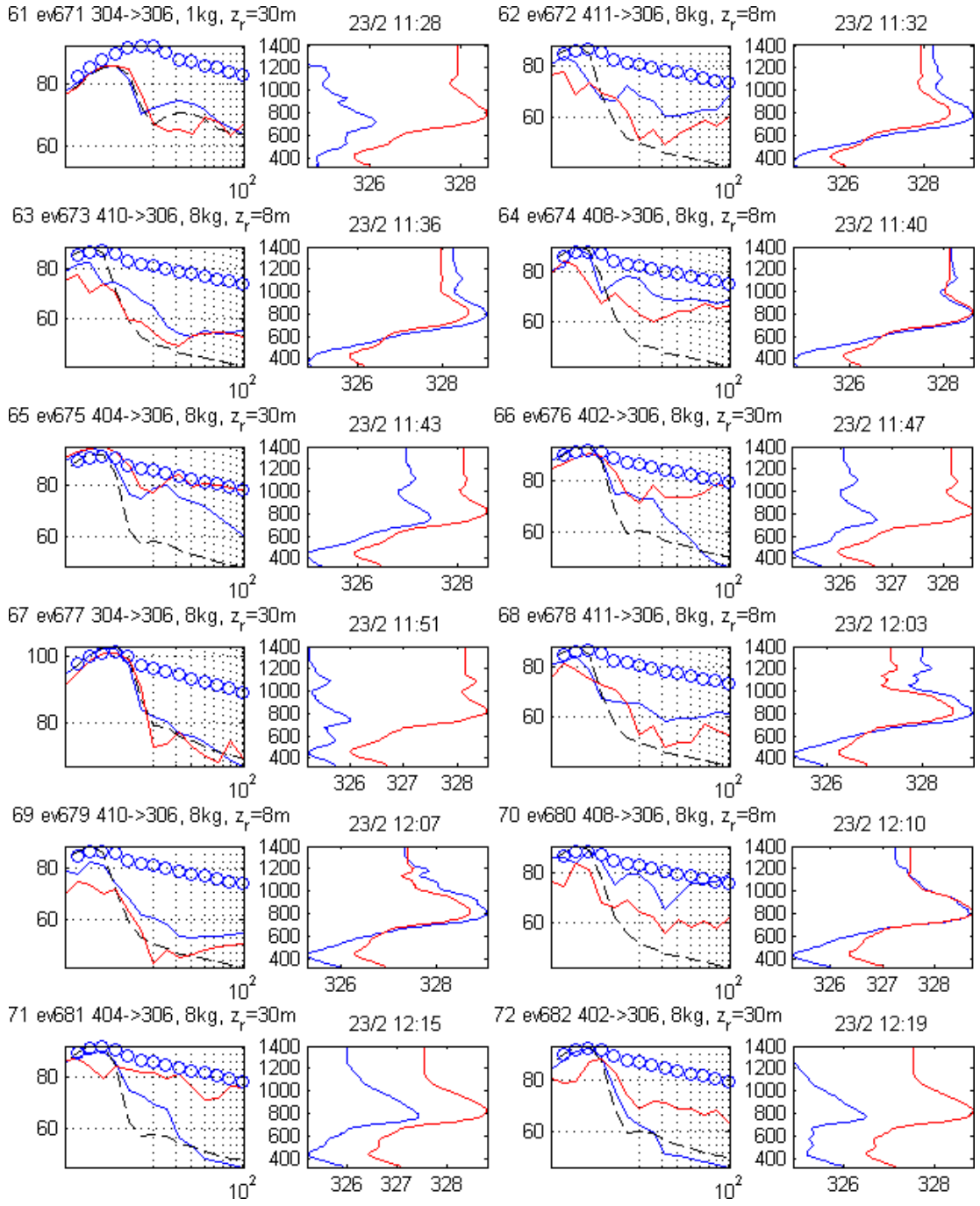
61 ev671 304->306, 1kg, z_r=30m
23/2 11:28
62 ev672 411->306, 8kg, z_r=8m
23/2 11:32
63 ev673 410->306, 8kg, z_r=8m
23/2 11:36
64 ev674 408->306, 8kg, z_r=8m
23/2 11:40
65 ev675 404->306, 8kg, z_r=30m
23/2 11:43
66 ev676 402->306, 8kg, z_r=30m
23/2 11:47
67 ev677 304->306, 8kg, z_r=30m
23/2 11:51
68 ev678 411->306, 8kg, z_r=8m
23/2 12:03
69 ev679 410->306, 8kg, z_r=8m
23/2 12:07
70 ev680 408->306, 8kg, z_r=8m
23/2 12:10
71 ev681 404->306, 8kg, z_r=30m
23/2 12:15
72 ev682 402->306, 8kg, z_r=30m
23/2 12:19
10^2

Figure A.28

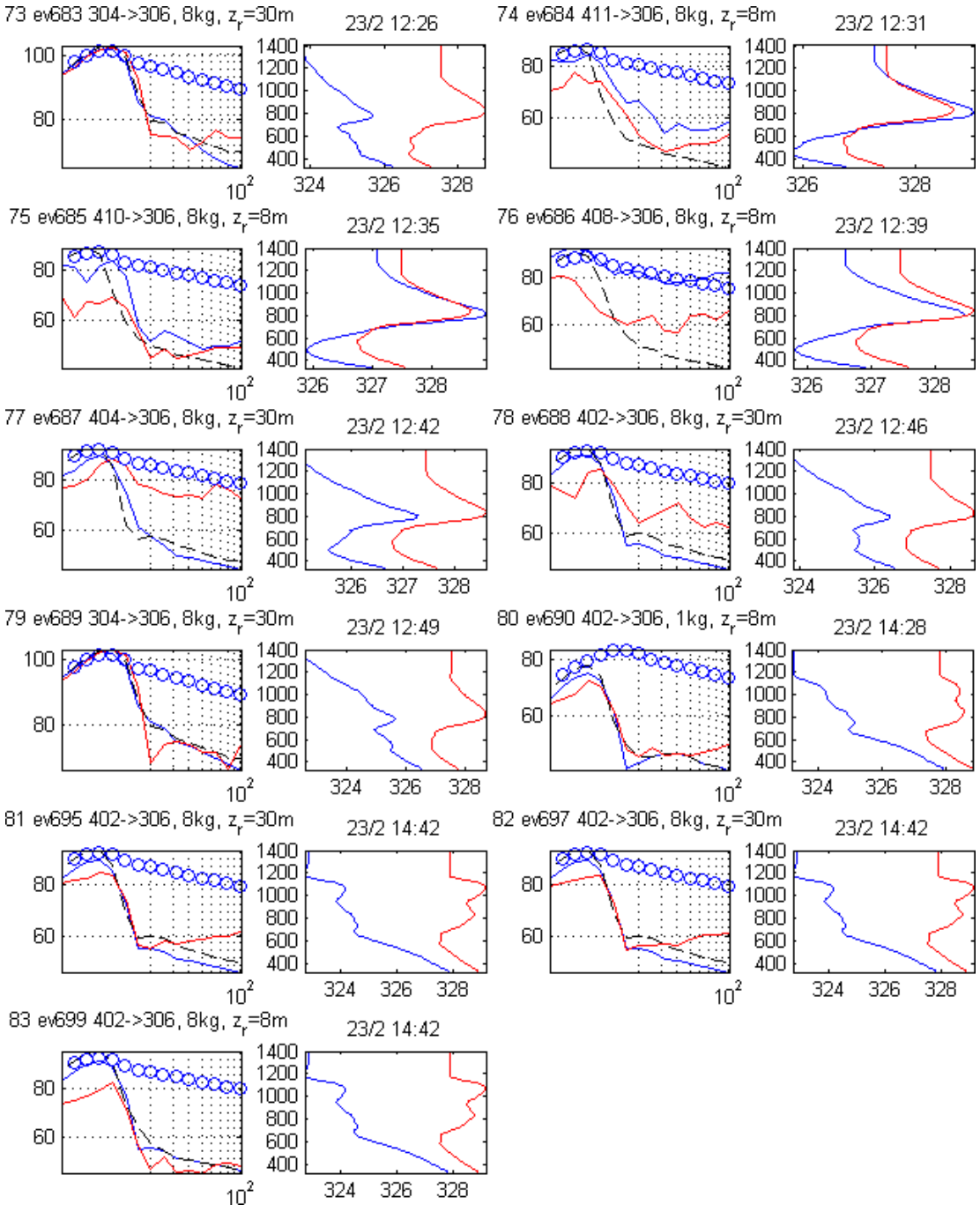
73 ev683 304->306, 8kg, z_r=30m
23/2 12:26
74 ev684 411->306, 8kg, z_r=8m
23/2 12:31
75 ev685 410->306, 8kg, z_r=8m
23/2 12:35
76 ev686 408->306, 8kg, z_r=8m
23/2 12:39
77 ev687 404->306, 8kg, z_r=30m
23/2 12:42
78 ev688 402->306, 8kg, z_r=30m
23/2 12:46
79 ev689 304->306, 8kg, z_r=30m
23/2 12:49
80 ev690 402->306, 1kg, z_r=8m
23/2 14:28
81 ev695 402->306, 8kg, z_r=30m
23/2 14:42
82 ev697 402->306, 8kg, z_r=30m
23/2 14:42
83 ev699 402->306, 8kg, z_r=8m
23/2 14:42
10^2

Figure A.29

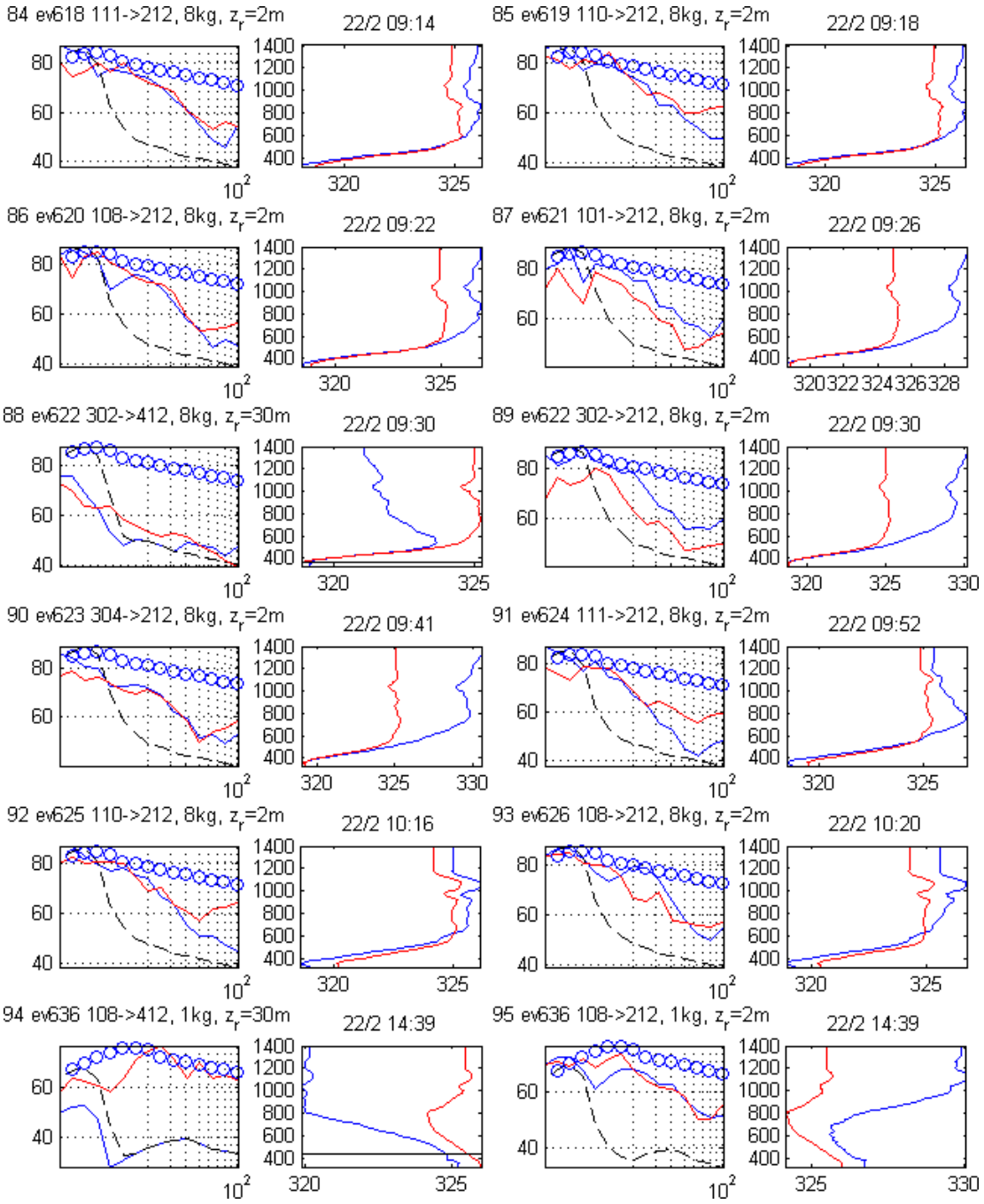
84 ev618 111->212, 8kg, z_r=2m
22/2 09:14
85 ev619 110->212, 8kg, z_r=2m
22/2 09:18
86 ev620 108->212, 8kg, z_r=2m
22/2 09:22
87 ev621 101->212, 8kg, z_r=2m
22/2 09:26
88 ev622 302->412, 8kg, z_r=30m
22/2 09:30
89 ev622 302->212, 8kg, z_r=2m
22/2 09:30
90 ev623 304->212, 8kg, z_r=2m
22/2 09:41
91 ev624 111->212, 8kg, z_r=2m
22/2 09:52
92 ev625 110->212, 8kg, z_r=2m
22/2 10:16
93 ev626 108->212, 8kg, z_r=2m
22/2 10:20
94 ev636 108->412, 1kg, z_r=30m
22/2 14:39
95 ev636 108->212, 1kg, z_r=2m
22/2 14:39

Figure A.30

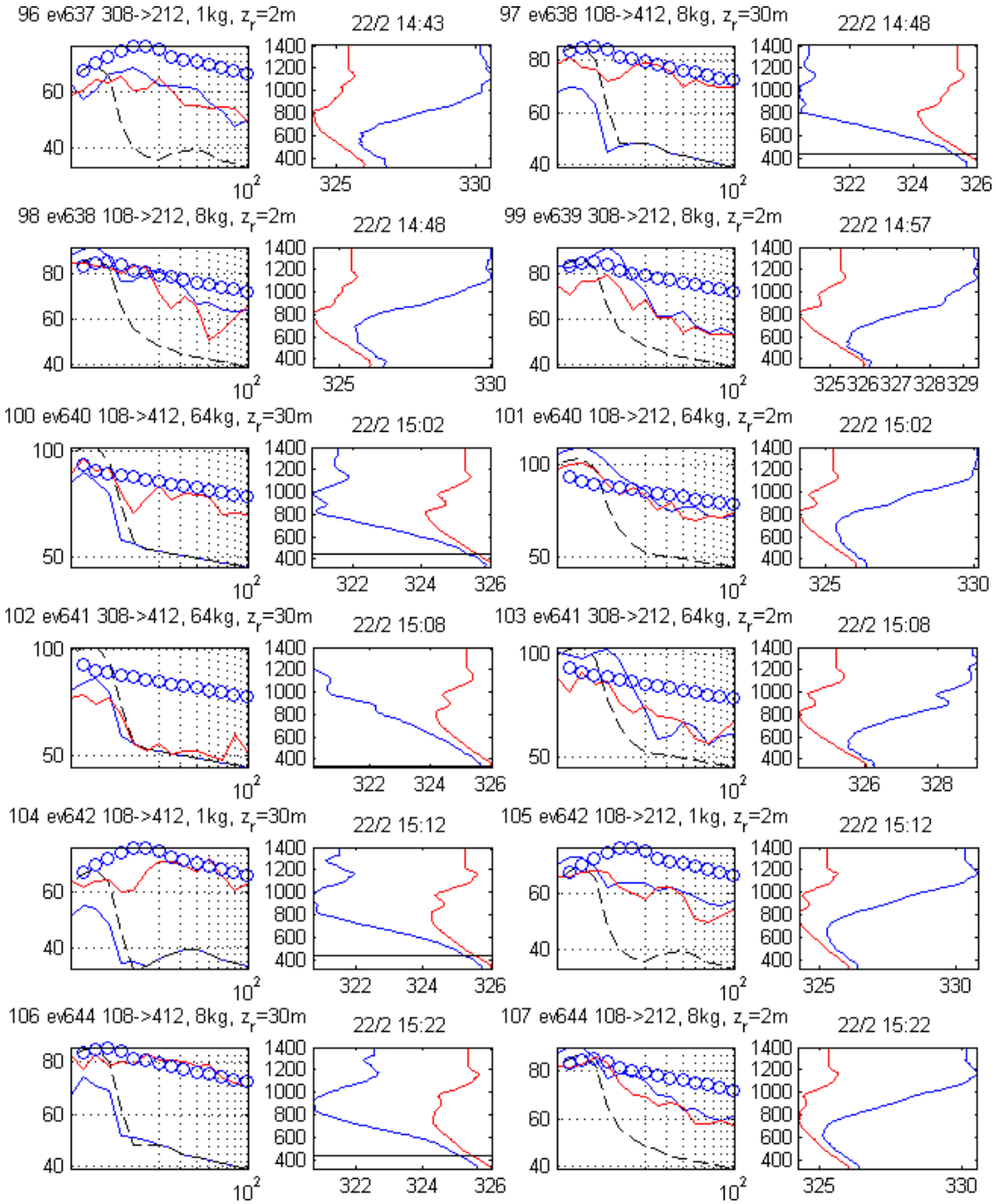
96 ev637 308->212, 1kg, z_r=2m
22/2 14:43
97 ev638 108->412, 8kg, z_r=30m
22/2 14:48
98 ev638 108->212, 8kg, z_r=2m
22/2 14:48
99 ev639 308->212, 8kg, z_r=2m
22/2 14:57
100 ev640 108->412, 64kg, z_r=30m
22/2 15:02
101 ev640 108->212, 64kg, z_r=2m
22/2 15:02
102 ev641 308->412, 64kg, z_r=30m
22/2 15:08
103 ev641 308->212, 64kg, z_r=2m
22/2 15:08
104 ev642 108->412, 1kg, z_r=30m
22/2 15:12
105 ev642 108->212, 1kg, z_r=2m
22/2 15:12
106 ev644 108->412, 8kg, z_r=30m
22/2 15:22
107 ev644 108->212, 8kg, z_r=2m
22/2 15:22
10^2

Figure A.31

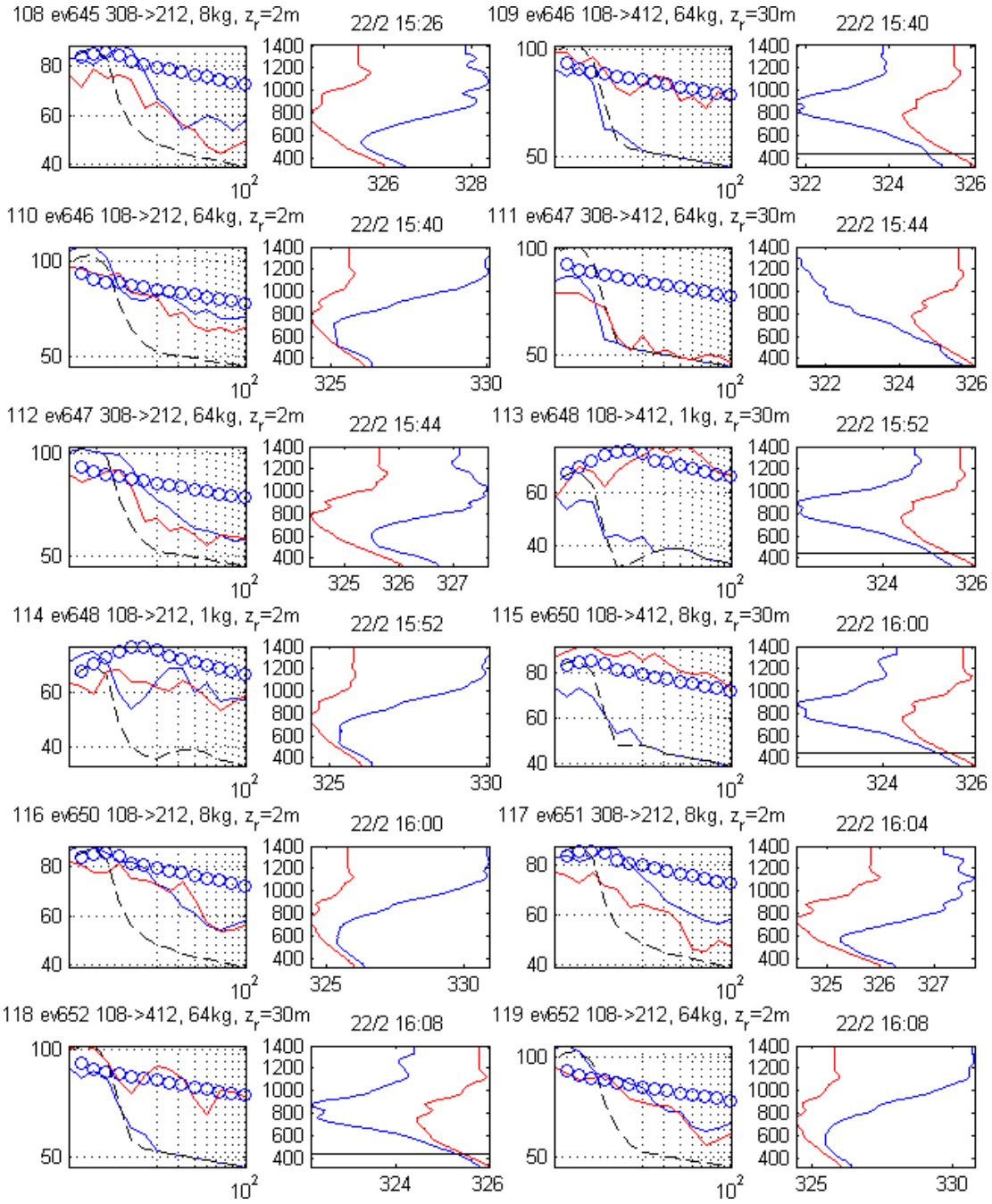
108 ev645 308->212, 8kg, z_r=2m
22/2 15:26
109 ev646 108->412, 64kg, z_r=30m
22/2 15:40
110 ev646 108->212, 64kg, z_r=2m
22/2 15:40
111 ev647 308->412, 64kg, z_r=30m
22/2 15:44
112 ev647 308->212, 64kg, z_r=2m
22/2 15:44
113 ev648 108->412, 1kg, z_r=30m
22/2 15:52
114 ev648 108->212, 1kg, z_r=2m
22/2 15:52
115 ev650 108->412, 8kg, z_r=30m
22/2 16:00
116 ev650 108->212, 8kg, z_r=2m
22/2 16:00
117 ev651 308->212, 8kg, z_r=2m
22/2 16:04
118 ev652 108->412, 64kg, z_r=30m
22/2 16:08
119 ev652 108->212, 64kg, z_r=2m
22/2 16:08

Figure A.32

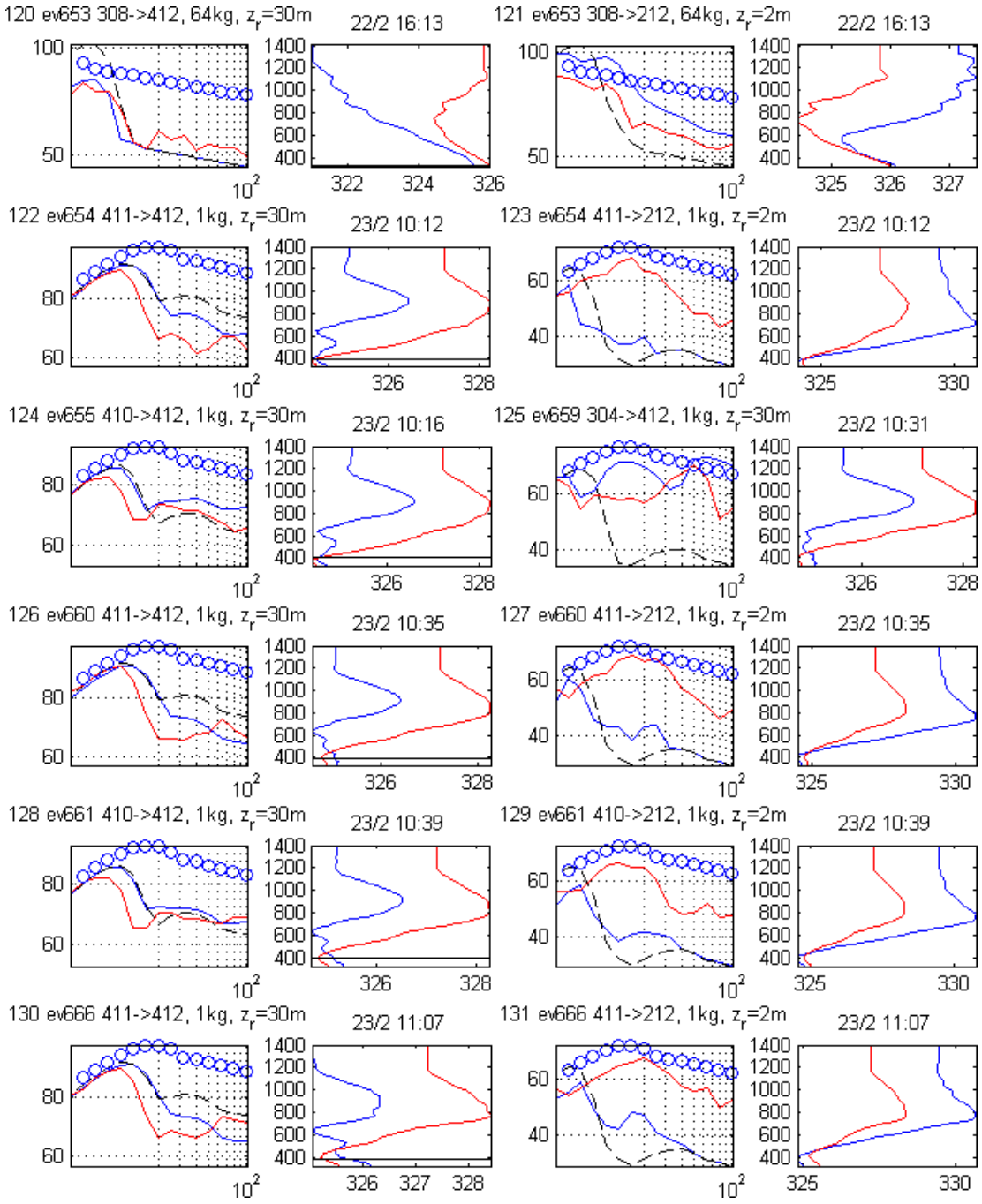
120 ev653 308->412, 64kg, z_r=30m
22/2 16:13
121 ev653 308->212, 64kg, z_r=2m
22/2 16:13
122 ev654 411->412, 1kg, z_r=30m
23/2 10:12
123 ev654 411->212, 1kg, z_r=2m
23/2 10:12
124 ev655 410->412, 1kg, z_r=30m
23/2 10:16
125 ev659 304->412, 1kg, z_r=30m
23/2 10:31
126 ev660 411->412, 1kg, z_r=30m
23/2 10:35
127 ev660 411->212, 1kg, z_r=2m
23/2 10:35
128 ev661 410->412, 1kg, z_r=30m
23/2 10:39
129 ev661 410->212, 1kg, z_r=2m
23/2 10:39
130 ev666 411->412, 1kg, z_r=30m
23/2 11:07
131 ev666 411->212, 1kg, z_r=2m
23/2 11:07
10^2

Figure A.33

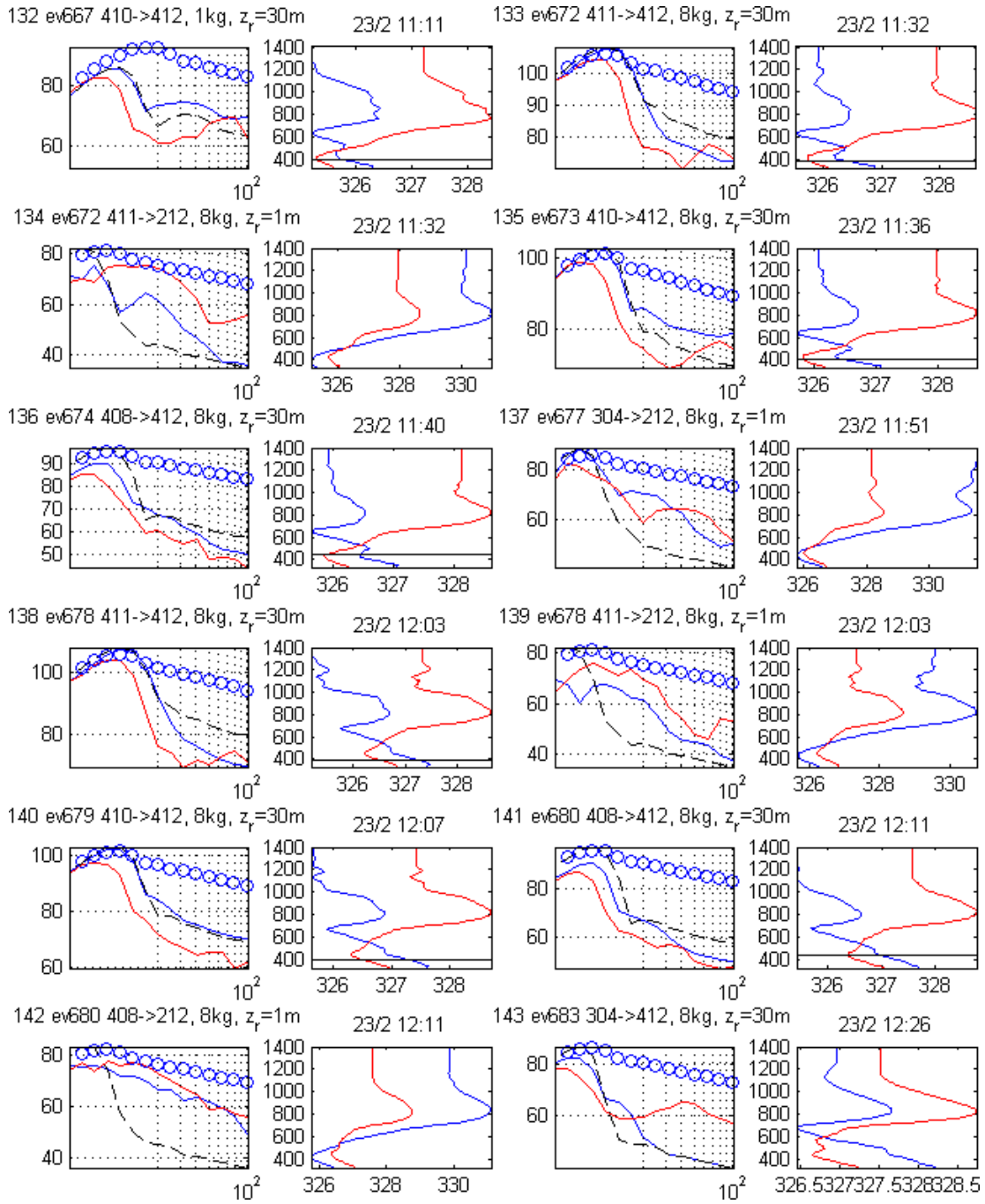
132 ev667 410->412, 1kg, z_r=30m
23/2 11:11
133 ev672 411->412, 8kg, z_r=30m
23/2 11:32
134 ev672 411->212, 8kg, z_r=1m
23/2 11:32
135 ev673 410->412, 8kg, z_r=30m
23/2 11:36
136 ev674 408->412, 8kg, z_r=30m
23/2 11:40
137 ev677 304->212, 8kg, z_r=1m
23/2 11:51
138 ev678 411->412, 8kg, z_r=30m
23/2 12:03
139 ev678 411->212, 8kg, z_r=1m
23/2 12:03
140 ev679 410->412, 8kg, z_r=30m
23/2 12:07
141 ev680 408->412, 8kg, z_r=30m
23/2 12:11
142 ev680 408->212, 8kg, z_r=1m
23/2 12:11
143 ev683 304->412, 8kg, z_r=30m
23/2 12:26
10^2
326.5327327.5328328.5

Figure A.34

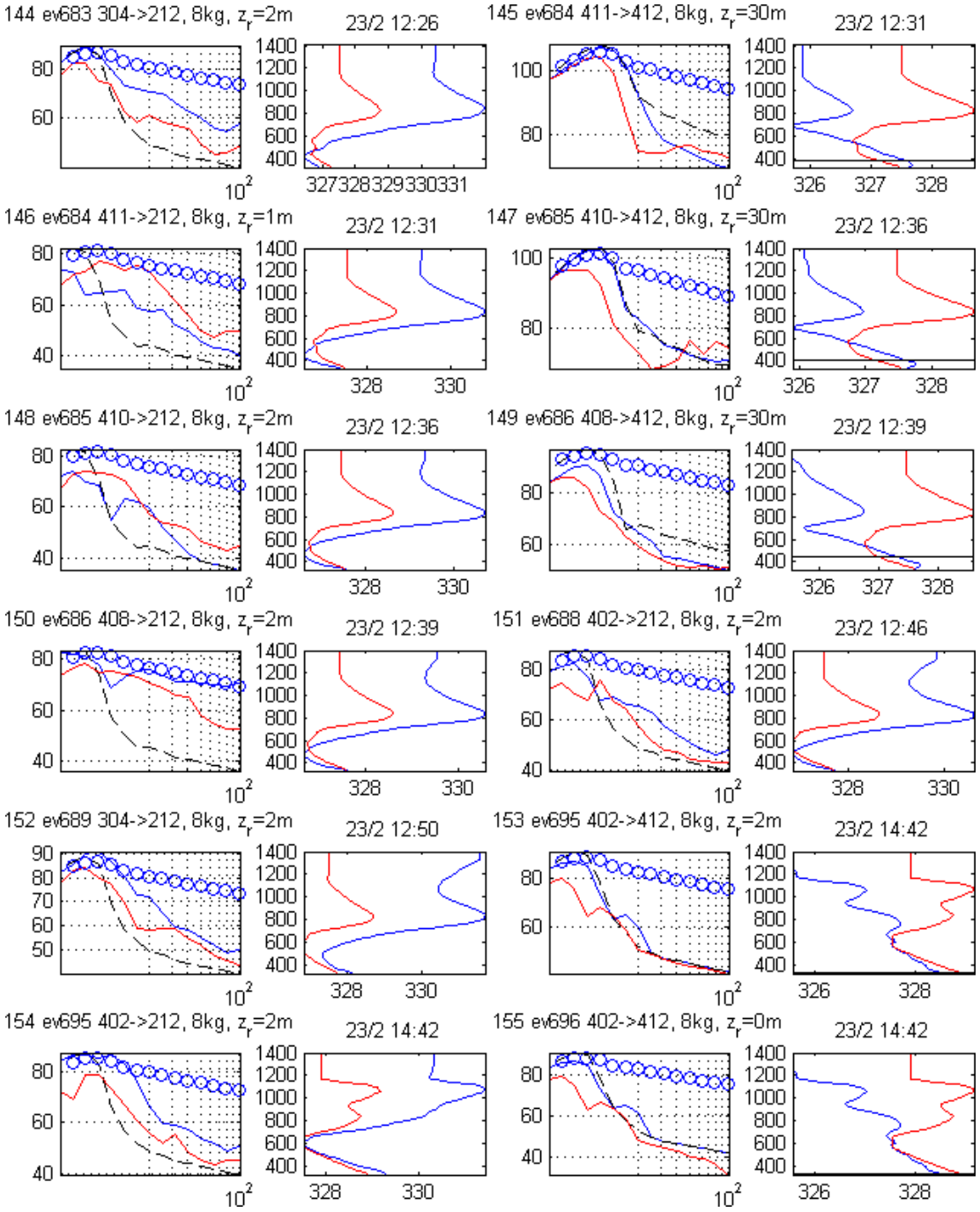
144 ev683 304->212, 8kg, z_r=2m
23/2 12:26
145 ev684 411->412, 8kg, z_r=30m
23/2 12:31
146 ev684 411->212, 8kg, z_r=1m
23/2 12:31
147 ev685 410->412, 8kg, z_r=30m
23/2 12:36
148 ev685 410->212, 8kg, z_r=2m
23/2 12:36
149 ev686 408->412, 8kg, z_r=30m
23/2 12:39
150 ev686 408->212, 8kg, z_r=2m
23/2 12:39
151 ev688 402->212, 8kg, z_r=2m
23/2 12:46
152 ev689 304->212, 8kg, z_r=2m
23/2 12:50
153 ev695 402->412, 8kg, z_r=2m
23/2 14:42
154 ev695 402->212, 8kg, z_r=2m
23/2 14:42
155 ev696 402->412, 8kg, z_r=0m
23/2 14:42

Figure A.35

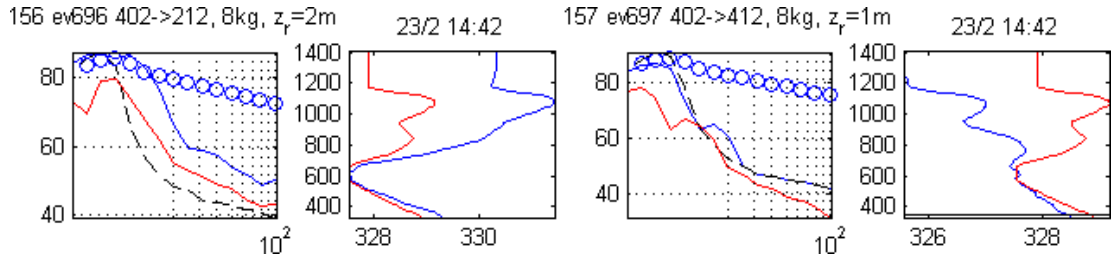
156 ev696 402->212, 8kg, z_r=2m
23/2 14:42
157 ev697 402->412, 8kg, z_r=1m
23/2 14:42
80
60
40
10^2
1400
1200
1000
800
600
400
328
330
326
328

Figure A.36

A.3 Tethersonde data processing

Summer data:

```
% Read tethersonde data
[z3,ws3,wd3,at3raw,ap3,t3raw] = gettethparams_mod_kw(403,1994,metbase94); %Raw T-data
[z3,ws3,wd3,at3,ap3,t3] = gettethparams(403,1994,metbase94);

tsep01_94=date2num('01-Sep-1994','00:00:00.000');

tstart=tsep01_94-1;


%Remove bad data(usually when sonde just had a break)
jT=find(t3raw-tstart<21.289 & t3raw-tstart>21.28);%Botched T-data
at3raw(jT)=at3raw(jT(end));
jT=find(t3-tstart<21.289 & t3-tstart>21.28);%Botched T-data
at3(jT)=at3(jT(end));
wd3(jT)=wd3(jT(end));
ws3(jT)=ws3(jT(end));
z3(jT)=z3(jT(end));
jT=find(t3-tstart<22.3 & t3-tstart>22.2);%Botched T-data
at3(jT)=at3(jT(end));
wd3(jT)=wd3(jT(end));
ws3(jT)=ws3(jT(end));
jT=find(t3-tstart<13.564 & t3-tstart>13.559);%Botched T-data
at3(jT)=interp1(t3([jT(1),jT(end)]),at3([jT(1),jT(end)]),t3(jT));
wd3(jT)=interp1(t3([jT(1),jT(end)]),wd3([jT(1),jT(end)]),t3(jT));
ws3(jT)=interp1(t3([jT(1),jT(end)]),ws3([jT(1),jT(end)]),t3(jT));
jT=find(t3-tstart<13.65 & t3-tstart>13.63);%Botched T-data
at3(jT)=at3(jT(1));
wd3(jT)=wd3(jT(1));
ws3(jT)=ws3(jT(1));
jT=find(t3-tstart<14.352 & t3-tstart>14.33);%Botched T-data
at3(jT)=at3(jT(end));
wd3(jT)=wd3(jT(end));
ws3(jT)=ws3(jT(end));
jT=find(t3-tstart<19.362 & t3-tstart>19.31);%Botched T-data
at3(jT)=at3(jT(end));
wd3(jT)=wd3(jT(end));
ws3(jT)=ws3(jT(end));
```

```
38 jT=find(t3-tstart<20.303 & t3-tstart>20.3);%Botched T-data
39 at3(jT)=at3(jT(end));
40 wd3(jT)=wd3(jT(end));
41 ws3(jT)=ws3(jT(end));
42 jT=find(t3-tstart<20.48 & t3-tstart>20.405);%Botched T-data
43 at3(jT)=at3(jT(1));
44 wd3(jT)=wd3(jT(1));
45 ws3(jT)=ws3(jT(1));
46 jT=find(t3-tstart<20.524 & t3-tstart>20.5);%Botched T-data
47 at3(jT)=at3(jT(end));
48 wd3(jT)=wd3(jT(end));
49 ws3(jT)=ws3(jT(end));
50 jT=find(not (t3-tstart<22.303 & t3-tstart>22.1) );%Botched T-
       data (remove)
51 z3=z3(jT);
52 t3=t3(jT);
53 at3=at3(jT);
54 wd3=wd3(jT);
55 ws3=ws3(jT);
56 jT=find(not (t3-tstart<14.7 & t3-tstart>14.623) );%Botched T-
       data (remove)
57 z3=z3(jT);
58 t3=t3(jT);
59 at3=at3(jT);
60 wd3=wd3(jT);
61 ws3=ws3(jT);
62 jT=find(not (t3-tstart<23 & t3-tstart>22.530) );%Botched T-data
       (remove)
63 z3=z3(jT);
64 t3=t3(jT);
65 at3=at3(jT);
66 wd3=wd3(jT);
67 ws3=ws3(jT);
68
69
70 cosEW3=cos((90-wd3)*pi/180);
71 cosNS3=cos(wd3*pi/180);
72 uwe=ws3.*(-cosEW3);
73 usn=ws3.*(-cosNS3);
74
75 %Replace 21/9 with raw data.
76 tsep=t3-tstart;
77 jt=find(abs(tsep-21.5)<.5);
78 tsepraw=t3raw-tstart;
79 jtraw=find(abs(tsepraw-21.5)<.5);
80 at3(jt)=at3raw(jtraw);
```

```
81
82
83  %Interpolation to cartesian grid
84  [tt,zz]=meshgrid(13:.02:23,10:5:1010);
85  TT=griddata(t3-tstart,z3/5000,at3,tt,zz/5000);%Note scaling of z
86  uu=griddata(t3-tstart,z3/5000,uwe,tt,zz/5000);
87  vv=griddata(t3-tstart,z3/5000,usn,tt,zz/5000);
88
89
90  %Above the grid etc:
91  [nz nt]=size(tt);
92  maxh = tethpeak_kw(z3,200); %Upper height of each tethersonde
        flight
93  ttops=t3(maxh(:,2))-tstart;
94  ztops=maxh(:,1);
95  t=tt(1,:);
96  zcut=interp1(ttops,ztops,t,'linear','extrap');
97
98  for jt=1:nt %Loop over times in interp grid
99       iinan=find(isnan(TT(:,jt)) | zz(:,jt)>zcut(jt));
100      iinan=min(iinan);
101      iinan=max(2,iinan);
102      TT(iinan:end,jt)=TT(iinan-1,jt);
103      iinan=find(isnan(uu(:,jt)) | zz(:,jt)>zcut(jt));
104      iinan=min(iinan);
105      iinan=max(2,iinan);
106      uu(iinan:end,jt)=uu(iinan-1,jt);
107      iinan=find(isnan(vv(:,jt)) | zz(:,jt)>zcut(jt));
108      iinan=min(iinan);
109      iinan=max(2,iinan);
110      vv(iinan:end,jt)=vv(iinan-1,jt);
111 end
112
113 %Outside data, set to 0:
114 TT(isnan(TT))=0;
115 uu(isnan(uu))=0;
116 vv(isnan(vv))=0;
117
118 %Save to file readable by write_weatherfile.m
119 save tethdatainterp2 tt zz uu vv TT t zcut
```

Winter data:

```
1  % Read tethersonde data:
2  [z3,ws3,wd3,at3,ap3,t3] = gettethparams(403,1996,metbase96);
3  wd1=wd1-180;
4  h3=320+z3;
```

```
5
6  tfeb01_96=date2num('01-Feb-1996','00:00:00.000');
7  tstart=tfeb01_96-1;
8
9
10 jyes3=find(z3>0);
11 z3=z3(jyes3);ws3=ws3(jyes3);wd3=wd3(jyes3);at3=at3(jyes3);t3=t3(
       jyes3);
12
13
14 jyes3=find(z3<1050);
15 z3=z3(jyes3);ws3=ws3(jyes3);wd3=wd3(jyes3);at3=at3(jyes3);t3=t3(
       jyes3);
16
17 jyes3=find(at3<-2.5);
18 z3=z3(jyes3);ws3=ws3(jyes3);wd3=wd3(jyes3);at3=at3(jyes3);t3=t3(
       jyes3);
19
20 whichdate=floor(t3-tstart);
21 jyes3=find( whichdate~=22  |  (at3<-8 & whichdate==22)  );
22 z3=z3(jyes3);ws3=ws3(jyes3);wd3=wd3(jyes3);at3=at3(jyes3);t3=t3(
       jyes3);
23 whichdate=floor(t3-tstart);
24 jyes3=find( whichdate~=21  |  (at3>-11 & whichdate==21)  );
25 z3=z3(jyes3);ws3=ws3(jyes3);wd3=wd3(jyes3);at3=at3(jyes3);t3=t3(
       jyes3);
26 jyes3=find(t3-tstart>21.531);
27 z3=z3(jyes3);ws3=ws3(jyes3);wd3=wd3(jyes3);at3=at3(jyes3);t3=t3(
       jyes3);
28 jyes3=find(t3-tstart<21.6505   | t3-tstart>21.652);
29 z3=z3(jyes3);ws3=ws3(jyes3);wd3=wd3(jyes3);at3=at3(jyes3);t3=t3(
       jyes3);
30 jyes3=find(t3-tstart>22.345   | t3-tstart<22.3);
31 z3=z3(jyes3);ws3=ws3(jyes3);wd3=wd3(jyes3);at3=at3(jyes3);t3=t3(
       jyes3);
32 jyes3=find(t3-tstart<21.6505   | t3-tstart>21.653);
33 z3=z3(jyes3);ws3=ws3(jyes3);wd3=wd3(jyes3);at3=at3(jyes3);t3=t3(
       jyes3);
34 jyes3=find(t3-tstart<22.385   | t3-tstart>22.3856);
35 z3=z3(jyes3);ws3=ws3(jyes3);wd3=wd3(jyes3);at3=at3(jyes3);t3=t3(
       jyes3);
36 jyes3=find(t3-tstart<21.613   | t3-tstart>21.615);
37 z3=z3(jyes3);ws3=ws3(jyes3);wd3=wd3(jyes3);at3=at3(jyes3);t3=t3(
       jyes3);
38 jyes3=find(t3-tstart<22.436   | t3-tstart>22.489);
39 z3=z3(jyes3);ws3=ws3(jyes3);wd3=wd3(jyes3);at3=at3(jyes3);t3=t3(
```

```
    jyes3);
jyes3=find(t3-tstart <23.374    | t3-tstart >23.377);
z3=z3(jyes3);ws3=ws3(jyes3);wd3=wd3(jyes3);at3=at3(jyes3);t3=t3(
    jyes3);
jyes3=find(t3-tstart <23.438    | t3-tstart >23.445);
z3=z3(jyes3);ws3=ws3(jyes3);wd3=wd3(jyes3);at3=at3(jyes3);t3=t3(
    jyes3);

jyes3=find(ws3>0 & ws3<8);
z3=z3(jyes3);ws3=ws3(jyes3);wd3=wd3(jyes3);at3=at3(jyes3);t3=t3(
    jyes3);
jyes3=find(t3-tstart <22.48    | t3-tstart >22.51);
z3=z3(jyes3);ws3=ws3(jyes3);wd3=wd3(jyes3);at3=at3(jyes3);t3=t3(
    jyes3);


%uEW=ws3.*cosWE3;
c_of_T = @(T) 20.03*sqrt(T+273.15);%linear: cst=340+.6*(T-15);
cosEW3=cos((90-wd3)*pi/180);
cosNS3=cos(wd3*pi/180);
uwe=ws3.*(-cosEW3);
usn=ws3.*(-cosNS3);

%Interpolation of thethersonde data
[tt,zz]=meshgrid(21:.002:29,0:5:1010);
TT=griddata(t3-tstart,z3/5000,at3,tt,zz/5000);%Note scaling of z
uu=griddata(t3-tstart,z3/5000,uwe,tt,zz/5000);
vv=griddata(t3-tstart,z3/5000,usn,tt,zz/5000);


%Above the grid etc:
[nz nt]=size(tt);
maxh = tethpeak_kw(z3, 800); %Upper height of each tethersonde
    flight
ttops=t3(maxh(:,2))-tstart;
ztops=maxh(:,1);
t=tt(1,:);
zcut=interp1(ttops,ztops,t,'linear','extrap');

for jt=1:nt %Loop over times in interp grid
    iinan=find(zz(:,jt)>zcut(jt));
    iinan=min(iinan);
    iinan=max(2,iinan);
    TT(iinan:end,jt)=TT(iinan-1,jt);
    iinan=find(zz(:,jt)>zcut(jt));
    iinan=min(iinan);
```

```
80      iinan=max(2,iinan);
81      uu(iinan:end,jt)=uu(iinan-1,jt);
82      iinan=find( zz(:,jt)>zcut(jt));
83      iinan=min(iinan);
84      iinan=max(2,iinan);
85      vv(iinan:end,jt)=vv(iinan-1,jt);
86  end
87
88
89  %Outside data, set to 0:
90  TT(isnan(TT))=griddata(t3-tstart,z3/5e3,at3,tt(isnan(TT)),zz(
        isnan(TT))/5e3, 'nearest');
91  uu(isnan(uu))=griddata(t3-tstart,z3/5e3,uwe,tt(isnan(uu)),zz(
        isnan(uu))/5e3, 'nearest');
92  vv(isnan(vv))=griddata(t3-tstart,z3/5e3,usn,tt(isnan(vv)),zz(
        isnan(vv))/5e3, 'nearest');
93
94  %Save to file readable by write_weatherfile.m
95  save tethdatainterpF96 tt zz uu vv TT
```

A.4 Lists of NORTRIAL data selections

This section lists the selected data from the NORTRIAL database. We provide a case number (case, defined in this report), a detonation event number (event, defined in NORTRIAL), the receiver position (rec), and receiver height in m (h(m)). The latter three pieces of information uniquely define the recording. We also list the measured (SELCnt) and simulated (SELCpe) C-weighted SEL values.

A.4.1 Summer quality A data

case	event	rec	h(m)	SELCnt	SELCpe
5	70	306	2	84	87
7	73	112	30	77	78
11	76	306	2	88	89
13	77	112	4	108	106
14	81	412	4	84	81
16	82	306	8	98	101
18	83	112	30	107	105
19	83	306	1	56	74
20	84	306	1	61	76
21	87	306	1	86	89
23	88	306	1	99	101
25	91	306	1	63	69

26	92	306	1	77	83
27	93	306	1	88	89
29	94	306	1	99	101
30	139	112	2	102	98
32	143	306	1	65	70
34	144	306	8	85	86
36	149	306	0	65	69
37	150	306	8	71	84
38	151	112	2	103	97
40	157	112	2	103	99
41	159	112	0	93	84
42	160	306	2	71	85
43	161	306	8	81	86
45	162	306	8	95	92
46	163	112	4	101	98
47	164	112	2	84	91
48	166	112	8	69	70
49	167	306	8	81	86
51	168	306	8	97	92
53	169	112	4	99	97
54	170	112	2	90	90
55	172	306	8	71	79
57	173	306	8	86	89
59	174	306	8	94	93
60	177	306	1	72	69
61	178	306	2	77	84
63	179	306	1	91	95
65	180	306	8	86	90
66	182	112	16	91	86
67	182	306	0	65	60
69	183	112	16	93	94
70	183	306	0	74	69
72	184	306	8	80	85
73	185	306	8	91	97
75	186	306	8	95	104
77	188	112	0	91	86
79	189	112	8	95	94
80	189	306	1	79	71
81	189	412	0	79	70
83	190	306	8	80	84
84	191	306	8	91	96
86	192	306	8	96	104
88	194	112	0	93	87
90	195	112	2	96	96
91	195	306	8	78	70
93	196	306	8	85	85

94	197	306	8	97	97
97	199	306	8	82	75
99	200	306	8	78	76
101	202	306	8	71	73
102	204	412	1	93	92
103	205	306	8	80	77
105	206	306	8	75	77
107	207	306	8	81	81
108	208	306	0	74	78
109	211	306	8	82	67
110	212	306	8	78	65
112	213	306	8	80	71
113	214	306	2	73	80
114	215	306	1	73	73
115	216	306	0	74	75
116	217	306	8	87	84
118	218	306	8	86	87
120	219	306	1	79	86
121	220	306	8	71	77
122	220	212	1	67	65
123	221	306	8	75	79
124	222	306	1	72	82
126	223	306	8	79	81

A.4.2 Summer quality B1 data

case	event	rec	h(m)	SELCnt	SELCpe
5	65	112	30	98	96
7	66	112	30	90	88
9	67	112	30	77	79
15	71	112	30	98	96
17	72	112	30	90	88
23	77	412	8	74	67
25	79	112	30	81	83
27	79	412	8	80	75
31	80	412	8	76	81
34	82	112	30	77	50
35	82	412	8	83	70
36	83	412	8	74	73
38	84	112	30	99	96
39	84	412	8	77	72
42	85	112	30	82	84
43	85	412	8	77	82
47	87	412	8	85	65
49	88	412	8	82	58

51	89	112	30	106	106
52	90	112	30	97	97
53	90	412	8	79	59
56	91	112	30	79	84
57	91	412	8	74	68
61	92	412	8	77	74
64	93	412	8	73	64
66	94	112	30	81	52
67	94	412	8	73	59
70	140	112	30	90	92
72	141	112	30	78	91
81	145	112	30	98	97
83	146	112	30	89	89
86	147	112	30	83	86
96	152	112	30	89	89
99	153	112	30	79	82
107	158	112	30	96	94
115	160	112	30	77	69
119	161	112	30	74	73
122	162	112	30	72	72
133	165	112	30	92	80
141	168	112	30	70	71
152	171	112	30	88	84
157	172	112	30	70	57
173	177	112	30	85	82
174	177	412	8	72	62
187	181	112	30	75	74
194	183	412	8	76	67
195	183	212	8	73	64
204	187	112	30	78	73
210	188	412	8	71	61
212	189	212	8	71	62
227	195	412	8	77	70
228	195	212	2	71	65
254	207	112	30	72	77
264	209	412	8	78	81
269	210	412	8	92	91
273	211	412	1	78	46
274	211	212	8	75	71
287	215	412	8	77	80
290	216	412	8	88	90
305	222	112	30	72	56
321	226	306	8	74	60

A.4.3 Winter quality A data

case	event	rec	h(m)	SELCnt	SELCpe
1	603	306	30	75	59
2	604	306	30	66	68
3	605	306	30	80	79
4	608	306	30	61	51
5	609	306	30	65	60
6	610	306	30	66	65
7	611	306	30	79	78
8	613	306	20	51	69
9	614	306	30	59	62
10	616	306	30	67	66
11	617	306	30	79	77
12	618	306	30	73	64
13	619	306	30	67	64
14	620	306	30	72	67
15	621	306	30	83	84
16	622	306	30	94	95
17	623	306	30	101	99
18	624	306	30	67	66
19	625	306	8	65	69
20	626	306	30	74	74
21	627	306	30	84	84
22	628	306	30	92	94
23	629	306	30	94	99
24	630	306	8	64	65
25	631	306	8	64	65
26	632	306	8	68	67
27	633	306	30	81	80
28	634	306	30	82	95
29	635	306	30	95	96
30	638	306	30	84	61
31	639	306	30	83	92
32	640	306	30	76	80
33	641	306	30	89	104
34	642	306	8	72	59
35	643	306	8	79	79
36	644	306	8	78	79
37	645	306	8	91	95
38	646	306	8	84	97
39	647	306	30	88	104
40	648	306	8	69	79
41	649	306	8	80	79
42	650	306	8	79	86
43	651	306	30	75	92

44	652	306	8	88	96
45	653	306	8	102	107
46	656	306	8	73	70
47	657	306	8	72	77
48	658	306	8	72	78
49	659	306	30	81	80
50	660	306	0	64	63
51	661	306	0	57	57
52	662	306	8	71	67
53	663	306	30	80	85
54	664	306	30	78	85
55	665	306	30	81	79
56	666	306	0	59	63
57	667	306	0	56	56
58	668	306	8	73	66
59	669	306	30	78	84
60	670	306	30	82	79
61	671	306	30	79	80
62	672	306	8	66	73
63	673	306	8	64	69
64	674	306	8	74	79
65	675	306	30	89	83
66	676	306	30	85	80
67	677	306	30	92	92
68	678	306	8	67	71
69	679	306	8	62	69
70	680	306	8	71	84
71	681	306	30	85	77
72	682	306	30	79	79
73	683	306	30	94	92
74	684	306	8	65	72
75	685	306	8	61	73
76	686	306	8	71	88
77	687	306	30	84	76
78	688	306	30	77	77
79	689	306	30	94	92
80	690	306	8	61	62
81	695	306	30	73	76
82	697	306	30	73	76
83	699	306	8	70	78
84	618	212	2	75	75
85	619	212	2	77	76
86	620	212	2	76	75
87	621	212	2	72	78
88	622	412	30	58	58
89	622	212	2	71	79

90	623	212	2	71	72
91	624	212	2	73	72
92	625	212	2	75	74
93	626	212	2	74	79
94	636	412	30	77	44
95	636	212	2	70	69
96	637	212	2	64	67
97	638	412	30	81	54
98	638	212	2	79	81
99	639	212	2	71	82
100	640	412	30	85	69
101	640	212	2	87	94
102	641	412	30	66	68
103	641	212	2	78	91
104	642	412	30	76	45
105	642	212	2	65	67
106	644	412	30	85	57
107	644	212	2	75	78
108	645	212	2	68	79
109	646	412	30	89	73
110	646	212	2	84	91
111	647	412	30	65	69
112	647	212	2	81	89
113	648	412	30	82	47
114	648	212	2	67	70
115	650	412	30	90	58
116	650	212	2	76	78
117	651	212	2	67	79
118	652	412	30	92	73
119	652	212	2	82	88
120	653	412	30	68	68
121	653	212	2	75	88
122	654	412	30	80	85
123	654	212	2	65	42
124	655	412	30	77	82
125	659	412	30	73	78
126	660	412	30	81	85
127	660	212	2	68	45
128	661	412	30	77	79
129	661	212	2	64	45
130	666	412	30	82	85
131	666	212	2	68	47
132	667	412	30	75	81
133	672	412	30	94	100
134	672	212	1	74	62
135	673	412	30	86	93

136	674	412	30	69	77
137	677	212	1	71	74
138	678	412	30	94	100
139	678	212	1	70	62
140	679	412	30	84	92
141	680	412	30	70	77
142	680	212	1	74	71
143	683	412	30	70	66
144	683	212	2	67	75
145	684	412	30	94	100
146	684	212	1	72	61
147	685	412	30	86	92
148	685	212	2	65	60
149	686	412	30	70	77
150	686	212	2	72	79
151	688	212	2	64	68
152	689	212	2	69	78
153	695	412	2	62	71
154	695	212	2	66	77
155	696	412	0	61	71
156	696	212	2	67	77
157	697	412	1	61	71

Bibliography

[1] Eyvind Aker. NORTRIAL - innlegging av måledata fra finnskogen 1994 og 1996. Technical report, 20071037-3, Norwegian Geotechnical Institute, 2007.

[2] Eyvind Aker. NORTRIAL databasen. Technical report, 20061034-2, Norwegian Geotechnical Institute, 2007.

[3] Roy D. Ford, David J. Saunders, and Geoffrey Kerry. The acoustic pressure waveform from small unconfined charges of plastic explosive. *The Journal of the Acoustical Society of America*, 94(1), 1993.

[4] LR Hole, Y Gjessing, and T De Lange. Meteorological measurements during Norwegian trials. In *International congress on noise control engineering*, pages 605–610, 1996.

[5] M Huseby, R Rahimi, JA Teland, I Dyrdal, H Fykse, B Hugsted, CE Wasberg, E Aker, R Cleave, F Løvholt, H Olsen, SÅ Storeheier, and Taraldsen. G. Final report: Improvement of the computational methods of the Norwegian defence estates agency for computing noise from the Norwegian defence training ranges. *Norwegian Defence Research Establishment report*, 2008.

[6] Morten Huseby. Noise emission data for M109, 155 mm field howitzer, 2007.

[7] Morten Huseby, Reza Rahimi, Jan Arild Teland, and Idar Dyrdal. Støy fra skytefelt. Technical report, Technical Report FFI/RAPPORT-2005/00471, Norwegian Defence Research Establishment, 2005.

[8] Amir M Kaynia, Finn Løvholt, and Christian Madshus. Effects of a multi-layered poro-elastic ground on attenuation of acoustic waves and ground vibration. *Journal of Sound and Vibration*, 330(7):1403–1418, 2011.

[9] Finn Løvholt. Statistical modelling of sound propagation. *NGI report*, pages 20071037–6, 2007.

[10] Christian Madshus, Finn Løvholt, Amir Kaynia, Lars Robert Hole, Keith Attenborough, and Shahram Taherzadeh. Air-ground interaction in long range propagation of low frequency sound and vibration - field tests and model verification. *Applied Acoustics*, 66(5):553–578, 2005.

[11] RA Sack and M West. A parabolic equation for sound propagation in two dimensions over any smooth terrain profile: the generalised terrain parabolic equation (GT-PE). *Applied acoustics*, 45(2):113–129, 1995.

[12] Erik M Salomons. *Computational Atmospheric Acoustics*. Springer Netherlands, 2001.

[13] S.Å. Storeheier. Estimates of acoustic impedance of ground surfaces at Haslemoen and Finnskogen sites, during the Norwegian Trials 1994-1996. main results. Technical report, Sintef Memo 40-NO980231, 1998.

[14] S.Å. Storeheier. Nye markslagstyper. Technical report, Sintef, 1998.

[15] S.Å. Storeheier and S Stensby. Land-cover classification at the Finnskogen site – a satellite photo approach. Technical report, Sintef Memo 40-NO980117, 1998.

[16] Michelle E Swearingen, Morten Huseby, and Reza Rahimi. *Comparison of Sound Propagation Codes: Milstøy, BNoise and a PE-method*. Forsvarets Forskningsinstitutt, 2009.

[17] G. Taraldsen. The Delany-Bazley impedance model and Darcy's law. *Acta Acustica united with Acustica*, 91(1):41–50, 2005-01-01T00:00:00.

[18] Knut Waagan. Low-frequency long-range atmospheric noise propagation modelling with the PE method. Technical report, FFI/RAPPORT-2014/00260, Norwegian Defence Research Establishment, 2014.

[19] Knut Waagan. Noise mapping with the PE method – a case study from interior Norway. Technical report, FFI/RAPPORT-2015/00809, Norwegian Defence Research Establishment, 2015.

[20] D Keith Wilson, Matthew S Lewis, John W Weatherly, and Edgar L Andreas. Dependence of predictive skill for outdoor narrowband and broadband sound levels on the atmospheric representation. *Noise Control Engineering Journal*, 56(6):465–477, 2008.

[21] Cornelis Zwikker and Cornelis Willem Kosten. *Sound absorbing materials*. Elsevier, 1949.

About FFI

The Norwegian Defence Research Establishment (FFI) was founded 11th of April 1946. It is organised as an administrative agency subordinate to the Ministry of Defence.

FFI's MISSION

FFI is the prime institution responsible for defence related research in Norway. Its principal mission is to carry out research and development to meet the requirements of the Armed Forces. FFI has the role of chief adviser to the political and military leadership. In particular, the institute shall focus on aspects of the development in science and technology that can influence our security policy or defence planning.

FFI's VISION

FFI turns knowledge and ideas into an efficient defence.

FFI's CHARACTERISTICS

Creative, daring, broad-minded and responsible.

Om FFI

Forsvarets forskningsinstitutt ble etablert 11. april 1946. Instituttet er organisert som et forvaltningsorgan med særskilte fullmakter underlagt Forsvarsdepartementet.

FFIs FORMÅL

Forsvarets forskningsinstitutt er Forsvarets sentrale forskningsinstitusjon og har som formål å drive forskning og utvikling for Forsvarets behov. Videre er FFI rådgiver overfor Forsvarets strategiske ledelse. Spesielt skal instituttet følge opp trekk ved vitenskapelig og militærteknisk utvikling som kan påvirke forutsetningene for sikkerhetspolitikken eller forsvarsplanleggingen.

FFIs VISJON

FFI gjør kunnskap og ideer til et effektivt forsvar.

FFIs VERDIER

Skapende, drivende, vidsynt og ansvarlig.

FFI's organisation

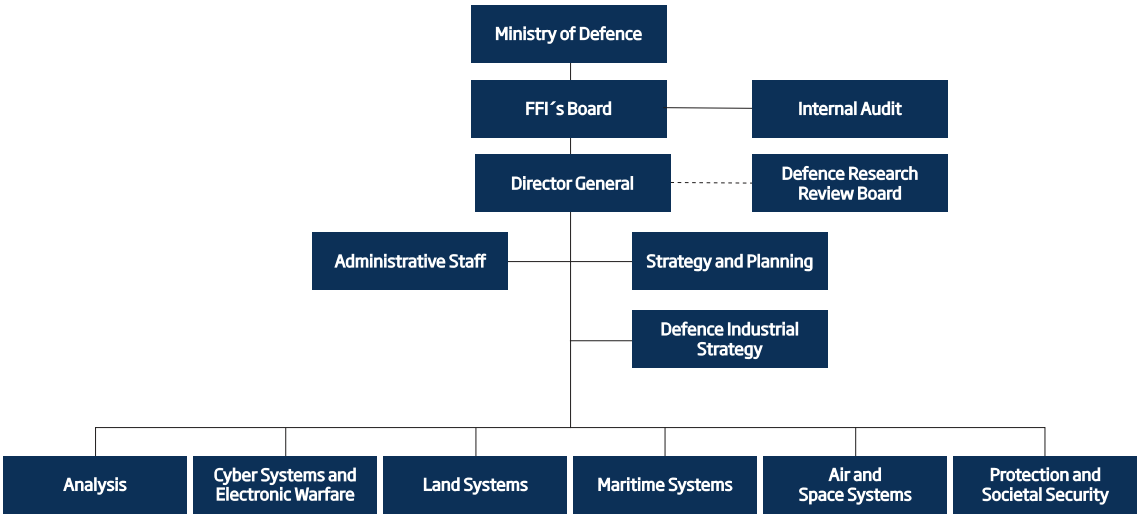

Forsvarets forskningsinstitutt
Postboks 25
2027 Kjeller

Besøksadresse:
Instituttveien 20
2007 Kjeller

Telefon: 63 80 70 00
Telefaks: 63 80 71 15
Epost: ffi@ffi.no

Norwegian Defence Research Establishment (FFI)
P.O. Box 25
NO-2027 Kjeller

Office address:
Instituttveien 20
N-2007 Kjeller

Telephone: +47 63 80 70 00
Telefax: +47 63 80 71 15
Email: ffi@ffi.no

FFI Forsvarets forskningsinstitutt